

NASA Contractor Report 4250

Interpretation of F106B and CV580 In-Flight Lightning Data and Form Factor Determination

T. Rudolph, J. Horembala,
F. J. Eriksen, H. S. Weigel,
J. R. Elliott, S. L. Parker,
and R. A. Perala
Electro Magnetic Applications, Inc.
Lakewood, Colorado

Prepared for
Langley Research Center
under Contract NAS1-17748



National Aeronautics and
Space Administration
Office of Management
Scientific and Technical
Information Division

1989

TABLE OF CONTENTS

Chapter	Title	
1	INTRODUCTION	1-1
2	ANALYSIS OF THE 1985 AND 1986 F106B TRANSIENT FLIGHT DATA	2-1
2.1	Introduction	2-1
2.2	Linear Triggered Lightning Modeling	2-2
2.2.1	Description of the Linear Triggered Lightning Models	2-2
2.2.2	Results of the Linear Triggered Lightning Modeling	2-4
2.3	Database Development for the 1985 Data	2-8
2.3.1	Results of the Database Development for the 1985 Data	2-9
2.4	Lightning Current Derivative Peak Value Correlation Study	2-9
2.4.1	Results of the Lightning Current Derivative Peak Value Correlation Study	2-10
2.5	Summary and Conclusions	2-14
3	F106B FIELD MILL MODELING	3-1
3.1	Introduction	3-1
3.2	Calculated Field Enhancements and Calibration Matrices	3-3
3.3	Application of Form Factors to Measured Data	3-7
4	EXPERIMENTAL DETERMINATION OF F106B FORM FACTORS	4-1
4.1	Description of Electrolytic Tank Experiment	4-1
4.2	Electrolytic Tank Anomalies	4-4
4.2.1	Possible Explanations for Anomalies	4-5
4.3	Numerical Validation of Experimental Techniques	4-6
4.3.1	Time Domain Finite Difference Technique	4-6
4.3.2	Potential Technique	4-7
4.3.3	Comparison of Numerical and Experimental Results for Finite Cylinder	4-11
4.4	Experimental Form Factors for the F106B	4-12
5	ANALYSIS OF THE 1987 CV580 IN-FLIGHT LIGHTNING DATA	5-1
5.1	Introduction	5-1
5.1.1	Terminology	5-3
5.2	General Comments	5-5
5.2.1	Initial Responses	5-5
5.2.2	Multiple Surges	5-6
5.2.3	Continuing Current Sizes	5-6
5.2.4	Type of Channel	5-8

LIST OF FIGURES

Figure	Title	
2.1	Entry Channel Geometries	2-3
2.2	Comparison of Nose Attachment Models with the Measured Data for Flight 85-028 Run 001 Strike 001	2-7
2.3	Peak Value Scatter Diagram 1 Derived from 1985 Measured I-dot and B-dot Longitudinal Response Data	2-11
2.4	Peak Value Scatter Diagram 2 Derived from 1985 Measured I-dot and B-dot Right Wing Response Data	2-11
2.5	Peak Value Scatter Diagram 3 Derived from 1985 Measured I-dot and B-dot Left Wing Response Data	2-12
2.6	Peak Value Scatter Diagram 4 Derived from 1985 Measured I-dot and D-dot Forward Response Data	2-12
2.7	Peak Value Scatter Diagram 5 Derived from 1985 Measured I-dot and D-dot Tail Response Data	2-13
2.8	Peak Value Scatter Diagram 6 Derived from 1985 Measured I-dot and D-dot Right Wing Response Data	2-13
3.1	F106B Showing Field Mill Locations	3-4
3.2a	Calculated Ambient Fields Just Prior to the Strike for the Coarsely Modeled F106B (Strike Time Is at 14 Seconds)	3-9
3.2b	Calculated Ambient Fields Just Prior to the Strike for the Finely Modeled F106B (Strike Time Is at 14 Seconds)	3-10
3.3a	Calculated Ambient Fields Just Prior to the Strike for the Coarsely Modeled F106B (Strike Time Is at 48 Seconds)	3-11
3.3b	Calculated Ambient Fields Just Prior to the Strike for the Finely Modeled F106B (Strike Time Is at 48 Seconds)	3-12
3.4a	Calculated Ambient Fields Just Prior to the Strike for the Coarsely Modeled F106B (Strike Time Is at 40 Seconds)	3-13
3.4b	Calculated Ambient Fields Just Prior to the Strike for the Finely Modeled F106B (Strike Time Is at 40 Seconds)	3-14
3.5a	Calculated Ambient Fields Just Prior to the Strike for the Coarsely Modeled F106B (Strike Time Is at 15 Seconds)	3-15

LIST OF FIGURES

Figure

Title

5.8	E-Field and Current Sensor Records from Flash 7, 11 August 1987	5-20
-----	--	------

CHAPTER 1 INTRODUCTION

This report is the last in a series of reports [1-6] documenting the interpretation of lightning data gathered by aircraft in flight. A majority of the investigation has centered on data collected by the NASA F106B Thunderstorm Research Aircraft. This report also contains analysis of analog data generated by the CV580 aircraft flown by the Federal Aviation Administration and Wright-Patterson Air Force Base.

The current report is concerned mostly with two topics. The first is the direct interpretation of data collected by the F106B and CV580 aircraft. In the case of the F106B, the investigation is done using finite difference computer models to predict lightning currents and attach points. This was done for a variety of observed 1985 strikes to the aircraft. The measured and calculated data from these strikes was also subjected to statistical analysis and the information entered into a database created under an earlier effort [6]. The small amount of 1986 data was not considered suitable for making these predictions and was not included in the database. The data from the CV580 aircraft which was analyzed was all in the form of analog data. Because of the long times involved (on the order of tens of microseconds to many milliseconds) and the low frequency bandwidth of the data the finite difference analysis of the type performed on the F106B data was not possible for the CV580 data. Hence the analysis presented here is more in the nature of statistical analysis of data in the form of current bursts per second, continuing current amplitudes and durations, and the like.

The second topic dealt with in this report is the investigation of ambient electric fields and charges within the lightning environment through the analysis of field mill data and the determination of aircraft form factors. Form factors are investigated both experimentally and numerically, and application is made to field mill data collected on the F106B in 1985.

Individual chapters of the report can be summarized as follows. Chapter 2 reports on the investigation of 1985 direct strike data collected on the F106B. Correlations between I-dot nose peak values and other sensor peak values are made using both measured and predicted results. These correlations show that under selected conditions relationships between these peak quantities can usually be

CHAPTER 2

ANALYSIS OF THE 1985 AND 1986 F106B TRANSIENT FLIGHT DATA

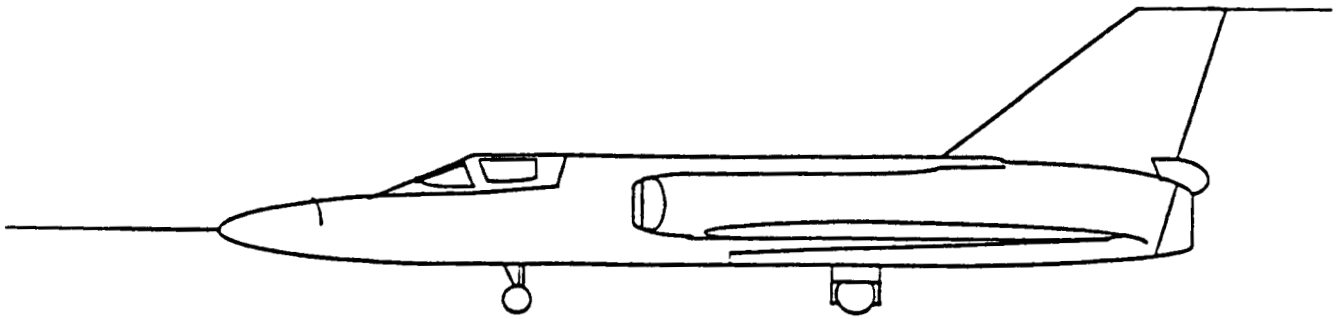
2.1 Introduction

The transient flight data gathered by the F106B during the 1985 and 1986 thunderstorm seasons [7] was analyzed to examine this data set for trends and to numerically calculate the electromagnetic sensor transients for further data characterization. The study supplements work completed in previous years as a part of a continuing effort to understand lightning/aircraft interaction.

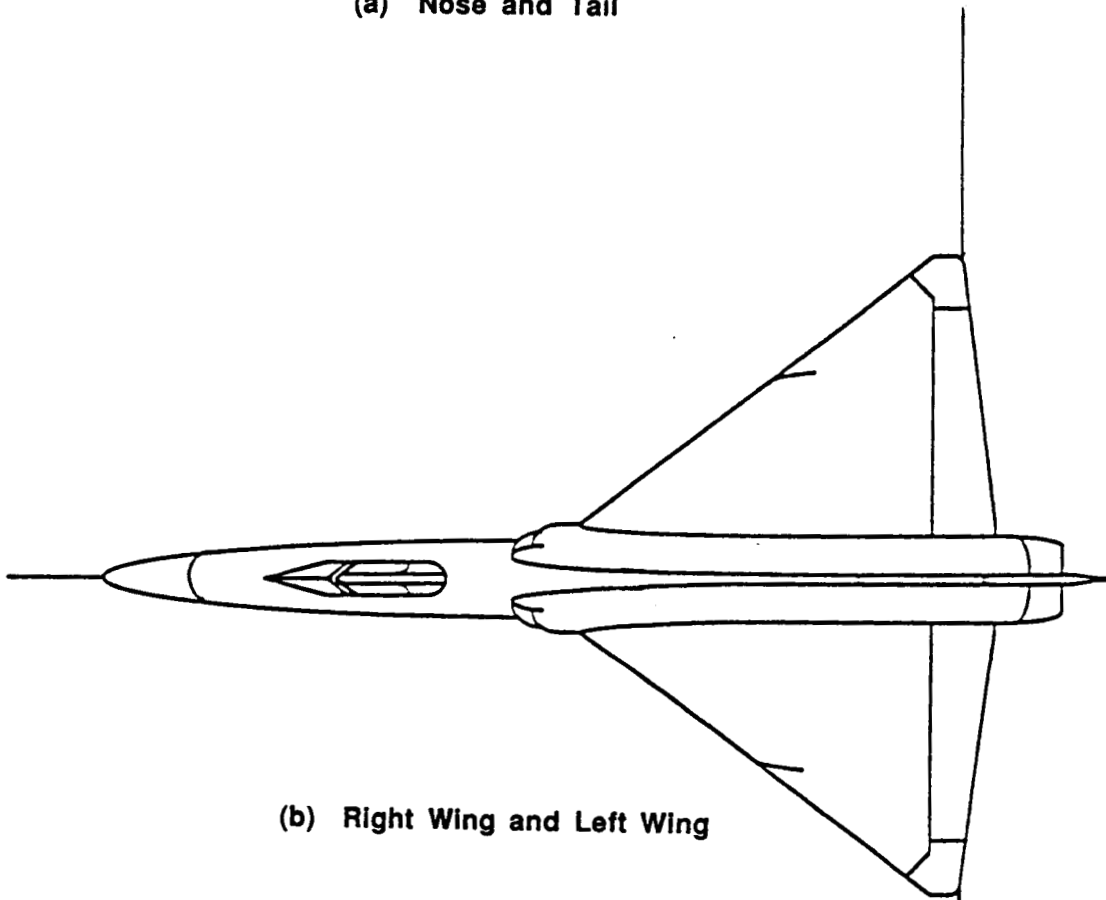
All of the events analyzed in detail in this report were from the 1985 thunderstorm season. For various reasons explained in Reference 7, 1986 produced only one large tail current measurement, but because none of the time derivative channels produced data that was usable for this type of analysis, 1986 data was not used.

The results of this investigation include a comparison of measured and calculated sensor transients for 27 separate events. The calculated waveforms were obtained using the linear triggered lightning model in conjunction with a lightning current source derived via the transfer function technique developed under an earlier phase [4]. As a new part of the triggered lightning analysis, four distinct lightning channel attachment geometries were considered for the simulations.

To complete the data interpretation, sensor waveform characteristics were generated for the 27 simulated events and for 29 events from the measured data. The characteristics were entered into the database formed during a previous effort [6] and then examined for correlations relating lightning current characteristics to the characteristics of the external sensors.



(a) Nose and Tail



(b) Right Wing and Left Wing

Figure 2.1 Entry Channel Geometries

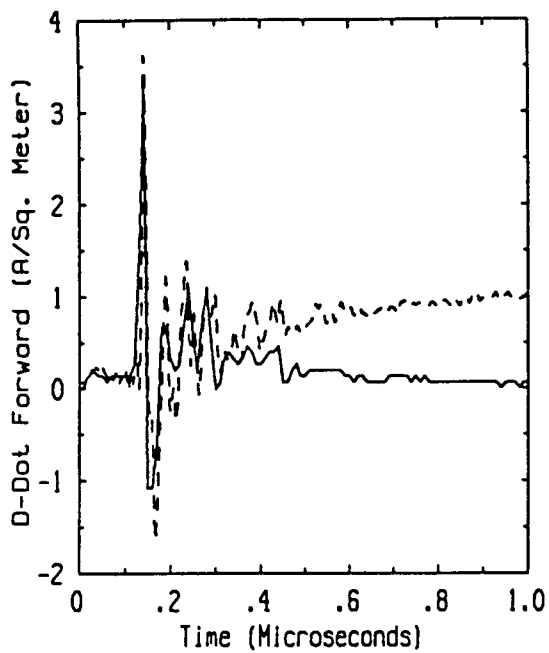
The numerical results indicate that from the 27 strikes analyzed, 20 fall into the category of nose attachments, 3 were left wing attachments, 3 were right wing attachments and a single tail attachment case is probable for Flight 85.035 Run 005 Strike 005. The large percentage of nose attachments witnessed in the measured data once again confirms the high probability of channel formation at this particular location on the F106B.

The current waveforms calculated during the analysis are, in many cases, similar to the data obtained in previous years. There is, however, a noticeable occurrence of some larger amplitude transients in the new data associated with the peak response period as compared to those seen in past years. The appearance of this characteristic in the derived waveforms is easily supported through an examination of the corresponding flight data for these events. The data obtained from the D-dot sensors on the F106B is particularly useful for this type of analysis since these waveforms have been observed in previous data to follow the pattern established by the current flowing on the aircraft.

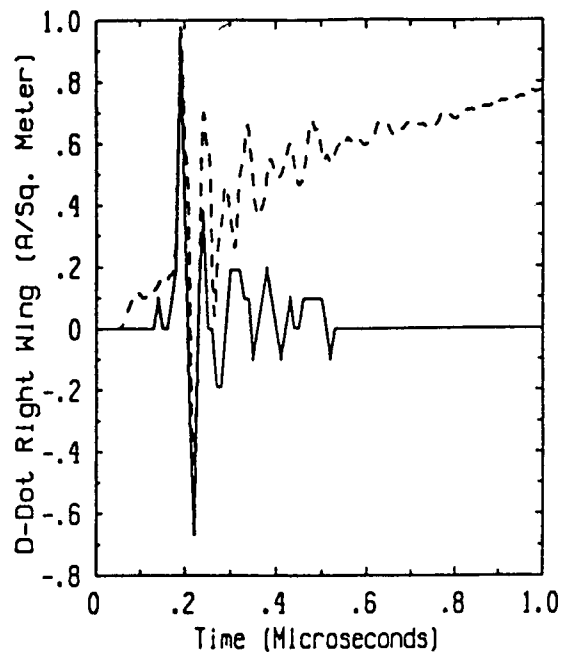
In general, the calculated sensor transients appearing in Appendix B provide a reasonably good representation of the measured sensor waveforms. The only major discrepancies in this set occur with the amplitudes of the calculated I-dot waveforms when compared to their measured counterparts and with the calculated transients exhibiting larger than expected oscillations at both early and late time for certain strikes.

A close examination of the measured and calculated I-dot transients shows that while the pairs generally agree in terms of overall waveshape, there remains some disagreement in the amplitude characteristics even after the filtering process. The differences noted here are probably due in part to the use of calculated waveforms essentially derived from differing aircraft sensors. This could result in differences in the derived currents which are clearly functions of not only the sensor type and sampling rate, but also location on the F106B surface. The addition of the supplementary operation of differentiation to this process might also tend to magnify any inaccuracies in the calculated sources.

The oscillations which appear in some of the calculated transients, predominantly during Flight 85.032, have their origins in the current sources derived

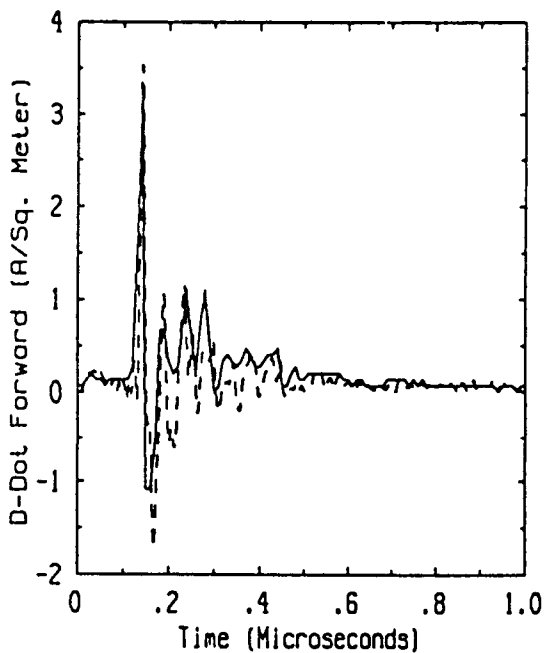


Flight 85.028 Run 001 Strike 001
- Measured -- Predicted

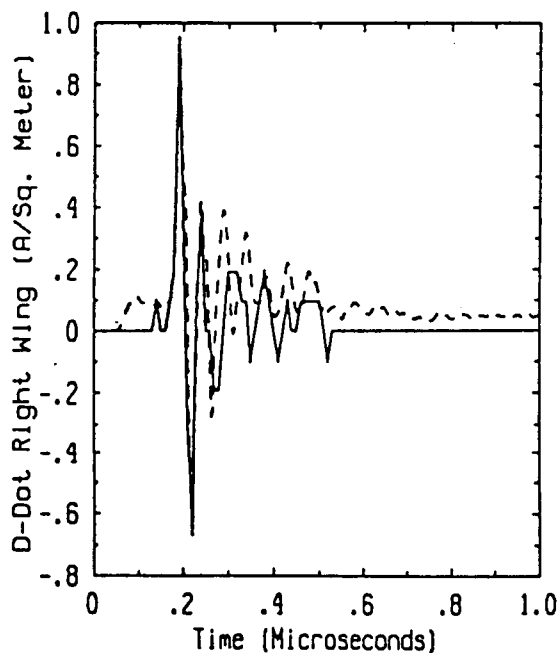


Flight 85.028 Run 001 Strike 001
- Measured -- Predicted

(a) No Exit Channel



Flight 85.028 Run 001 Strike 001
- Measured -- Predicted



Flight 85.028 Run 001 Strike 001
- Measured -- Predicted

(b) Exit Channel on Tail Section

Figure 2.2 Comparison of Nose Attachment Models with the Measured Data for Flight 85.028 Run 001 Strike 001

2.3.1 Results of the Database Development for the 1985 Data

Using the measured and calculated transient results, it was possible to produce 56 new entries in the characteristics database. From this number, 27 fall into the category of calculated data entries and 29 represent entries of characteristics obtained from the measured data. Although the relative size of this additional database segment is small in comparison with the 1984 section, it still represents a useful addition to this collection of strike characteristics.

In addition to providing the response data required by the database programs and the linear modeling segment, the measured windows produced as a part of the database development represent a set of transients which have a form and record length that is similar to the raw data sets obtained in previous years. This makes this particular data collection important because the transients of intermediate size obtained during this analysis can be compared directly to the measured transient data obtained in the past.

2.4 Lightning Current Derivative Peak Value Correlation Study

The new database entries were examined for possible correlations that would relate lightning current characteristics to the characteristics of other sensor responses on the surface of the F106B. After an evaluation of the new data, the study focused on relationships that might exist between the I-dot peak values and the peak values obtained for the B-dot and D-dot sensors. These correlations, if they can be shown to exist, are useful for making simple predictions of sensor or current characteristics when measurements are unavailable. For example, a correlation might be used to predict a peak I-dot response from a peak D-dot response when a lightning attachment occurred at a point not monitored by a current or current derivative sensor.

This brief study represents an attempt to relate the sensor characteristics through the use of scatter diagrams for probable nose attachment cases. The particular analysis was performed for the measured values obtained from strikes where a nose attachment geometry was supported by the transients calculated in Section 2.2. The limitation of the values to a single strike geometry was aimed at reducing the list of parameters that might influence the development of simple correlations.

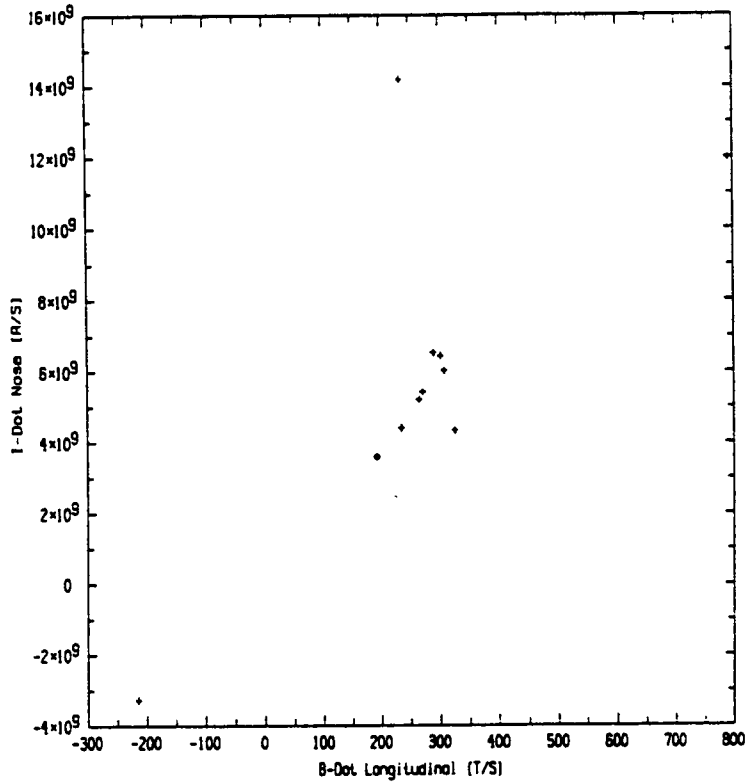


Figure 2.3 Peak Value Scatter Diagram 1 Derived from 1985 Measured I-dot and B-dot Longitudinal Response Data

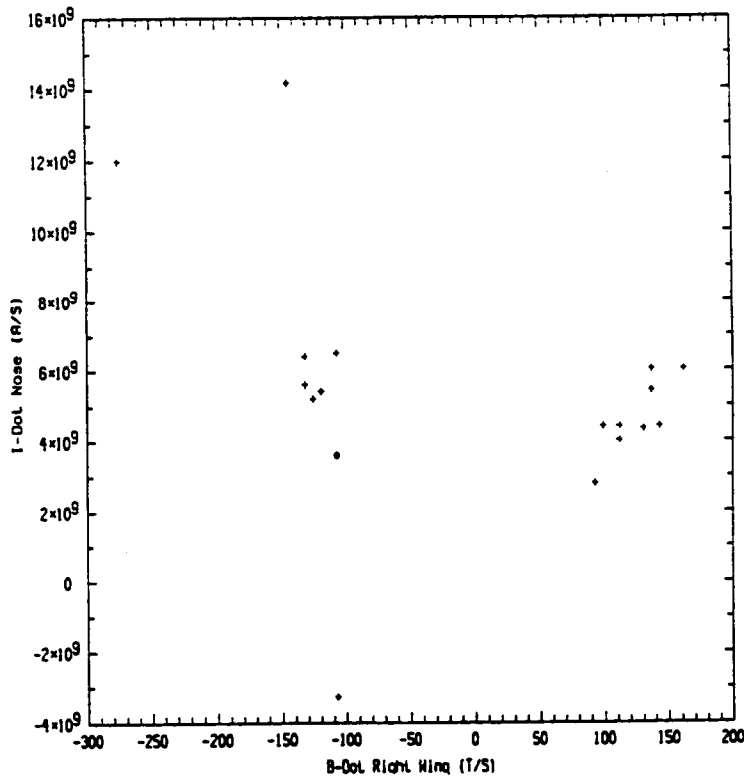


Figure 2.4 Peak Value Scatter Diagram 2 Derived from 1985 Measured I-dot and B-dot Right Wing Response Data

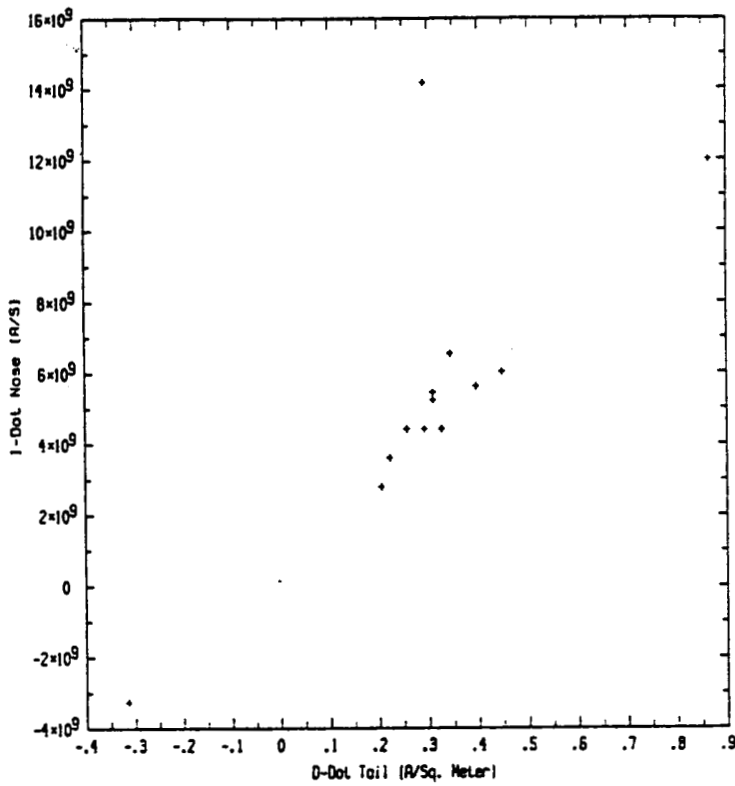


Figure 2.7 Peak Value Scatter Diagram 5 Derived from 1985 Measured I-dot and D-dot Tail Response Data

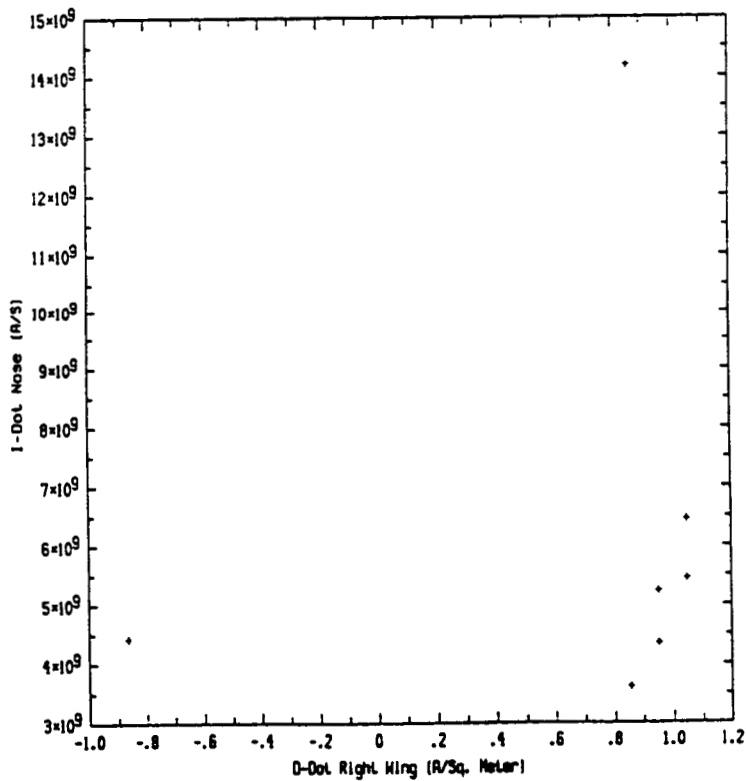


Figure 2.8 Peak Value Scatter Diagram 6 Derived from 1985 Measured I-dot and D-dot Right Wing Response Data

attachment geometry tended to improve the relationships between variables, the data still exhibited deficiencies that limit the accuracy of simple representations. The results suggest that consideration of the interaction between lightning and aircraft as a multivariate event, including such characteristics as temperature and pressure, may be crucial to the development of elementary predictive tools.

CHAPTER 3

F106B FIELD MILL MODELING

3.1 Introduction

The NASA F106B thunderstorm research aircraft carried electric field mills which measured the local electric field at four locations on the surface of the aircraft. Given a calibration of those mills, the measurements can be used to infer the ambient electric field intensity and direction and the net charge on the aircraft under the assumption that the ambient field is uniform over the volume occupied by the aircraft. Calibrations of the system can be performed either experimentally or analytically. The term "calibration" here refers to the relationship between the local fields and the ambient field and charge, not to the relationship between the local field at the field mill and the actual output (usually in volts) of that mill. Both experimental and analytic techniques have drawbacks that introduce errors into the calibration. Difficulties with the experimental techniques are listed below.

- 1) The net aircraft charge is difficult to measure, especially for an in-flight aircraft. Hence the local fields produced by net charge alone are uncertain. This means that only for situations in which the net charge is small can the calibration be reliably used. For an aircraft on the ground the potential can be accurately controlled. This is equivalent to the net charge if the capacitance of the aircraft is constant. Unfortunately the presence of the ground plane beneath the aircraft changes both the effective capacitance of the aircraft and the charge distribution from what exists in flight for the same potential. Hence the ground calibration is unreliable for an in-flight aircraft.

- 2) Calibrations performed by an in-flight aircraft rely on an independent determination of the electric field at the location of the aircraft. Independent measurements can be done near the ground, assuming that the field does not vary much up to the altitude of the aircraft, or by tethered balloons. Even if the field is determined accurately, the problem of net charge discussed above in (1) remains.

The analytic calibration does not suffer from the above problems, but has unique difficulties of its own. The net charge on the aircraft can be precisely fixed, and

The locations of the field mills on the F106B are shown in Figure 3.1. The frequency response of the field mill system was from DC to 250 Hz. A previous report [6] documented some points of caution which should be kept in mind when evaluating the field mill system and analysis. These are repeated below for completeness.

For those four points only, "calibration" means the relationship between the electric field at the field mill location and the actual output of the sensor in volts.

- 1) The field mill system was considered to be developmental throughout the NASA F106B flight program.
- 2) Because of the developmental nature, the measurements were not primary, and often flights were made that did not record all field mill channels.
- 3) There were no satisfactory calibrations of the field mill system until 1986; nevertheless a number of events for three flights in 1985 were considered usable.
- 4) A special calibration of the field mill system was performed at the end of 1986 for the 1985 flights. That is the calibration used in the analysis documented here. The electronic configuration of the F106B was returned to the 1985 values to within component tolerances.

3.2 Calculated Field Enhancements and Calibration Matrices

The technique used here to calculate local field enhancements for an aircraft in a uniform ambient electric field is the finite difference solution of Maxwell's equations [9]. The ambient field is inserted as an initial condition into an empty problem space along one of the coordinate axes. The aircraft is then introduced into the problem space as a conductivity which increases in time. The conductivity is increased slowly so as to minimize oscillations which are caused by resonant behavior of the aircraft. After the conductivity of the aircraft has increased to a sufficiently high value, the electric fields on the surface and within the aircraft can be zeroed to simulate a perfectly conducting metallic object. The normal fields at the locations of the field mills then represent the local field enhancements. This process is

repeated for ambient fields along the other two coordinate directions.

The fields for a net charge are calculated by placing a net charge on the aircraft. This is done by running current channels from the problem space boundary to the surface of the aircraft. The time domain waveforms and locations of the charging currents are again chosen so as to minimize resonant behavior of the aircraft.

This process produces a matrix equation which gives the local fields at the field mill locations in terms of the components of the ambient field and the aircraft's net charge. Inverting this matrix gives one an equation for the ambient fields and net charge in terms of the local fields. In principle, then, one knows the ambient quantities as precisely as the calibration of the system allows. In practice analysis shows that errors in the ambient quantities can be quite large, even for calibrations that may seem adequate [8].

The matrix equations giving the electric fields at the location of the field mills in terms of the ambient fields and net charge are shown below as Equations 3.1 and 3.2. Equation 3.1 is the matrix equation previously reported for the more coarsely modeled F106B, and Equation 3.2 is the equation for the finely modeled aircraft. Note that the local fields are keyed to the field mills shown in Figure 3.1 and the ambient fields to the coordinate system shown in that figure. Also the fields are measured in volts per meter and the net charge in microcoulombs.

$$\begin{bmatrix} E_R \\ E_L \\ E_F \\ E_A \end{bmatrix} = \begin{bmatrix} -4.38 & -1.46 & .08 & 507 \\ -4.38 & 1.46 & .08 & 507 \\ -2.47 & 0.00 & 1.52 & 464 \\ .89 & .15 & 1.03 & 276 \end{bmatrix} \begin{bmatrix} E_x \\ E_y \\ E_z \\ Q \end{bmatrix} \quad (3.1)$$

$$\begin{bmatrix} E_x \\ E_y \\ E_z \\ Q \end{bmatrix} = \begin{bmatrix} .0012 & .041 & -.276 & .311 \\ -.352 & .352 & 0.00 & 0.00 \\ -.350 & -.384 & .905 & -.265 \\ .00115 & .00147 & -.00248 & .00253 \end{bmatrix} \begin{bmatrix} E_R \\ E_L \\ E_F \\ E_A \end{bmatrix} \quad (3.4)$$

The ideal situation in these two equations would be for each ambient field to be dominated by one of the field mill readings. That is, one would like for one number to be dominant in each row. This would imply that the field mills each respond to only one component of the ambient field or net charge and are recording independent quantities. The above equations clearly do not have this property, which is in any case difficult to achieve in practice.

The differences between Equations 3.3 and 3.4 are large enough that it was deemed useful to repeat the analysis of the field mill data done in Reference 6. The application of the new matrix equation and comparison with older results is the subject of the next section.

3.3 Application of Form Factors to Measured Data

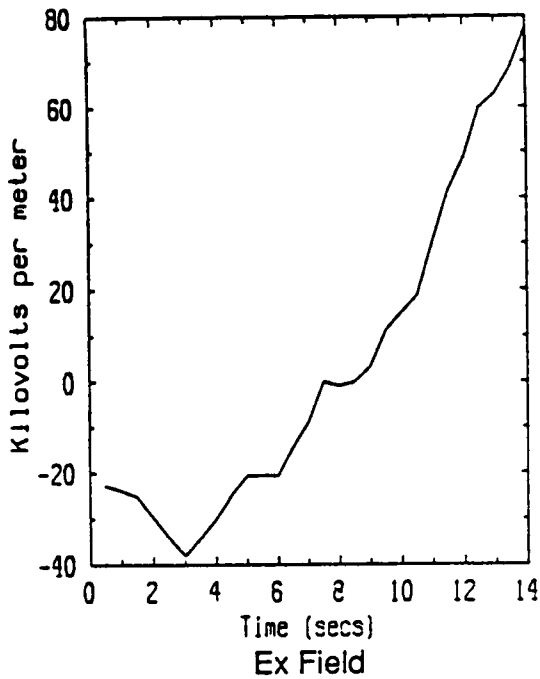
The observed field mill data used in this chapter were digitized by hand from hard copy records provided by NASA. The calibrations from sensor output to local electric field value were provided by NASA from a 1986 calibration as mentioned in Section 3.1. These calibrations are shown below, where the number is for a full scale reading.

E_R record: 227 kV/m

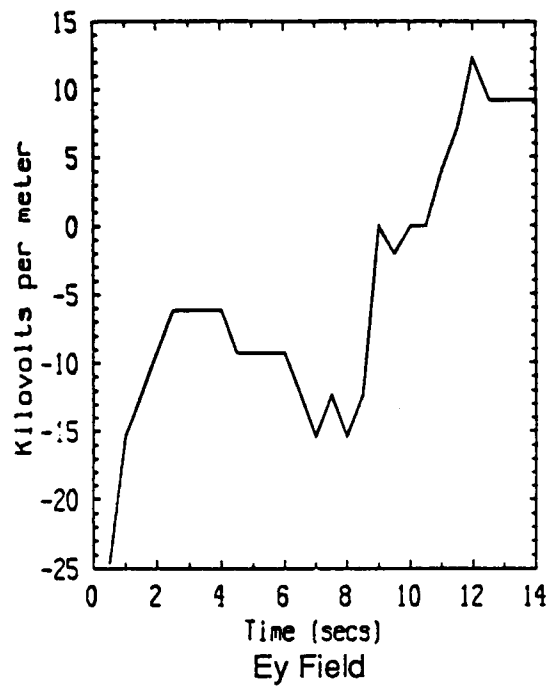
E_A record: 216 kV/m

E_L record: 232 kV/m

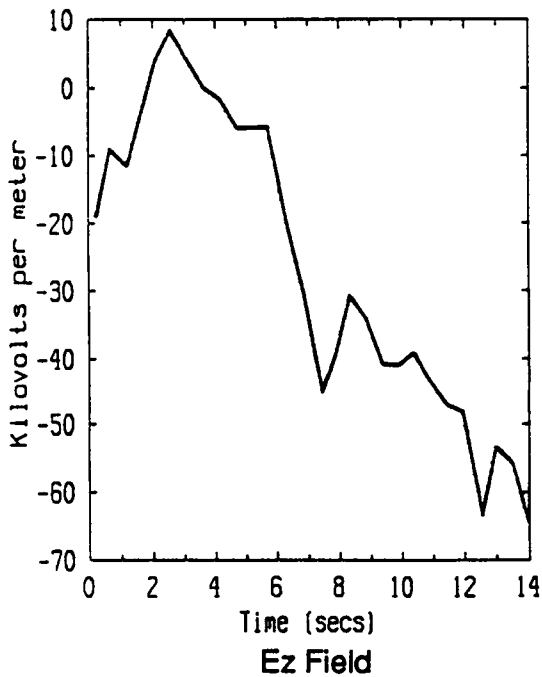
E_F record: 248 kV/m



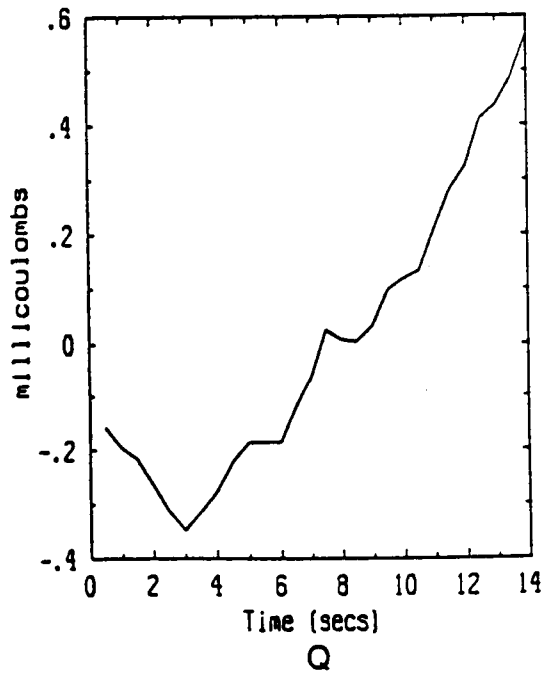
TRIGGER TIME = 19:31:34.8
Flight 85-26



TRIGGER TIME = 19:31:34.8
Flight 85-26

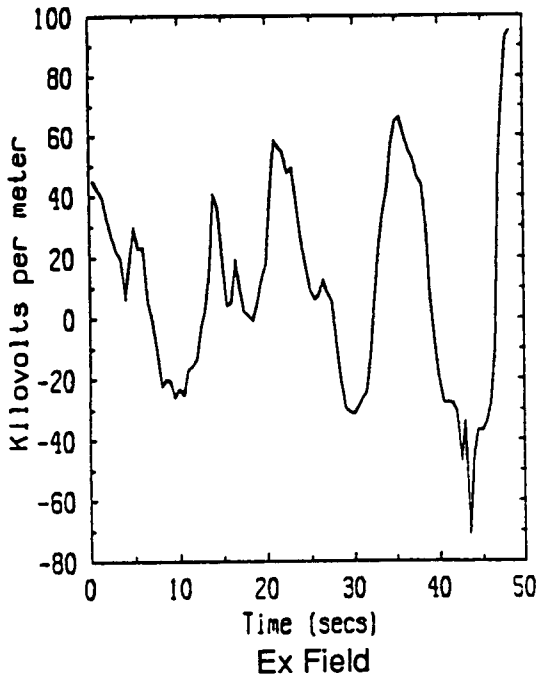


TRIGGER TIME = 19:31:34.8
Flight 85-26

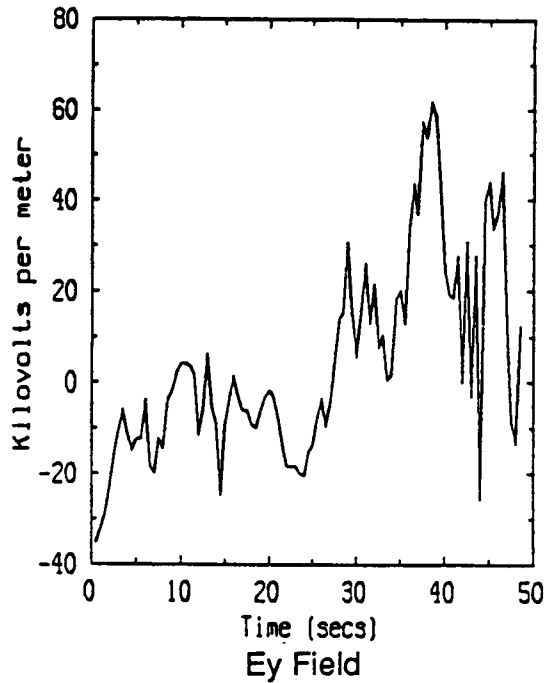


TRIGGER TIME = 19:31:34.8
Flight 85-26

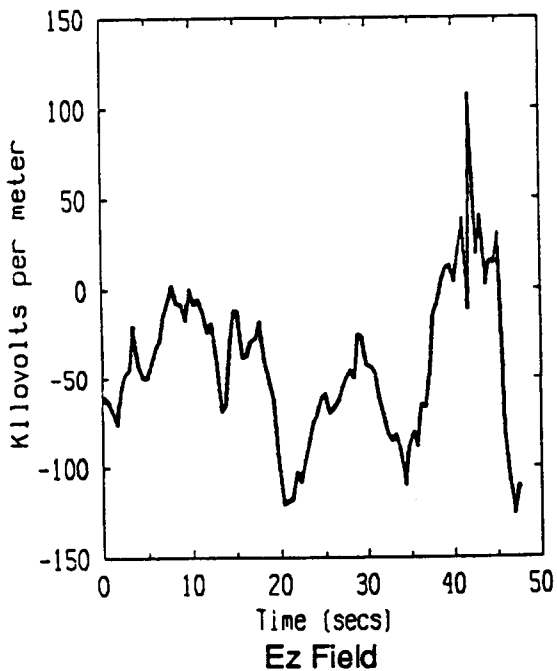
Figure 3.2a Calculated Ambient Fields Just Prior to the Strike for the Coarsely Modeled F106B (Strike Time Is at 14 Seconds)



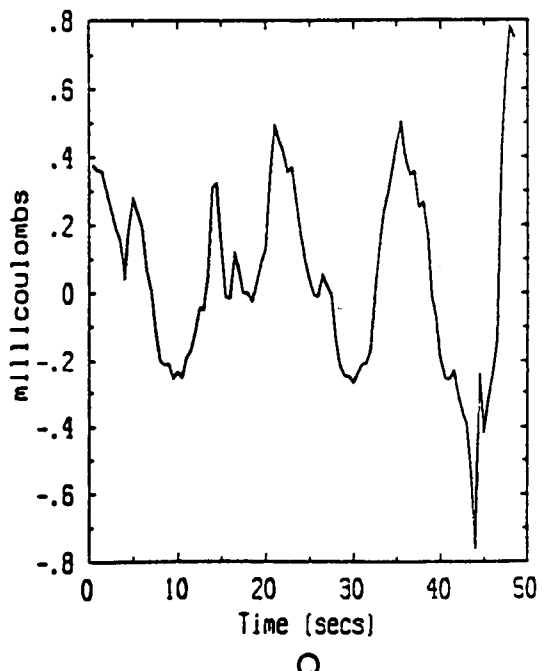
TRIGGER TIME = 20:13:15.2
Flight 85-26 CBW - FM



TRIGGER TIME = 20:13:15.2
Flight 85-26 CBW - FM

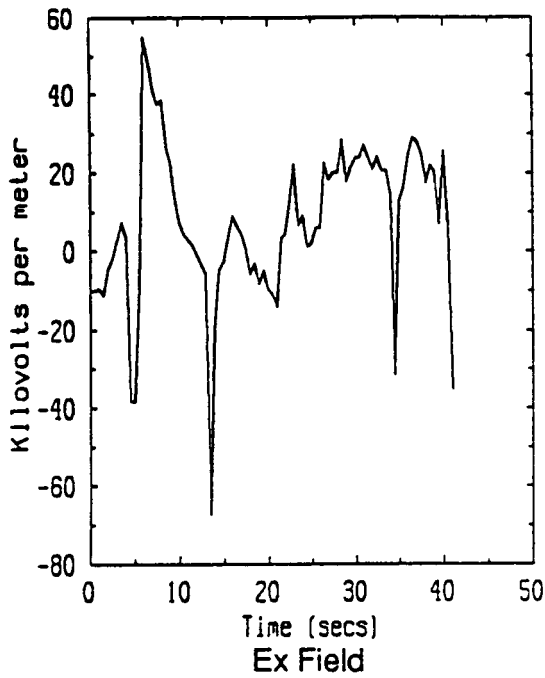


TRIGGER TIME = 20:13:15.2
Flight 85-26 CBW - FM

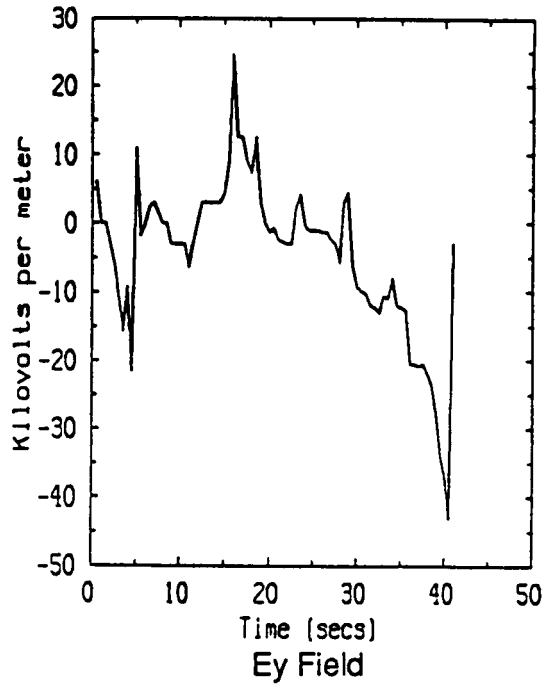


TRIGGER TIME = 20:13:15.2
Flight 85-26 CBW - FM

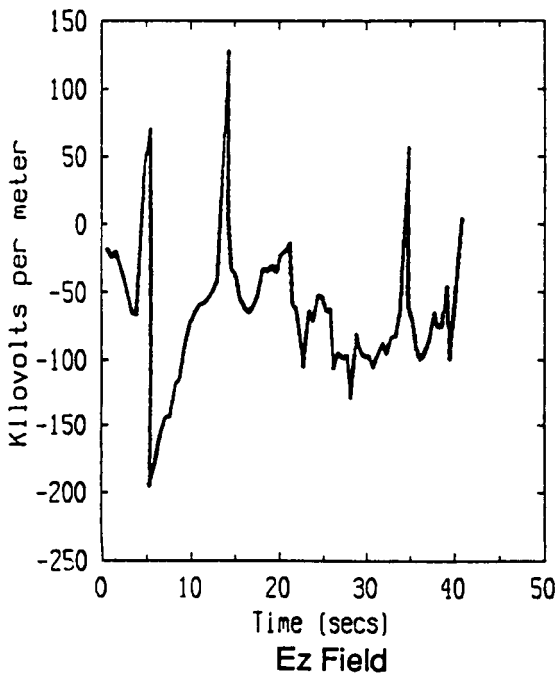
Figure 3.3a Calculated Ambient Fields Just Prior to the Strike for the Coarsely Modeled F106B (Strike Time Is at 48 Seconds)



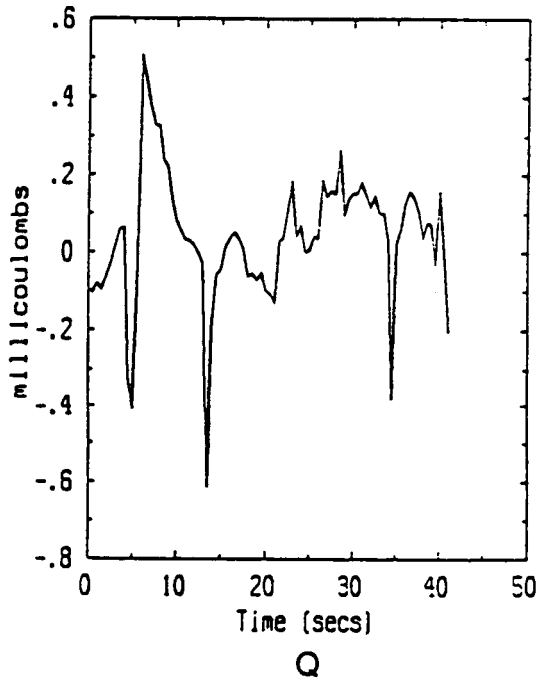
TRIGGER TIME = 19:51:21.8
Flight 85-26 CBW - FM



TRIGGER TIME = 19:51:21.8
Flight 85-26 CBW - FM

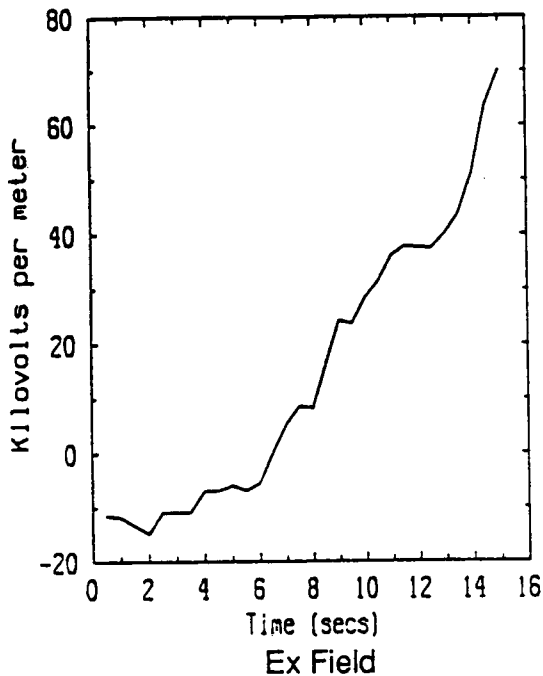


TRIGGER TIME = 19:51:21.8
Flight 85-26 CBW - FM

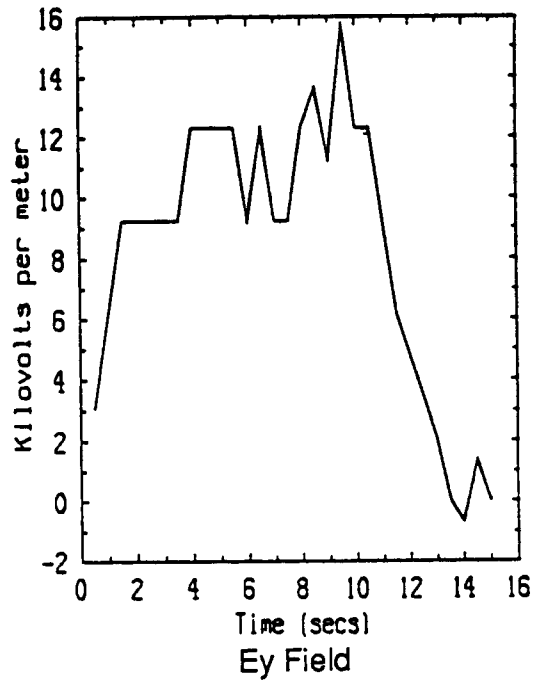


TRIGGER TIME = 19:51:21.8
Flight 85-26 CBW - FM

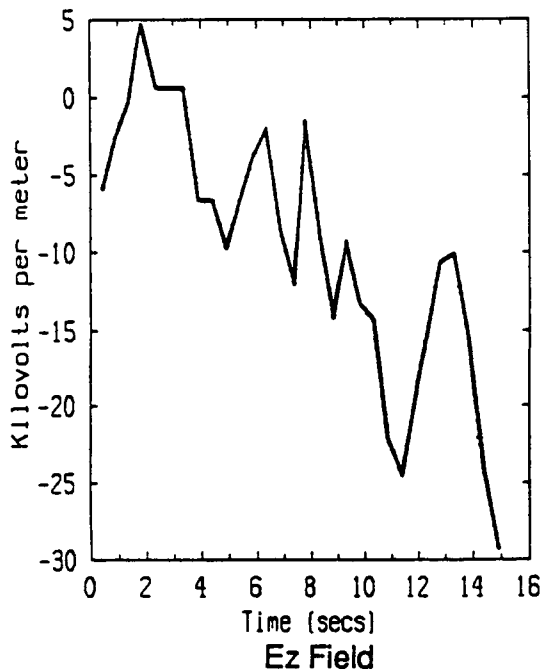
Figure 3.4a Calculated Ambient Fields Just Prior to the Strike for the Coarsely Modeled F106B (Strike Time Is at 40 Seconds)



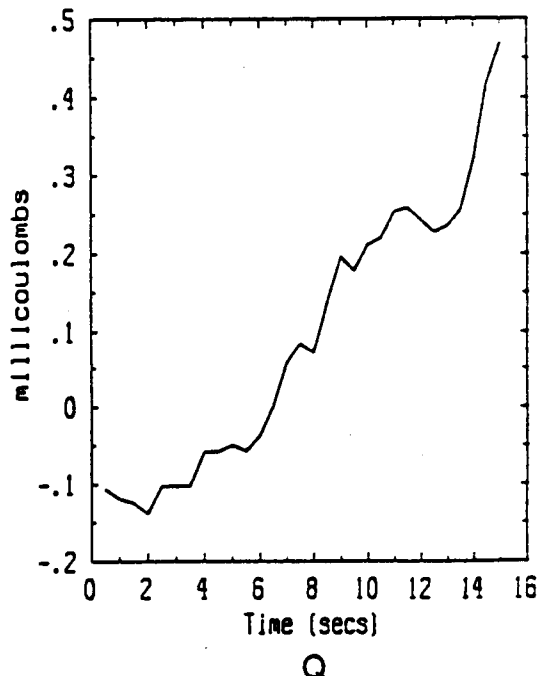
TRIGGER TIME = 18:32:45.9
Flight 85-28 CBW - FM



TRIGGER TIME = 18:32:45.9
Flight 85-28 CBW - FM

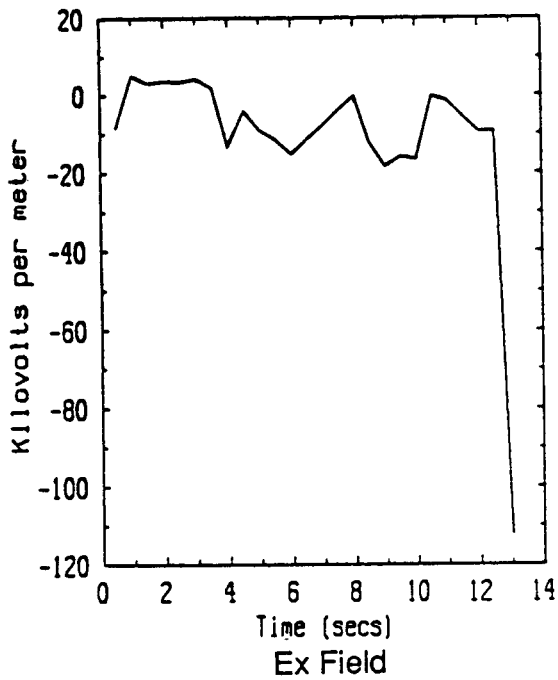


TRIGGER TIME = 18:32:45.9
Flight 85-28 CBW - FM

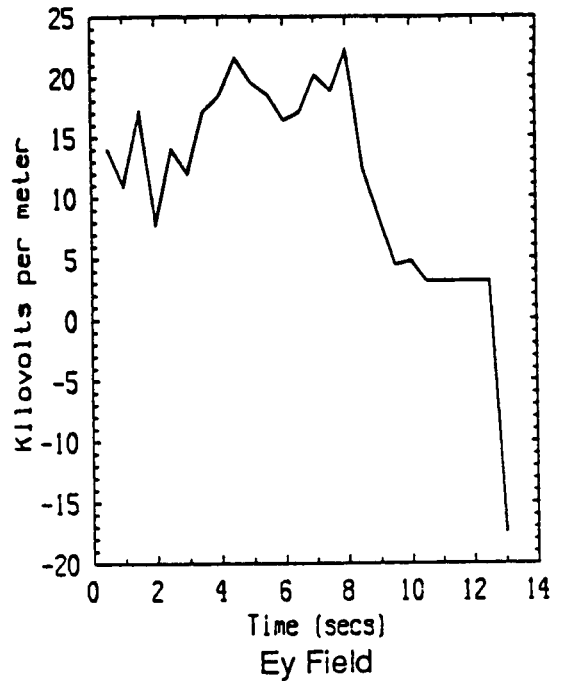


TRIGGER TIME = 18:32:45.9
Flight 85-28 CBW - FM

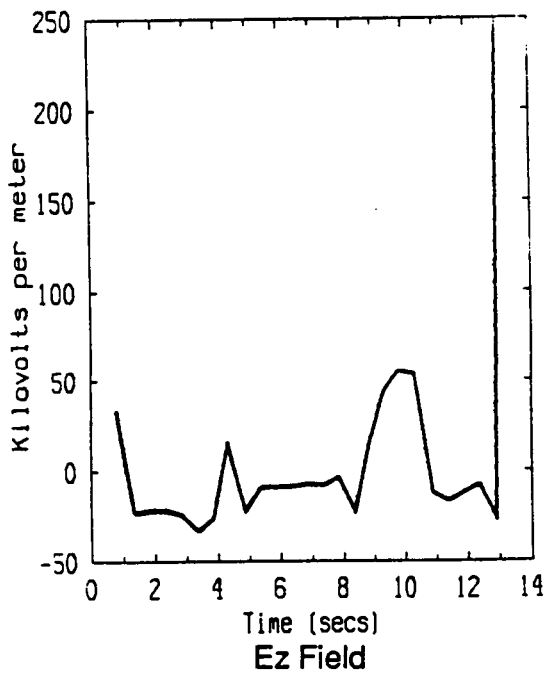
Figure 3.5a Calculated Ambient Fields Just Prior to the Strike for the Coarsely Modeled F106B (Strike Time Is at 15 Seconds)



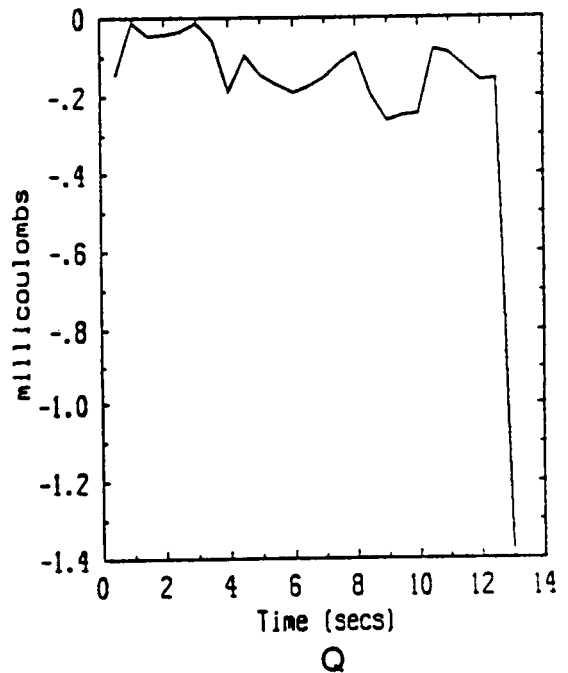
TRIGGER TIME = 17:04:44.2
Flight 85-29 CBW - FM



TRIGGER TIME = 17:04:44.2
Flight 85-29 CBW - FM

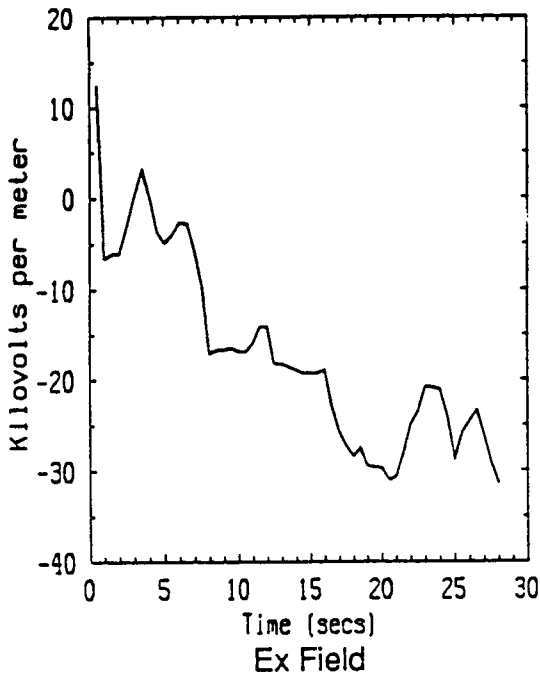


TRIGGER TIME = 17:04:44.2
Flight 85-29 CBW - FM

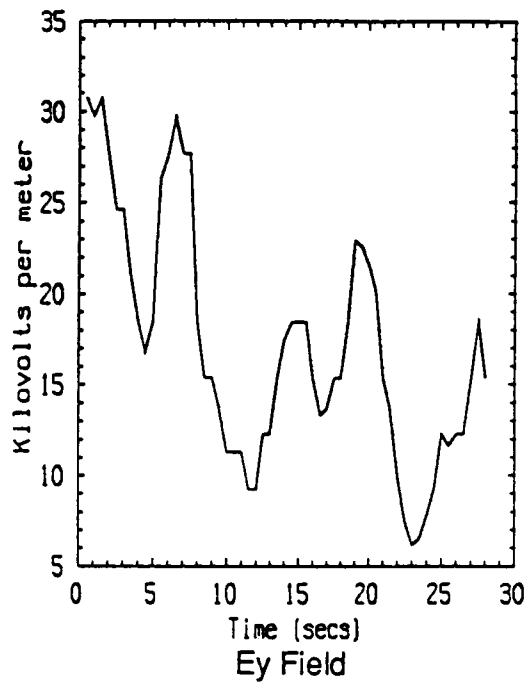


TRIGGER TIME = 17:04:44.2
Flight 85-29 CBW - FM

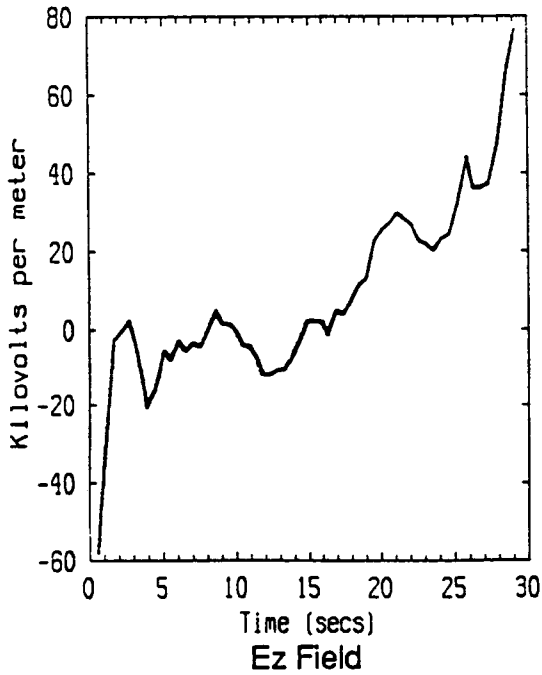
Figure 3.6a Calculated Ambient Fields Just Prior to the Strike for the Coarsely Modeled F106B (Strike Time Is at 13 Seconds)



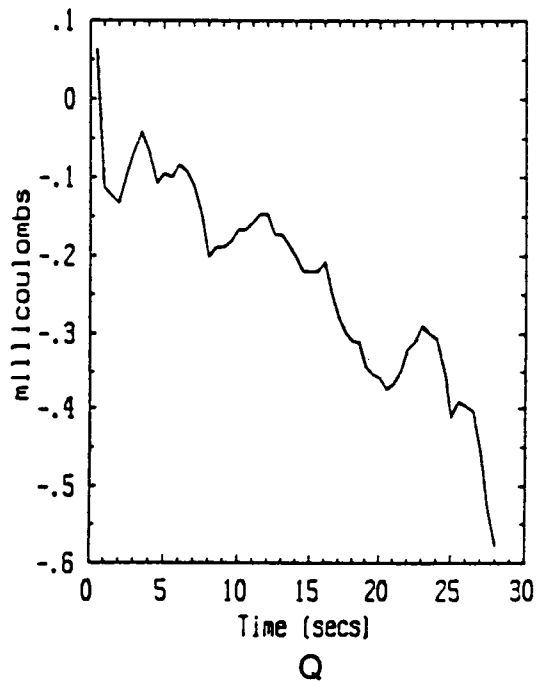
TRIGGER TIME = 16:54:22.9
Flight 85-29 CBW - FM



TRIGGER TIME = 16:54:22.9
Flight 85-29 CBW - FM



TRIGGER TIME = 16:54:22.9
Flight 85-29 CBW - FM



TRIGGER TIME = 16:54:22.9
Flight 85-29 CBW - FM

Figure 3.7a Calculated Ambient Fields Just Prior to the Strike for the Coarsely Modeled F106B (Strike Time Is at 28 Seconds)

components and net charge just before the strike occurred. The results of this analysis are shown in Tables 3.1, 3.2, and 3.3. Also shown is the total field calculated from the field components. The strike times shown in the tables should be considered approximate, in that they were read directly from the hard copy of the field mill observations. The electric fields are shown in kilovolts per meter and the net charge in microcoulombs.

TABLE 3.1
Derived Ambient Field Components for Strikes of Flight 85-026
(Finely Gridded Model)

Strike Time	E_x	E_y	E_z	E_t	Q
19:31:34.8	77.6	9.2	-69.9	104.8	566.8
19:51:21.8	-36.6	56.7	-12.0	68.5	-370.6
20:13:15.2	87.3	-30.8	-65.1	113.2	604.0
20:16:30.2	5.7	-17.1	-24.7	30.6	4.4

TABLE 3.2
Derived Ambient Field Components for Strikes of Flight 85-028
(Finely Gridded Model)

Strike Time	E_x	E_y	E_z	E_t	Q
18:32:45.9	70.1	0.0	-29.1	75.9	469.0

properly. The cause for this behavior is unknown but could be due to the presence of water, electrical corona, or some other unknown agency.

2) The field mill placement is such as to preclude accurate calibration

This was referred to earlier in the "coupling" between the waveforms of Ex and Q. This is caused by the placement of the field mills on the aircraft. The coupling occurs because the mills respond too strongly to certain components of the ambient field and charge (because of their location), and too weakly to other components.

3) The assumptions of the analysis are not satisfied

The assumption made in the analysis is that the ambient field is uniform over some volume which encloses the aircraft. If this is not satisfied the analysis technique cannot succeed, and the derived fields are in error by an unknown amount. Possible ways in which this may not be satisfied are in having charge centers too near the aircraft, or in having a natural lightning channel appear near the aircraft, triggering a branch to the (charged) channel.

CHAPTER 4

EXPERIMENTAL DETERMINATION OF F106B FORM FACTORS

4.1 Description of Electrolytic Tank Experiment

The electrolytic tank for the experimental determination of aircraft form factors was designed as an alternate method to the charge transfer technique used earlier [5]. In the earlier work it was felt that the introduction of probes into the enhanced electric field regions was disturbing the local field distribution and therefore producing inaccurate results. The electrolytic tank has the advantage of using non-intrusive probes, as will be described shortly. During the course of the experiment, several factors were discovered that created non-ideal conditions in the tank. These factors are described in Section 4.2. In this section the ideal experiment is described.

A schematic of the electrolytic tank is shown in Figure 4.1. Also shown is a nominal (spherical) test object. The tank is filled with a copper sulfate electrolyte solution, and has large (approximately 1 meter square) copper plates located on two sides. The plates are just slightly smaller than the dimensions of the tank itself and therefore nearly cover either side. They extend above the electrolyte solution by several inches, providing a convenient place for electrical connections. The plates are connected directly to a voltage source which provides the overall current for the electrolyte. The voltage source can be either direct or alternating; during this experiment an alternating 60 Hz voltage was usually used.

One of the plate electrodes is instrumented with a small circular (1/8" diameter) probe, which is actually a small electrically isolated region of the plate. This is done in order to measure the local current density on the plate. There were actually three such probes on the plate, but in general only one was monitored at a time. The current density on the plate is related to the local electric field at that location through the conductivity of the electrolyte, so the local electric field is known if the solution conductivity is known. For form factor determination, however, the conductivity need not be known, as the form factors are a ratio of current densities at the test object and the plate.

For an accurate determination of current density at the plate, care must be taken to ensure that the plate and the plate probe are at the same electrical potential.

This is the purpose of the voltmeter and variable resistor combination on the left of Figure 4.1. The resistor is adjusted until the voltmeter reads zero (within noise limits).

The test object is instrumented in much the same way as the plate electrode. The object is metalized with a small circular region electrically isolated. The circular region (probe) is located at the position where a form factor is desired. An ammeter is used to read the current flowing through the probe region on the test object. Once again, for an accurate determination of the proper current density at the probe, it is necessary to ensure that the probe and the test object are at the same electrical potential. The potential of the test object is fixed by its location between the plate electrodes. Because the probe is at a physically different location with respect to the electrical center of the rest of the test object, a variable resistor must be placed in series with the probe in order to equalize the potentials. The voltmeter again is used to adjust the resistor until the potentials are equal within noise limits.

When both voltmeters are zeroed to within noise tolerances (in practice the potential differences shown on the meters are minimized rather than zeroed), the currents are read from the two ammeters. If the electrolyte conductivity does not vary with location in the tank, and that the probes in the plate electrode and the test object are the same physical size, the form factor can be calculated as shown below.

$$\text{Form Factor} = \frac{E_n}{E_o} = \frac{J_{cn}/\sigma}{J_{co}/\sigma} \quad (4.1)$$

$$\text{Form Factor} = \frac{J_{cn}}{J_{co}} \quad (4.2)$$

In principle the form factor determined using this procedure should be independent of the electrolyte conductivity, the magnitude of the voltage applied to the plate electrodes, and the location of the test object within the tank. In addition, because the probes used to measure currents are in essence part of the surface itself, ideally no probe effects should be seen.

4.2.1 Possible Explanations for Anomalies

Three possible explanations for the observed anomalies have been developed. These are listed below with a brief discussion of each.

1) Electrolysis of Solution

It was observed that during the course of the experiment, bubbles appeared at the surface of the fluid near the driving plates and above the location of the probe in the plate. This was most easily seen when the plates were driven with the largest potentials. This is strong evidence that electrolysis of the fluid was occurring somewhere on the plate, almost certainly around the probe region. It was also observed that the probe current readings drifted during this time. Bubbles of gas forming on the probe and nearby region of the plate, causing significant local conductivity changes, can easily account for this drift. Further evidence of this is that scraping the plate with a wooden dowel caused an abrupt change in the probe current readings followed by a resumption of the drift.

2) Galvanic Effects

Many of the metalized models created for the tank experiment used copper probes embedded in a different metallic surface. For example, the spherical model was painted with a silver compound, as were the F106B scale models. Because the probes and the rest of the surface were of different materials, small galvanic (or battery) effects were expected. It was hoped that these effects would be small enough that derived enhancement factors would not be affected. Effects were observed by removing the driving potential from the plates. Ideally all potential differences would go to zero at that point. However, potential differences on the order of a hundred millivolts were observed between the probes and the surrounding metal regions. These potential differences slowly decayed on the scale of minutes. Because of other problems, these galvanic effects and their magnitude were not investigated in detail.

3) Coatings on Plates and Probes

In spite of efforts to use plates and fluid having similar metals (copper and copper sulfate), it was observed that coatings appeared on the copper plates. Visible

then the finite difference approximation to the problem of the finite cylinder in a uniform electric field.

The biggest problem with the above technique is that the solution depends on not one but two boundary conditions. The first is the condition that the electric field be zero within and on the surface of the conducting cylinder (i.e., that the cylinder be an equipotential surface). The other boundary condition is that used to truncate the cylindrical problem space. Ideally this boundary condition simulates free space beyond the problem space boundary. In practice, however, the condition is imperfect, and because of this it introduces error into the static solution. The magnitude of this error was in the past thought to be dependent on the cell size used in the code. That is, if one modeled the cylinder with smaller and smaller cells in a problem space that was physically the same size, it was thought that the error diminished, particularly at locations near the cylinder. It has since been found that the effect of the outer boundary condition is pervasive throughout the problem space, and in fact the errors in the solution were found to be significantly larger for a problem space in which the cell size was decreased by a factor of four.

Two numerical models of a 15" long by 1 5/8" diameter cylinder were constructed. One had a cell size of 1/4" and the other a cell size of 1/32". The problem space boundaries were placed roughly one-half cylinder length away in the r and z directions. Enhancement factors were found to be significantly larger for the 1/32" grid than for the 1/4" grid. Results for the two models are presented later in this section for comparison with the improved numerical solution.

4.3.2 Potential Technique

During the course of this task it was discovered that the finite difference technique for the determination of form factors on the finite conducting cylinder was inaccurate. Therefore a new technique was developed which does not suffer from the boundary condition deficiencies of the finite difference code. This technique makes use of the fact that one can model the conducting cylinder as a collection of surface patches (in this case cylindrical rings), each of which holds a uniform charge density. The modeled cylinder with sample surface patches is shown in Figure 4.2. The electric potential at any point due to a single one of these rings is easily calculated

as shown in Equation 4.3. It is assumed that there is no variation in the θ coordinate direction, as in the finite difference technique.

$$\Delta\phi = \int_0^{2\pi} \frac{\sigma r_s dr_s d\theta}{4\pi\epsilon_0 \sqrt{r_0^2 + r_s^2 - 2r_0 r_s \cos\theta + (z_s - z_0)^2}}, \text{ End caps of cylinder} \quad (4.3)$$

$$\Delta\phi = \int_0^{2\pi} \frac{\sigma r_s dz_s d\theta}{4\pi\epsilon_0 \sqrt{r_0^2 + r_s^2 - 2r_0 r_s \cos\theta + (z_s - z_0)^2}}, \text{ Side of cylinder}$$

Here r_s and z_s represent the location of the source charge, and r_0 and z_0 represent the location of the observation point. σ is the surface charge density of the patch. The integration over θ must be done even though the potential is not a function of θ .

The analog of the outer boundary condition of the finite difference code is that the potential at infinity of a ring must be zero. This is a much more rigorous condition than that used in the finite difference code.

Using this technique, enhancement factors on the cylinder are calculated in the following way. Because the cylinder is conducting, in the static limit it must represent an equipotential. The potential of any point on the cylinder is the sum of the potentials due to the charge densities on all of the patches plus that due to the ambient external field. Hence the potential of a patch is represented as a sum of terms involving all of the patch surface charge densities plus a constant term (depending on patch location, because of the uniform external electric field). The potential of each patch can be represented this way, and all of the potentials must be equal. This results in a matrix equation for the patch surface charge densities with the dimension of the matrix equal to the number of patches. The matrix equation in truncated form is shown below.

and therefore the enhancement factor theoretically approaches infinity, so very fine gridding is necessary to accurately determine the enhancement of points near the corner. However, if one is not interested in points near the corner (within .1"), as in the case of the experimental results, the numerical solution should be accurate to within the 1% mentioned above.

It should be emphasized that the potential technique as described above is applicable only to cylindrical geometries. However, the technique is easily generalized, and has in fact been applied to three dimensional cartesian geometries in a limited number of cases.

4.3.3 Comparison of Numerical and Experimental Results for Finite Cylinder

A comparison of the results obtained from the finite difference numerical technique, the potential technique, and the two experimental techniques is shown in Table 4.1.

TABLE 4.1
Comparison of Numerical and Experimental Results for Enhancement Factors on a Finite Length (15") Cylinder Oriented with Axis Along the Ambient Electric Field

Distance from End (Inches)	Finite Difference 1/32"	Difference 1/4"	Potential Technique	Charge Transfer Experiment	Electrolytic Tank
.25	12.8	8.2	7.6	7.1	---
.50	11.1	6.4	6.3	5.5	7.7 - 13.4
1.0	9.8	4.9	4.8	4.2	---
2.0	8.1	3.6	3.5	3.1	2.2 - 5.4
4.0	5.2	2.1	2.0	1.8	1.2 - 1.8
6.0	2.2	0.9	0.8	0.7	---

TABLE 4.2
Form Factors for Fixed Sphere with Varying Probe Diameter - Test
Sphere Diameter Is 3.3'

Probe Diameter	Measured Form Factor
.092"	2.68
.125"	2.68
.173"	2.64
.30"	2.63

TABLE 4.3
Form Factors for Varying Sphere Diameters but Fixed Probe (.125" dia.)

Sphere Diameter	Measured Form Factor
3.3"	2.68
2.0"	2.53
1.5"	2.44
1.2"	2.38

TABLE 4.4
Form Factors for Varying Cylinder Diameters but Fixed Probe (.125" dia.)
Long Cylinders Normal to Field

Cylinder Diameter	Measured Form Factor
3.1"	1.63
2.5"	1.59
1.6"	1.54
1.1"	1.45
.88"	1.40

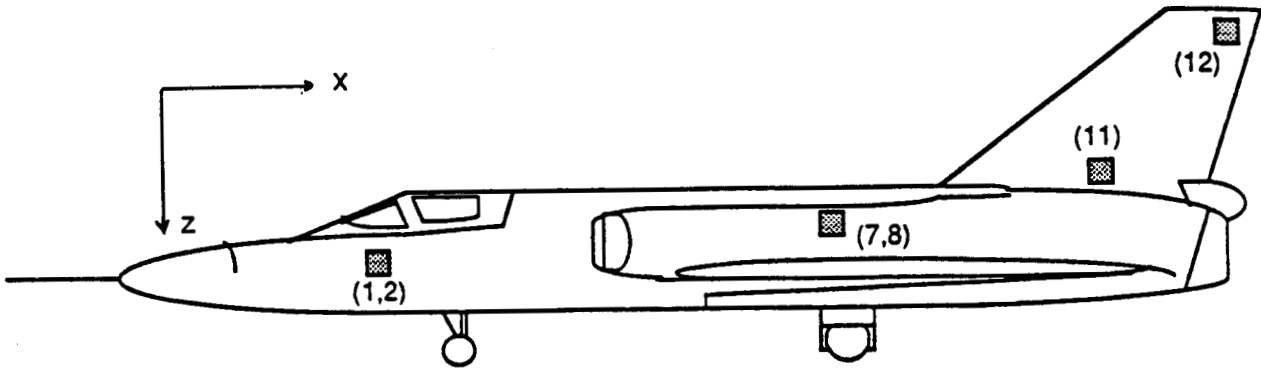


Figure 4.3 Side View of F106B Showing Test Point Locations

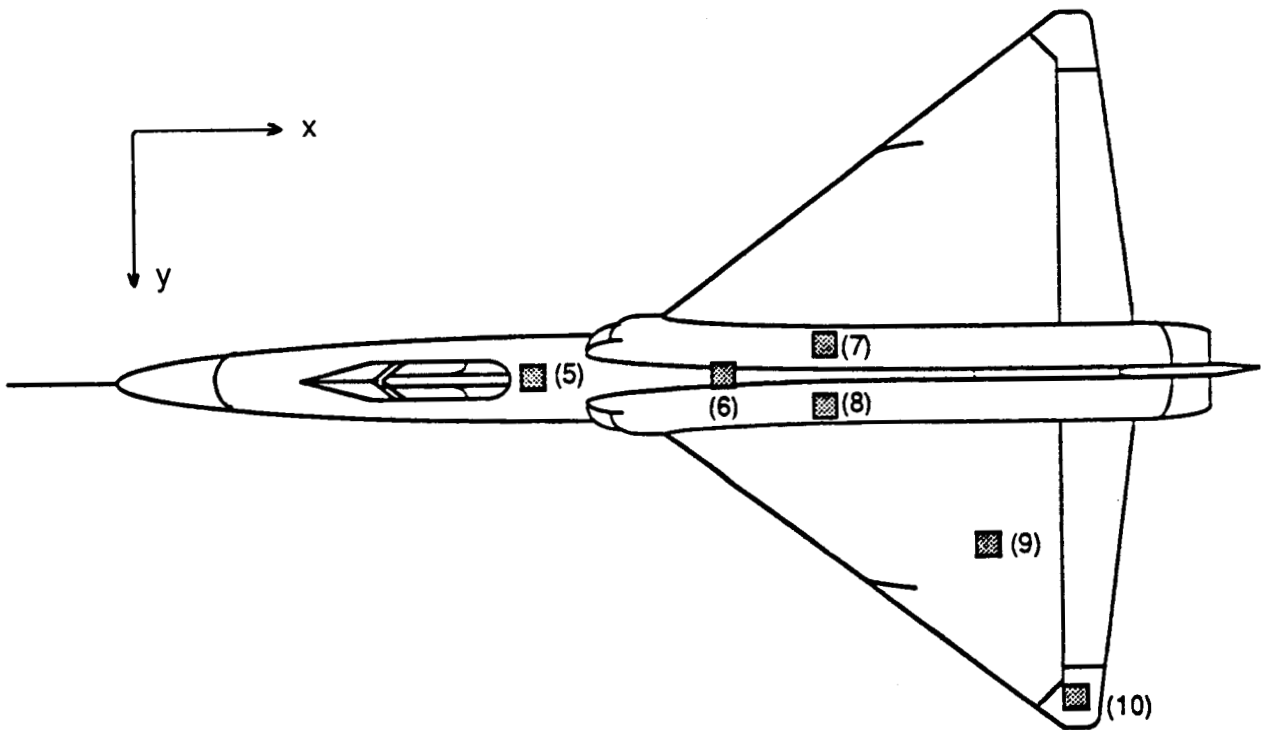


Figure 4.4 Top View of F106B Showing Test Point Locations

Huygens' surface. A potential technique solution for the F106B could be of much value in deciding this question.

In summary, although the electrolytic tank has not provided the ideal experimental platform for measuring form factors on scale models, it has driven a reexamination of numerical models for form factor calculation. This reexamination has led to a better numerical technique which showed that a previous experimental procedure (charge transfer technique) produced reliable results when applied to canonical shapes. These results are now felt to be better than can be reasonably achieved using the electrolytic tank. The new numerical technique has been used to calculate form factors on a finite length cylinder, and the results agree well with those found using the experimental charge transfer technique. Although not documented in this report, the numerical technique has also been applied to the canonical problem of a conducting sphere immersed in a uniform electric field. The results agreed to less than 1% with the known analytical result for all points on the sphere. A desirable further step in the use of this technique is to apply it to the F106B aircraft so comparisons can be made with results from the charge transfer experiment. Agreement there would increase confidence in the validity of both the numerical and experimental procedures.

CHAPTER 5

ANALYSIS OF THE 1987 CV580 IN-FLIGHT LIGHTNING DATA

5.1 Introduction

During a three year multiagency program (USAF, FAA, USN, and NASA) an instrumented Convair CV580 aircraft was flown from Cape Canaveral Air Force Station into central Florida thunderstorms at altitudes ranging from 2 to 18 kft in order to measure the electromagnetic environment during lightning attachments [10]. The aircraft was flown into the active thunderstorm regions during the 1984, 1985, and 1987 lightning seasons. Data from the 1984 and 1985 flights have been fairly extensively analyzed [10, 11] but the 1987 data have not yet been analyzed.

The purpose of this section is to present the first results of an analysis of the 1987 analog data. The review focuses on the most active records of the analog data which were the J_{nff} records and the current sensor records. Also, analog data have limited time resolution, about 30 microseconds, and so the primary features of the data that can be sensibly discussed are gross structure like initial field time dependence, multiple surge rates, and continuing current size.

The 1987 analog data included responses from an array of sensors. Figure 5.1 gives a schematic diagram of the aircraft and the location of the sensors whose data are analyzed here. The current sensors were mounted on booms that were approximately three feet in length.

Particularly active records were obtained from the forward upper fuselage sensor (J_{nff}). The data from this sensor were integrated by a passive integrator having a time constant of about 0.4 sec, and were DC coupled to a magnetic tape recorder.

Other active records were obtained from current sensors on the right (I_{rw}) and left (I_{lw}) wings, and on the vertical stabilizer (I_{vs}). The responses from these sensors were DC coupled to the tape recorder.

During the 1987 season, seven lightning flashes produced field and current records. Table 5.1 gives a summary of information about the seven flashes. The first flash, 16 July, occurred at 18 kft and all the other flashes occurred at 14 kft. Julian dates and times are listed in the "Notation" column. Note that for Flash 1, the Julian date is apparently wrong but, because it was supplied with the original data, is included unaltered for ease of data identification.

The results of the analysis will be presented in two parts. First, there will be a discussion of some general properties of the 1987 data including the character of the initial J_{nff} changes, multiple surge rates, and sizes of continuing currents. Second, there will be a detailed review of the seven flashes. The initial J_{nff} time dependence, the multiple surge character, probable attachment points and the sizes of currents will be subjects of each detailed review.

5.1.1 Terminology

Several terms in this discussion will be used with specific meanings and where possible the terms are consistent with SAE usage. 'Flash' will refer to the entire set of responses measured as the lightning occurs near, or is connected to, the aircraft. There were seven flashes in the 1987 data and they typically lasted 0.1 sec to 1.0 sec. The term 'record' will be used to describe the time response of a sensor for a given flash. 'Surge' will refer to a well defined pulse in a current sensor record. Typically, surges last less than 1-2 msec, and have shapes which are first monotonically increasing and then monotonically decreasing.

Certain responses in the current sensors show a multiple closely spaced sequence of surges sometimes with a continuing current. This will be referred to as a 'strike'. In SAE terminology a lightning strike is an attachment to the aircraft. Here 'strike' means an attachment and refers to currents or fields (perhaps many surges) that are associated with a particular breakdown and flow of current in some relatively short time period (often 10-20 msec). The term 'transition' will be used to describe changes in the J_{nff} fields. Typically there are fast and slow J_{nff} transitions in the J_{nff} records. Often, fast J_{nff} transitions occur simultaneously with surges in the current records. 'Group' will be used to describe a set of surges, a set of transitions, and/or occasionally several strikes together. Groups are typically 50-200 msec long

and the 1987 data have flashes with as few as one group and with as many as five. The groups are identified by the relatively quiet periods in J_{nff} between the groups and by common characteristics of the surges. In addition to groups, there are sets of surges closely spaced within a group which we denote subgroups.

In describing the sensor time records, 0 msec time will be defined starting at the first significant J_{nff} change. The starting time is marked in the records with a vertical line.

5.2 General Comments

The basic result of our analysis is that the 1987 data are similar to the 1984 and 1985 data and show no characteristics that are contradictory to the results obtained before [10]. The 1987 data taken together have several interesting trends, so before discussing the individual flashes, a summary of the trends will be given. Observations on the initial responses, the multiple surge rates, and the current sizes are included.

5.2.1 Initial Responses

Rustan et al. [10] have identified three general shapes for initial time dependences in the J_{nff} records. They denote the shapes by categories 1, 2, and 3 and explain them as a triggered flash, negative leader interception, and positive leader interception, respectively.

In the 1987 data, inspection of expanded data records shows that five of the seven flashes (1, 3, 4, 5, and 7) have category 1 initial J_{nff} changes. The category 1 changes consist of three steps: the first is a relatively slow increase in the field on a time scale of several milliseconds, the second is an abrupt decrease in the field in less than a millisecond, and the third is a subsequent rise in the field at a rate comparable to the first step. This sequence of field changes can be explained by a triggered strike.

Expanded data records of the remaining two of the seven flashes (2 and 6) show an initial J_{nff} change that starts with a very abrupt increase in the field, and in one case (event 2) there is a subsequent abrupt decrease in the field. Flash 2 appears to be a case of the aircraft in a branch of the main channel. In this case (flash

TABLE 5.2
Summary of the Multiple Surge Data for the 1987 CV580 Flights

Flash	Group A	Group B		Group C	Group D
1 surges s/sec * msec/s**	10 3300 0.33	4 800 1.25		7 10 10	None None None
2 none					
3 surges s/sec * msec/s**	12 13,000 0.074	7, 9 280, 209 3.5, 4.8		6 333 3.3	4 250 2.5
4 surges s/sec * msec/s**	None None None	14, 15, 7 280, 350, 210 3.5, 2.9, 4.8		4 240 4.1	9
5 surges s/sec * msec/s**	None None None	11 62 16		23, 12 135, 92 7.4, 10.8	5 30 33
6 surges s/sec * msec/s**	None None None	4, 5, 5 160, 167, 312 6.3, 6, 3.2		None None	None
7 surges s/sec * msec/s**	None None None	12 126 7.9		20 210 4.8	
AVERAGES					
Average number	10	9.5		8.4	
Av rate (s/sec)	5454	291		166	182
Av period (msec/s)	8.2	4.8		8.8	

* s/sec = surges per second

** msec/s = milliseconds per surge

Note: Grand Average Number Per Group = 9.1 surges/group

5.3 Flash 1, 16 July 1987

The data for this event are shown in Figure 5.2 and the major responses are in J_{nff} , I_{rw} , and I_{lw} . There are no significant other responses in the data records.

The initial behavior of J_{nff} is like Rustan et al.'s category 1 which shows that this flash is triggered, i.e., the leaders propagate out from the aircraft. This initial J_{nff} shape is also observed in flashes 3, 4, 5, and 7 of the 1987 data and is the most common shape in the old 1984 and 1985 data as well as the newer 1987 data.

There are three groups in this data and a summary of the surge rates and periods between surges is given in Table 5.3. In some cases the rates and periods are calculated from expanded time scale records of the data in Figure 5.2. The surges in the earlier groups are more closely spaced than for the later groups, and this is generally true in all the data.

The left wing current shows that this wing is a significant attachment point for this flash. The timing of the currents in the right and left wings is similar but there are unequal currents in these sensors. The measured I_{LW} current probably represents the total current into the aircraft, and there is a small branch of the exit channel attached to the right wing.

The current record for the left wing includes two continuing currents. The first transfers about 10.3 C of charge and the second about 32.2 C. Table 5.3 gives a summary of the 1987 continuing current properties. These continuing currents show that the channels for this flash were in contact with substantial charge centers in the surrounding cloud.

5.4 Flash 2, 30 July 1987

The data for this flash are shown in Figure 5.3. As in flash 1, the important responses are in the J_{nff} , I_{rw} and I_{lw} records. However this flash is substantially different than most of the other 1987 flashes because the process involved a branch attachment.

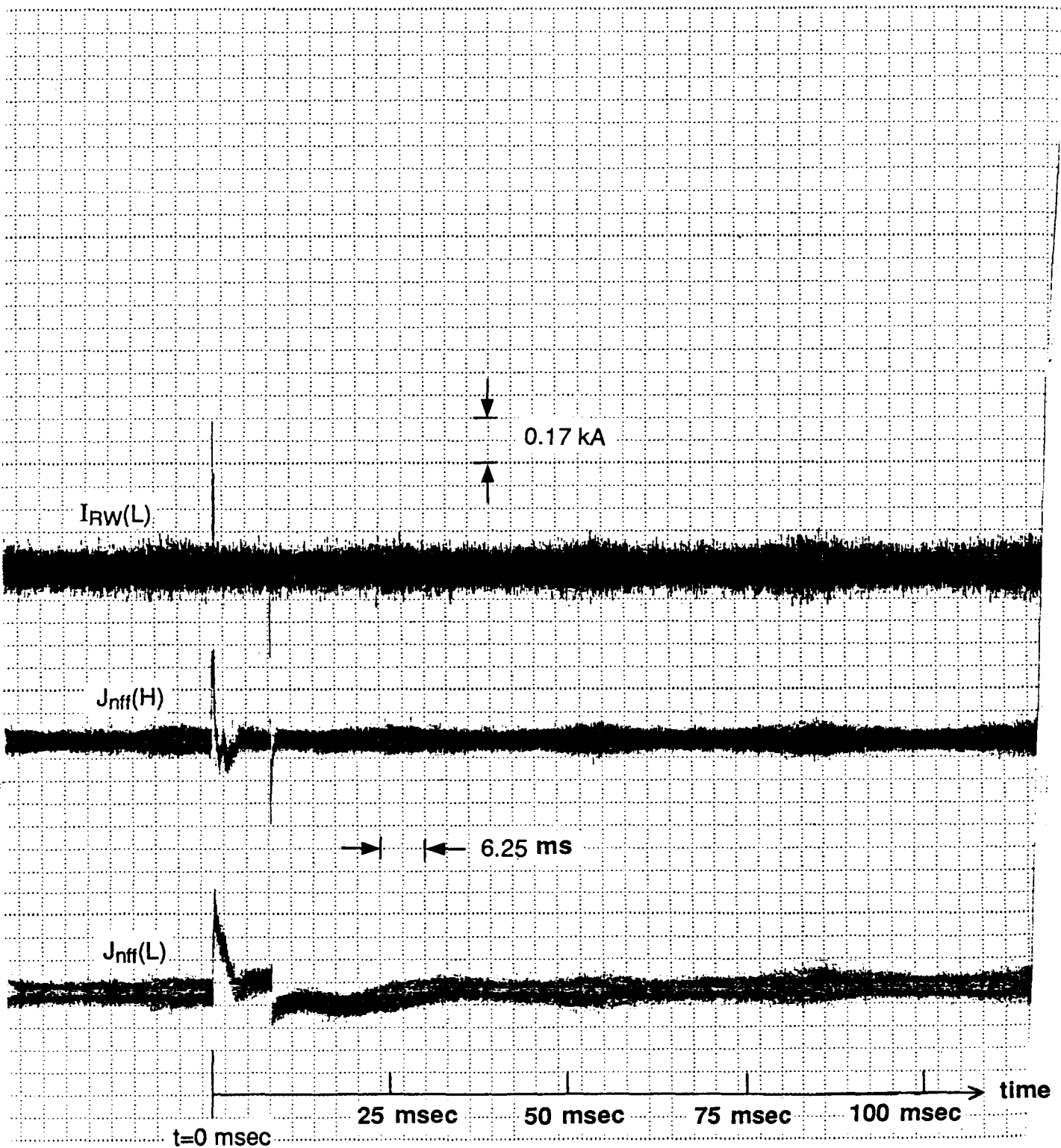


Figure 5.3 E-Field and Current Sensor Records from Flash 2, 30 July 1987

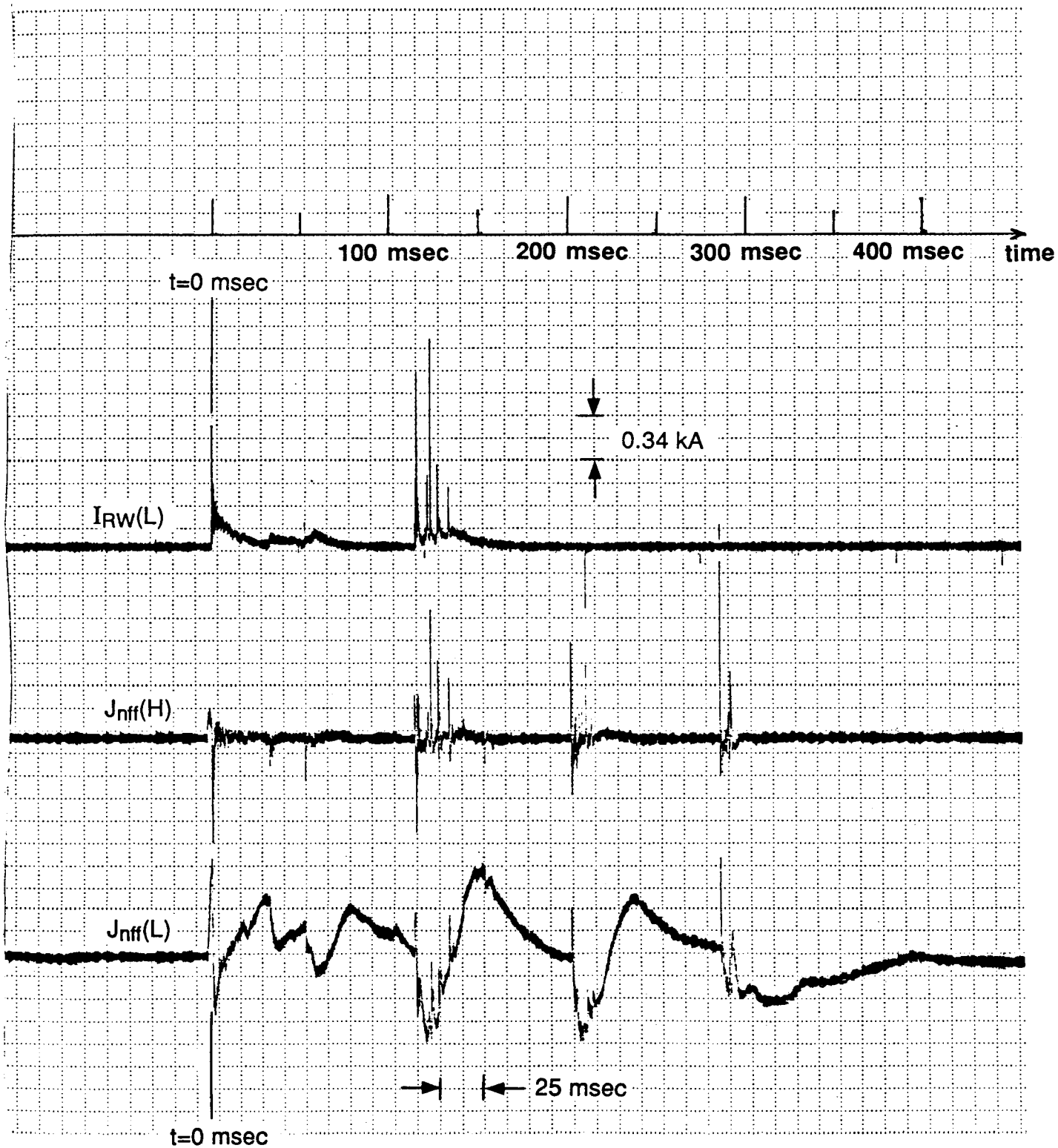


Figure 5.4 E-Field and Current Sensor Records from Flash 3, 31 July 1987

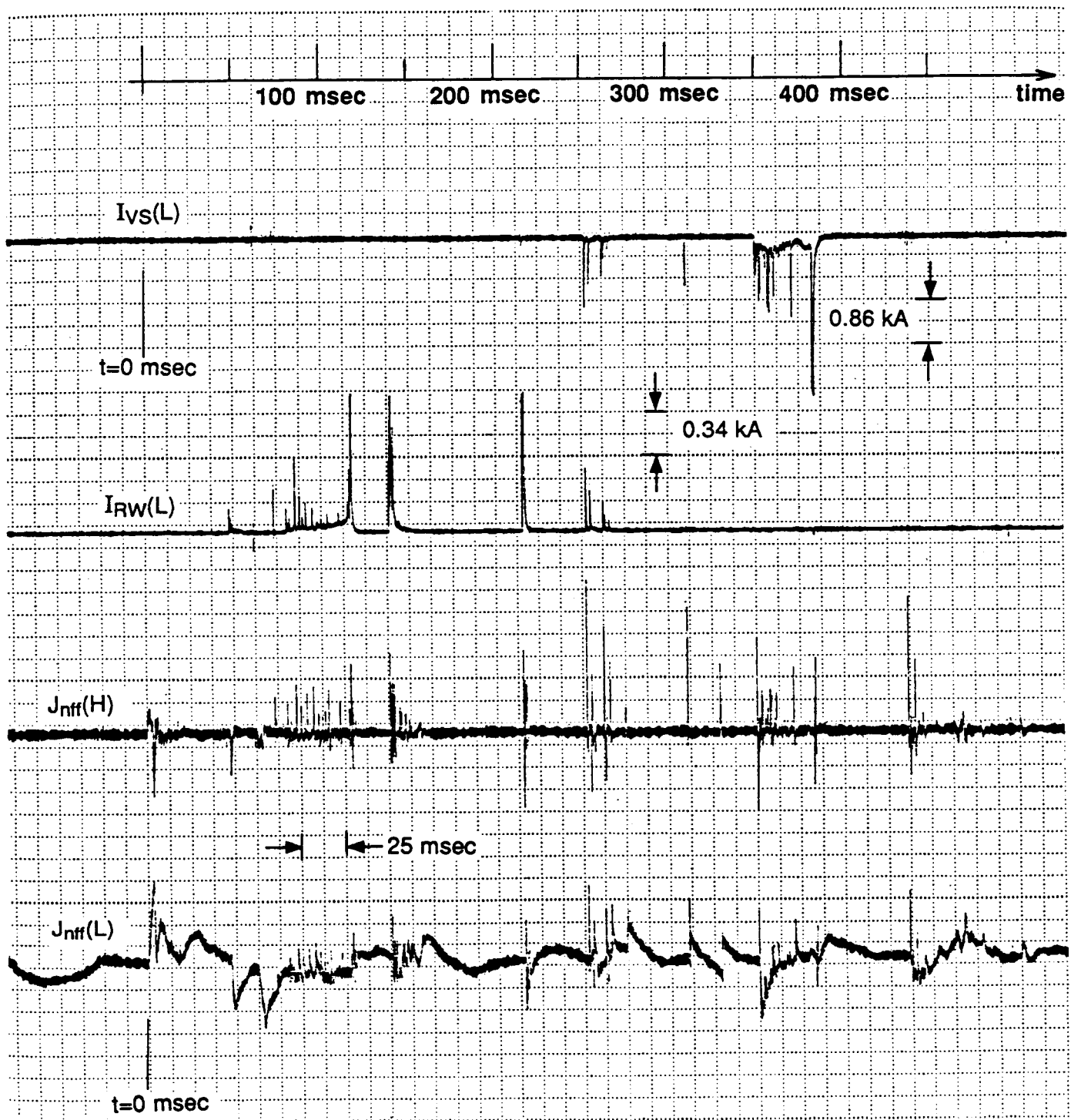


Figure 5.5 E-Field and Current Sensor Records from Flash 4, 4 August 1987

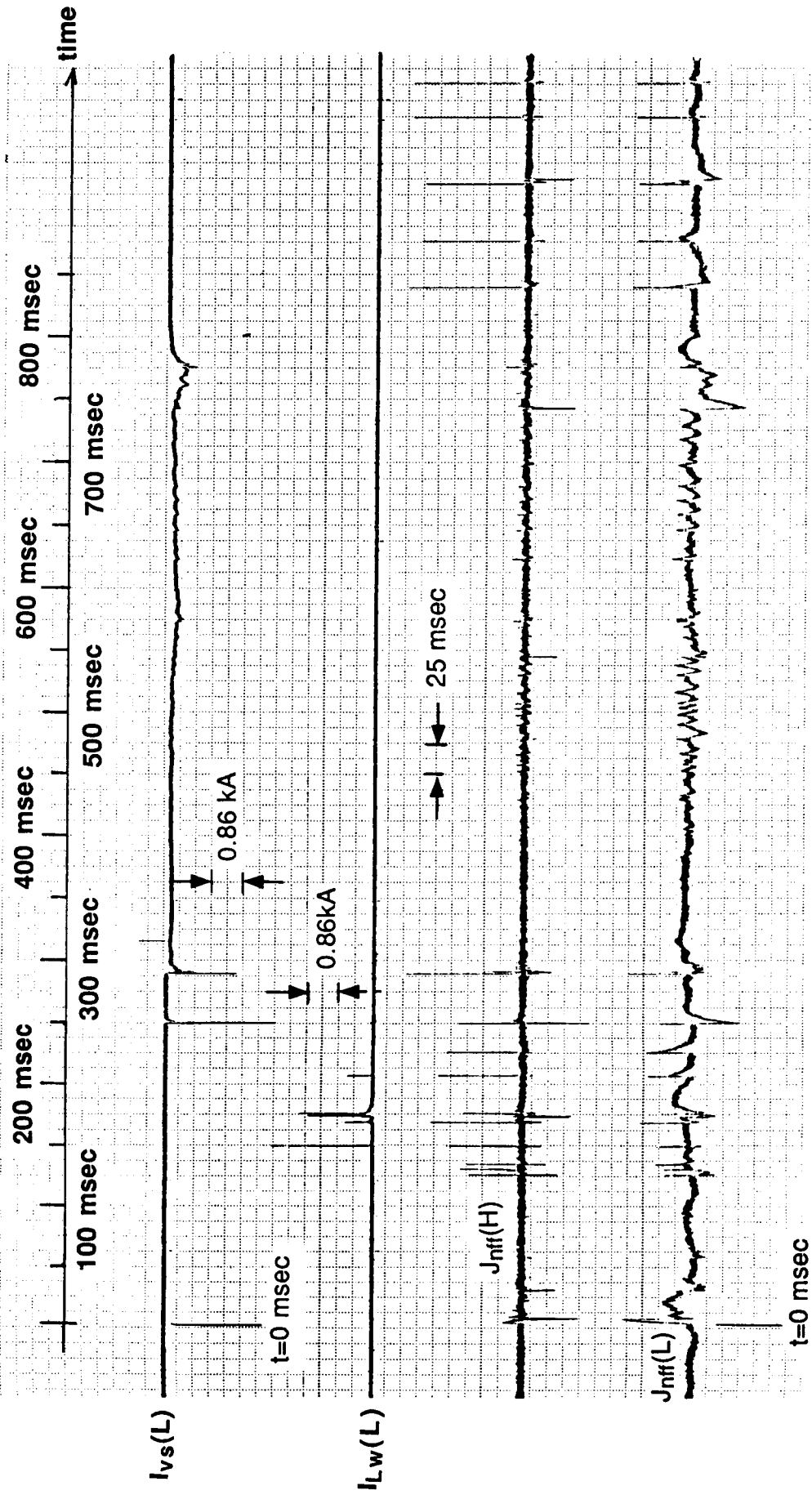


Figure 5.6 E-Field and Current Sensor Records from Flash 5, 4 August 1987

flashes 1, 3, 4, 5, and 7. At 200 msec, the channel connected to the aircraft is neutralizing charges from centers in the neighboring cloud. This is unlike the channel in flash 2 which did not neutralize any substantial charge centers.

The pair of currents in the right wing and vertical stabilizer at 200 msec are about the same size and have the same fine structure. These two currents are probably the only two occurring to the aircraft at the time 200 msec. There are no continuing currents during this time.

5.9 Flash 7, 11 August 1987

The data for this flash are shown in Figure 5.8. The most activity appears in the J_{nff} sensor. There are a few responses in the right wing and vertical stabilizer sensors, but these responses are small in magnitude (~200A) and are very fast in duration compared to the currents seen in other events. They do not appear to be channels carrying currents from charge centers in the cloud.

The initial J_{nff} change in this flash is similar to flashes 1, 3, 4, and 5, and is category 1 in Rustan et al.'s nomenclature. The flash is a triggered strike.

There are four groups in this flash with the first three (up to 300 msec) having the most activity. There are few surges in the current sensors and so the attachment points are not to the instrumented sensors and not identifiable.

5.10 Summary of Conclusions.

The main conclusion is that the principal responses in the 1987 analog data are in agreement with the 1984 and 1985 data. Secondary conclusions are:

1. Multiple Surge Testing: The average number of surges (or transitions) in a group is 9.1, and the average number of groups per flash is 3.4. The SAE specification [12] is 24 bursts/flash and 20 surges/burst. Thus, the SAE specification envelops the data presented here.

2. Triggering: Most, if not all, 1987 flashes are triggered.
3. Surge Size: The largest surge seen in the 1987 data was 3.0 kA. This is smaller than the largest surge (22.5 kA) in the 1984 and 1985 data.
4. Continuing Currents: The largest charge transferred in the 1987 data was 34 C. This is a little smaller than the largest charge transferred (> 100 C) in the 1984 and 1985 data.

CHAPTER 6

SUMMARY AND CONCLUSIONS

The research reported here has concentrated mostly on direct interpretation of measured in-flight lightning data and the determination of aircraft form factors with application to measured field mill data. Specifically the subjects covered include:

1) Interpretation of Digitized 1985 In-flight Data from F106B

Analysis of the 1985 data was performed using both the linear triggered lightning model described in previous reports and statistical analysis. The linear model was used to determine lightning attach points and current waveforms. More flexibility was allowed in attach points than in previous efforts. Left wing, right wing, and tail attachments were investigated in addition to nose attachments. Also it was found to be necessary to assume exit channels in a limited number of cases. This was necessary to avoid drifts in the calculated data, corresponding to net charging of the aircraft, which did not appear in the measured data. A relatively small percentage of attachments were found to require either non-nose attachment locations or exit channels. The statistical analysis was performed to identify trends and correlations in the data. The results of this portion of the analysis were very similar to what was found in previous years in that, under suitable restrictions, the peak values of current time derivatives can be related to the peak values of the time derivatives of the magnetic and electric field flux densities. Measured data from the 1986 thunderstorm season was also considered under this effort, but because of the small quantity of high resolution transient data recorded, no in-depth analysis was performed.

2) Field Mill Analysis

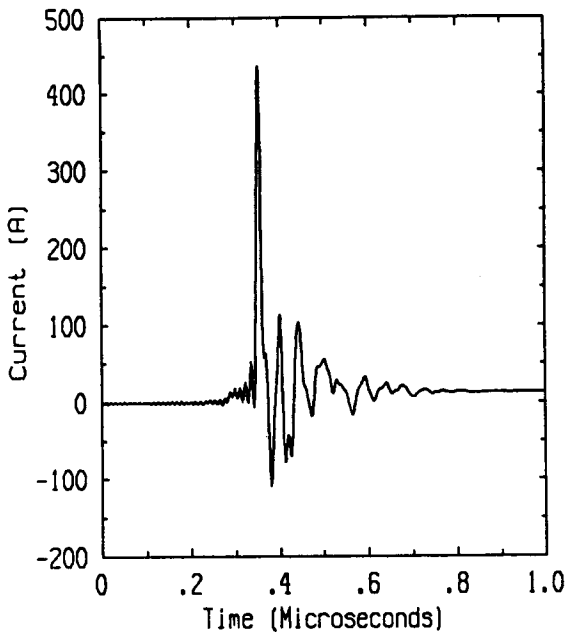
This effort concentrated on an improved numerical calculation of the form factors of the F106B using a more finely gridded model of the aircraft. The standard F106B finite difference model used for a majority of past analyses has a spatial resolution of one meter along the direction of the fuselage axis and one-half meter in the other two cartesian directions. The model used for the form factor analysis of this report has a spatial resolution of one-quarter meter in all three coordinate directions. The form factors calculated from the fine resolution model differed in a marginal sense from those calculated with the coarser model. The new form factors were used to redo

and properties inherent in the data. This included the statistics of multiple current bursts and continuing currents as well as physical interpretation of channel attachments and propagation directions. The observed statistical behavior was also found to be enveloped by the SAE recommendation for a multiple burst in-flight environment.

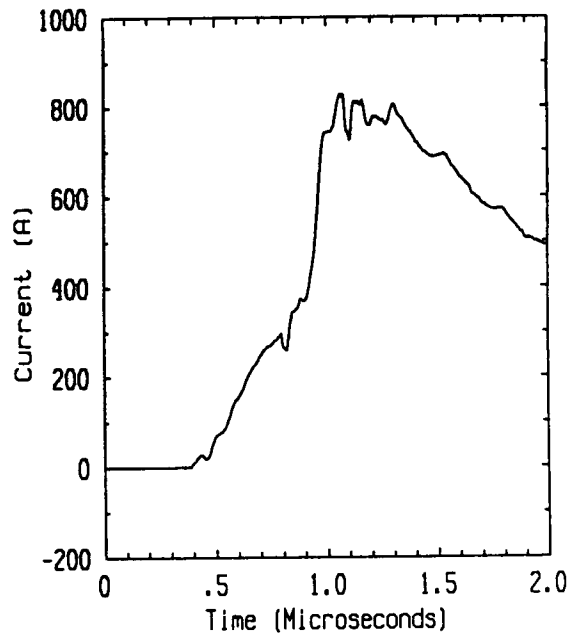
REFERENCES

1. Rudolph T., and R.A. Perala, "Interpretation Methodology and Analysis of In-Flight Lightning Data," NASA CR-3590, October 1982.
2. Rudolph, T.H., and R.A. Perala, "Linear and Nonlinear Interpretation of the Direct Strike Lightning Response of the NASA F106B Thunderstorm Research Aircraft," NASA CR-3746, March 1983.
3. Rudolph, T.H., R.A. Perala, P.M. McKenna, and S.L. Parker, "Investigations Into the Triggered Lightning Response of the F106B Thunderstorm Research Aircraft," NASA CR-3902, June 1985.
4. Rudolph, T.H., R.A. Perala, C.C. Easterbrook, and S.L. Parker, "Development and Application of Linear and Nonlinear Methods for the Interpretation of Lightning Strikes to In-Flight Aircraft," NASA CR-3974, September 1986.
5. Rudolph T., C.C. Easterbrook, P.H. Ng, R.W. Haupt, and R.A. Perala, "Experimental and Analytic Studies of the Triggered Lightning Environment of the F106B," NASA CR-4104, December 1987.
6. Ng, P.H., R.A. Dalke, J. Horembala, T. Rudolph, and R.A. Perala, "Application of Triggered Lightning Numerical Models to the F106B and Extension to Other Aircraft," NASA CR-4207, December 1988.
7. Zaepfel, K.P., and H.K. Carney, "1985 and 1986 Direct Strike Lightning Data," NASA TM-100533, March 1988.
8. Mazur, V., L.H. Ruhnke, and T. Rudolph, "Effect of E-Field Mill Location on Accuracy of Electric Field Measurements with Instrumented Airplane," Journal of Geophysical Research 92, No. D10, October 20, 1987, pp. 12,013-12,019.
9. Merewether, D.E., and R. Fisher, "Finite Difference Solution of Maxwell's Equations for EMP Applications," Defense Nuclear Agency 5301F (Contract No. DNA001-78-C-0231,) Electro Magnetic Applications, Inc., April 1980.
10. Burket, H.D., L.C. Walko, J. Reazer, and A. Serrano, "In-Flight Lightning Characterization Program on a CV-580 Aircraft: Final Report," AFWAL-TR-88-3024, Air Force Wright Aeronautical Laboratory, June 1988.
11. Rustan, P.L., B.P. Kuhlman, H.D. Burket, J. Reazer, and A. Serrano, "Low Altitude Lightning Attachment to an Aircraft," AFWAL-TR-86-3009, May 1987.
12. "Protection of Aircraft Electrical/Electronic Systems Against the Indirect Effects of Lightning," Draft Advisory Circular, Report of SAE Committee AE4L, AE4L-87-3, 4 February 1987.
13. Hartill, E.R., J.G. McQueen, and P.N. Robson, "A Deep Electrolytic Tank for the Solution of 2- and 3-Dimensional Field Problems in Engineering," Proceedings I.E.E., Paper, No. 2179M, October 1956.

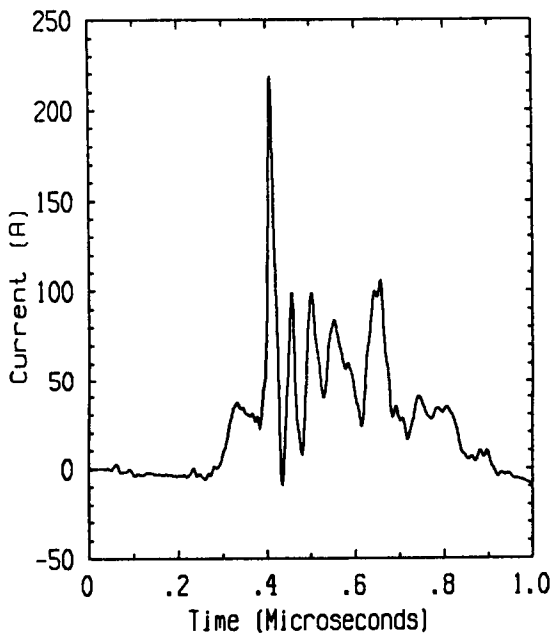
APPENDIX A
CALCULATED CURRENT SOURCES



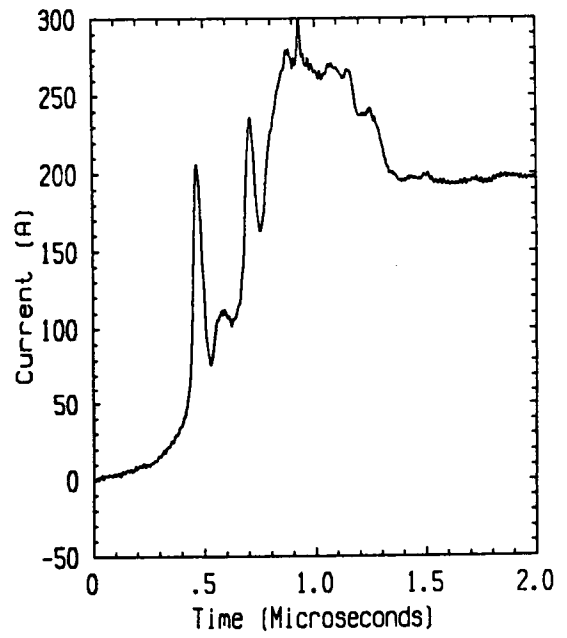
Flight 85.023 Run 005 Strike 002



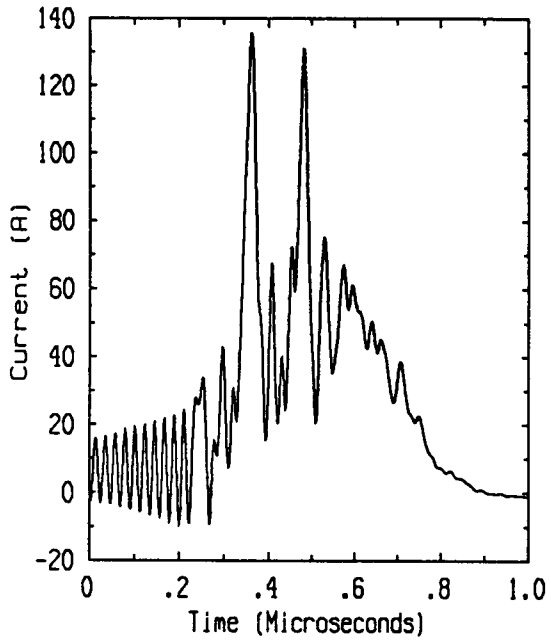
Flight 85.026 Run 002 Strike 002



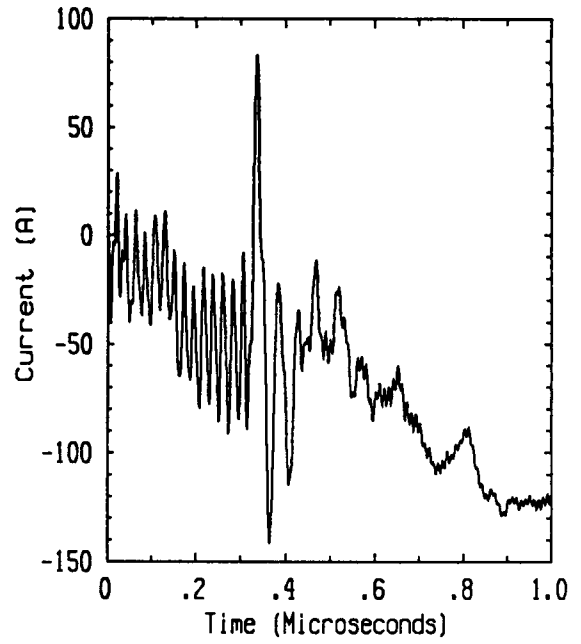
Flight 85.027 Run 001 Strike 001



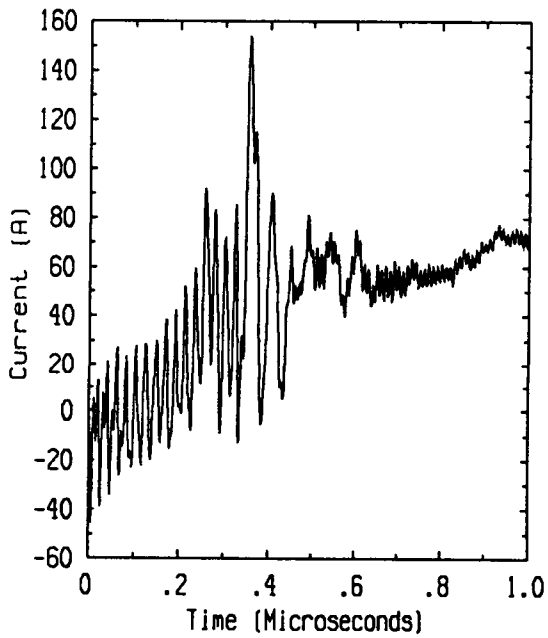
Flight 85.027 Run 002 Strike 002



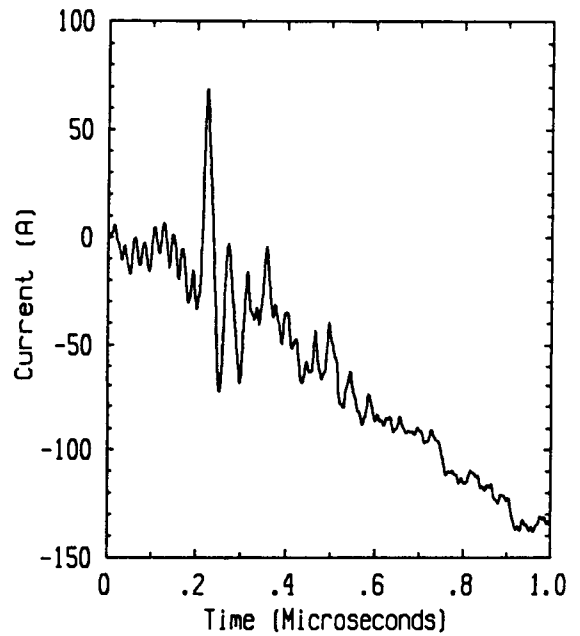
Flight 85.032 Run 002 Strike 002



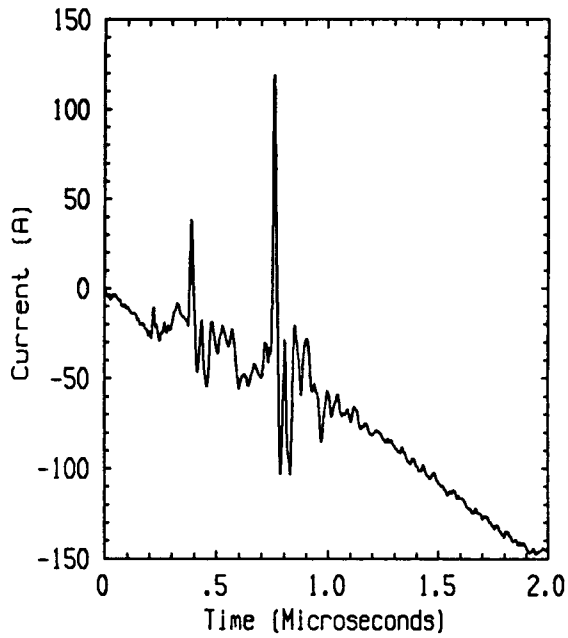
Flight 85.032 Run 003 Strike 003



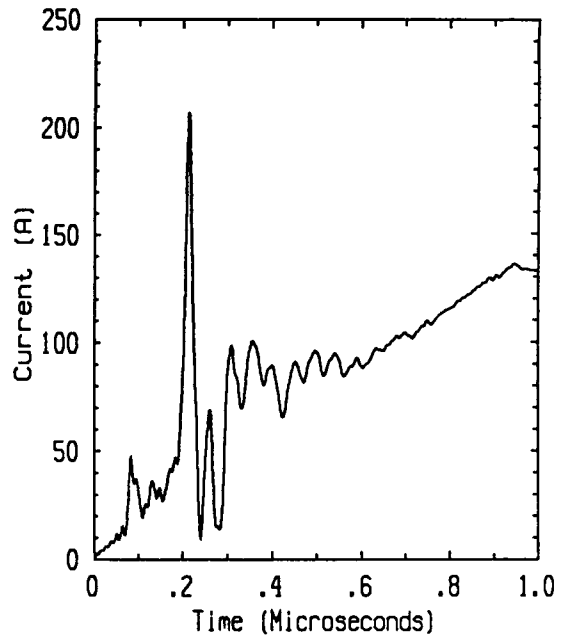
Flight 85.032 Run 004 Strike 004



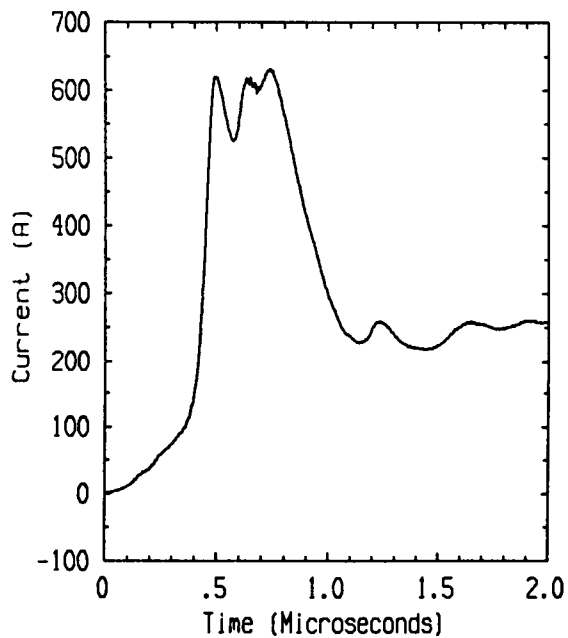
Flight 85.032 Run 005 Strike 005



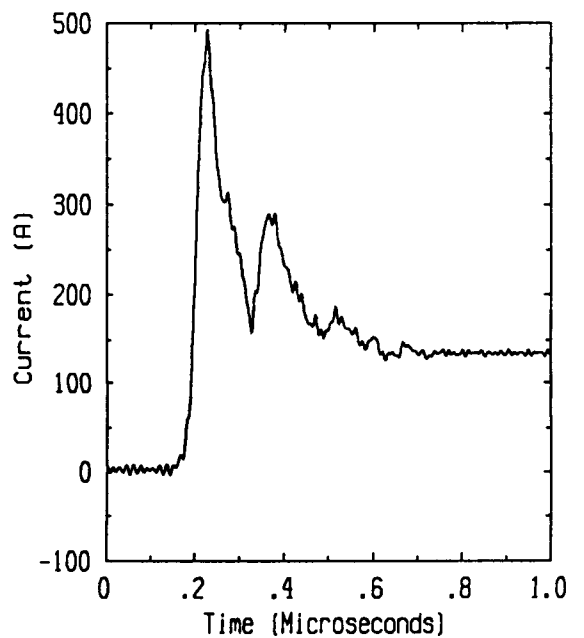
Flight 85.035 Run 002 Strike 002



Flight 85.035 Run 003 Strike 003



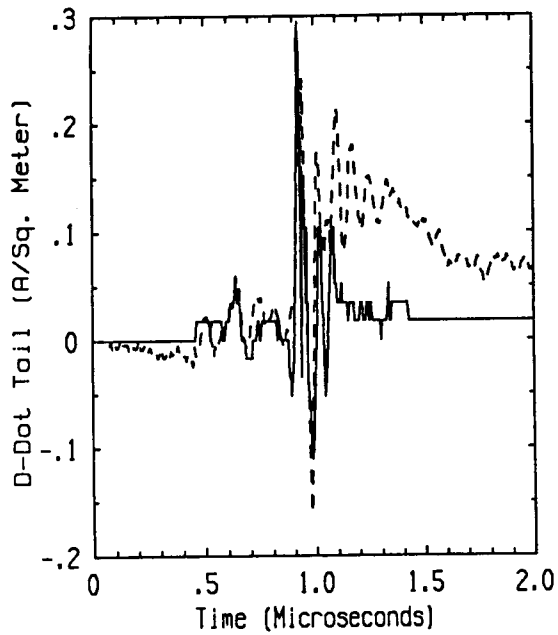
Flight 85.035 Run 004 Strike 004



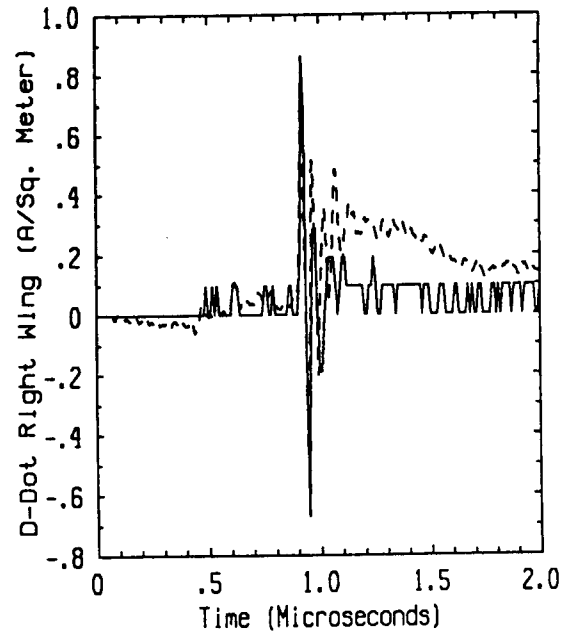
Flight 85.035 Run 005 Strike 005

APPENDIX B

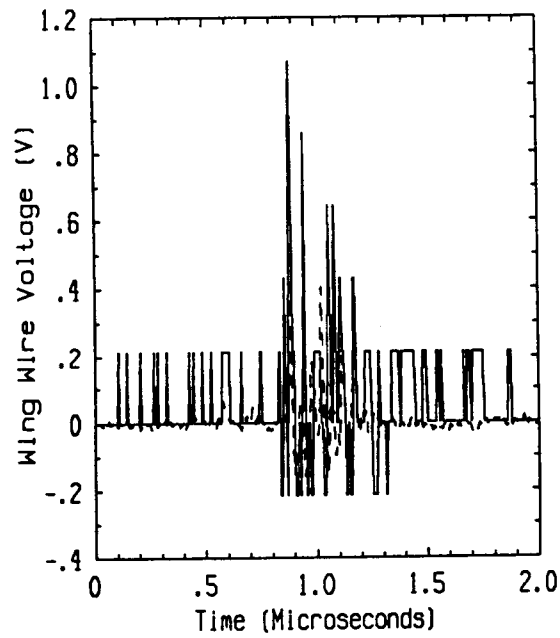
	PAGE #
MEASURED AND CALCULATED SENSOR TRANSIENTS FOR NOSE ATTACHMENTS	B-2 to B-40
MEASURED AND CALCULATED SENSOR TRANSIENTS FOR RIGHT WING ATTACHMENTS	B-42 to B-47
MEASURED AND CALCULATED SENSOR TRANSIENTS FOR LEFT WING ATTACHMENTS	B-49 to B-54
MEASURED AND CALCULATED SENSOR TRANSIENTS FOR TAIL ATTACHMENTS	B-56 to B-57



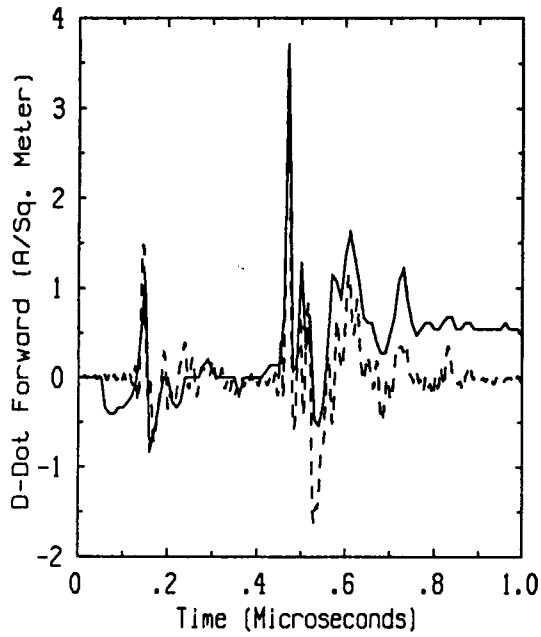
Flight 85.022 Run 004 Strike 004
 - Measured -- Predicted



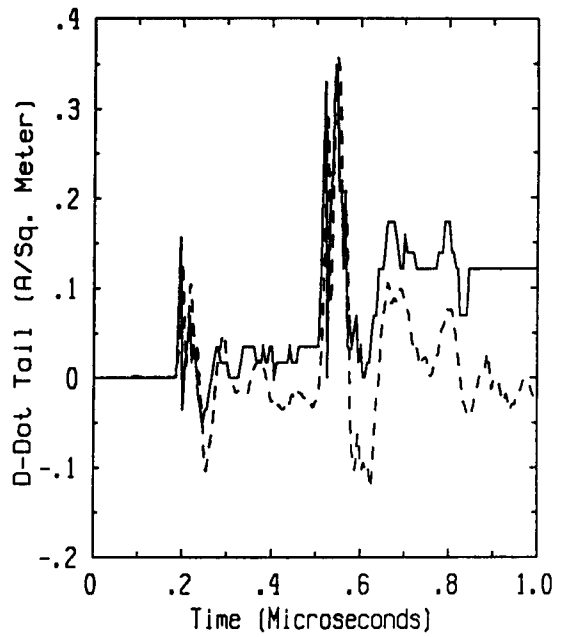
Flight 85.022 Run 004 Strike 004
 - Measured -- Predicted



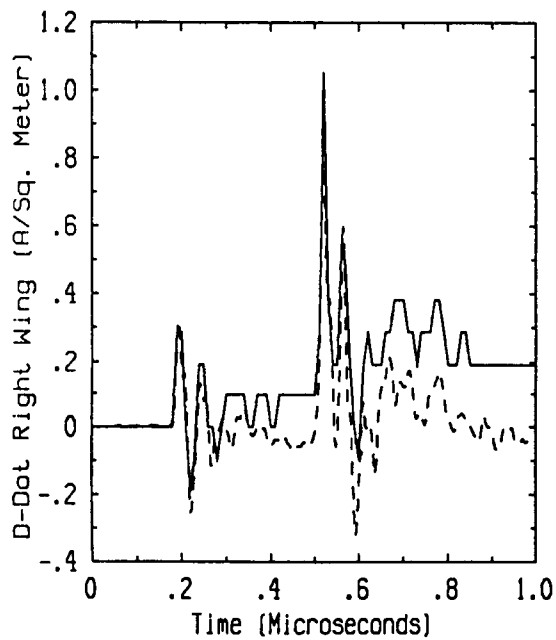
Flight 85.022 Run 004 Strike 004
 - Measured -- Predicted



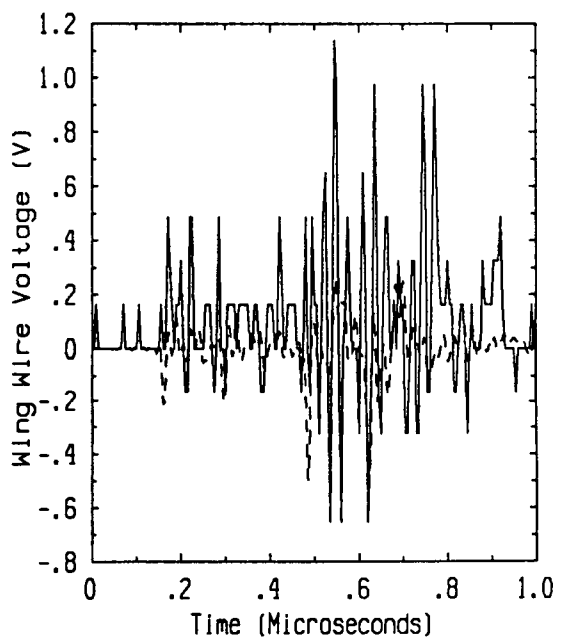
Flight 85.023 Run 003 Strike 001
 - Measured -- Predicted



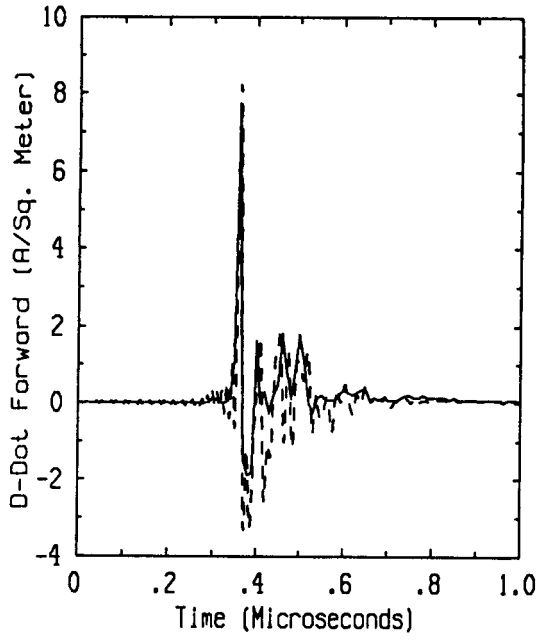
Flight 85.023 Run 003 Strike 001
 - Measured -- Predicted



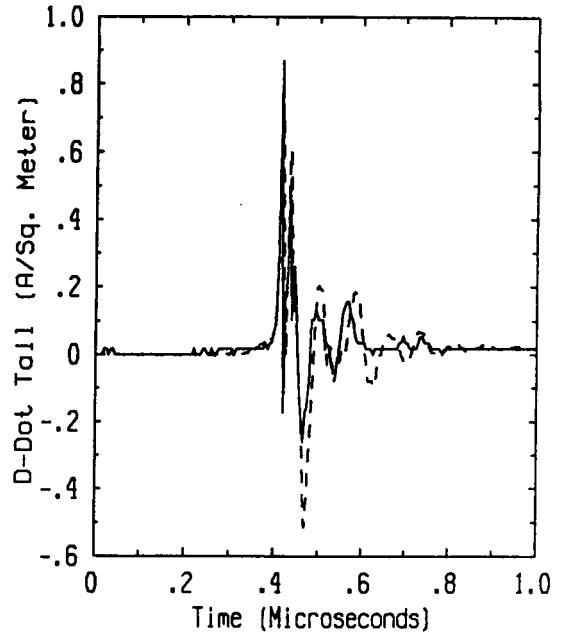
Flight 85.023 Run 003 Strike 001
 - Measured -- Predicted



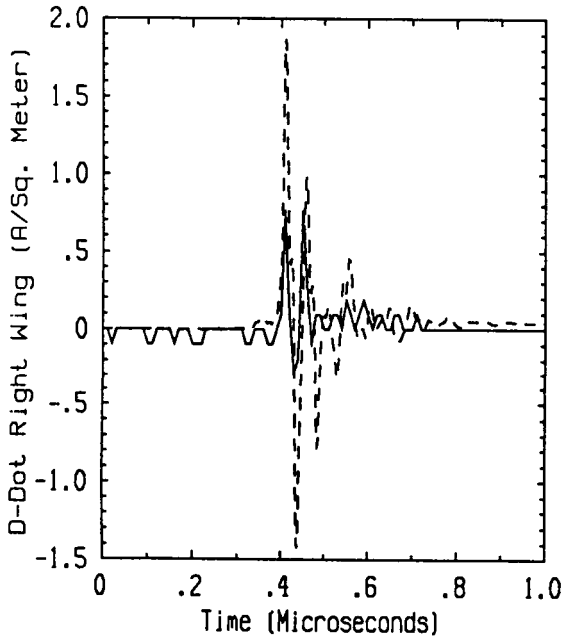
Flight 85.023 Run 003 Strike 001
 - Measured -- Predicted



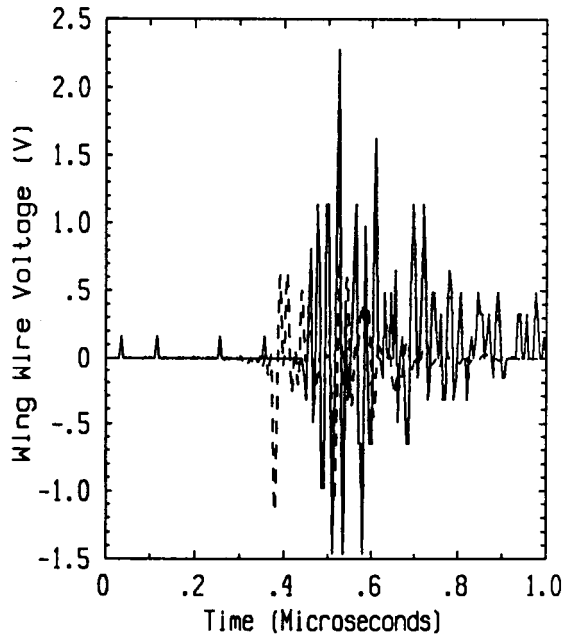
Flight 85.023 Run 005 Strike 002
 - Measured -- Predicted



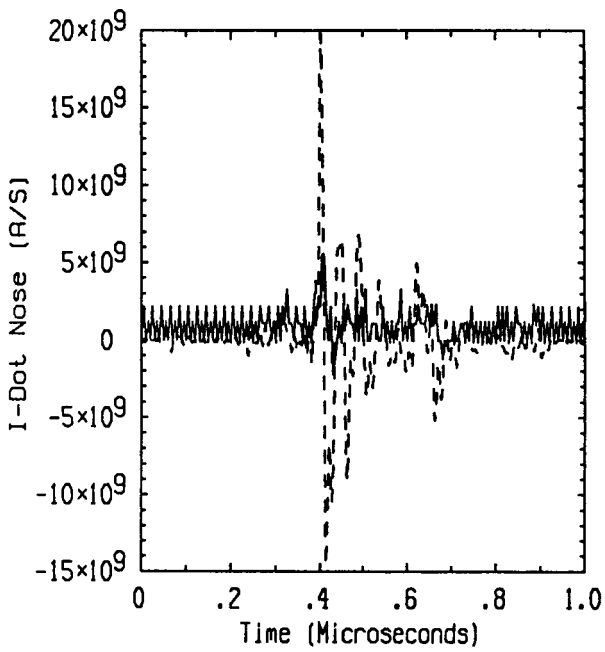
Flight 85.023 Run 005 Strike 002
 - Measured -- Predicted



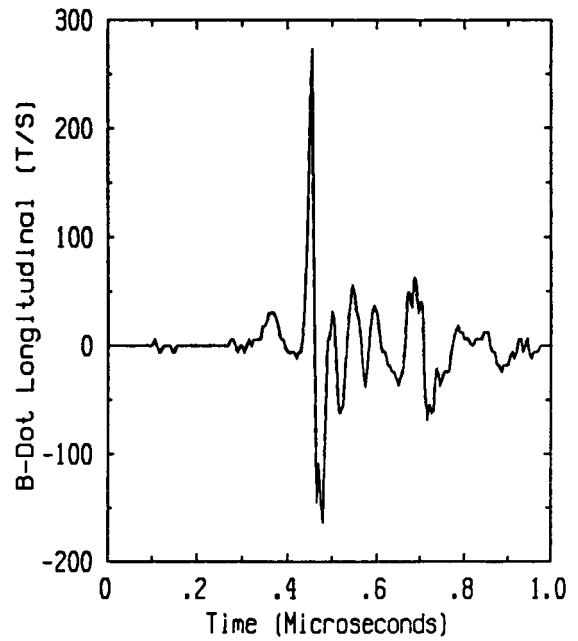
Flight 85.023 Run 005 Strike 002
 - Measured -- Predicted



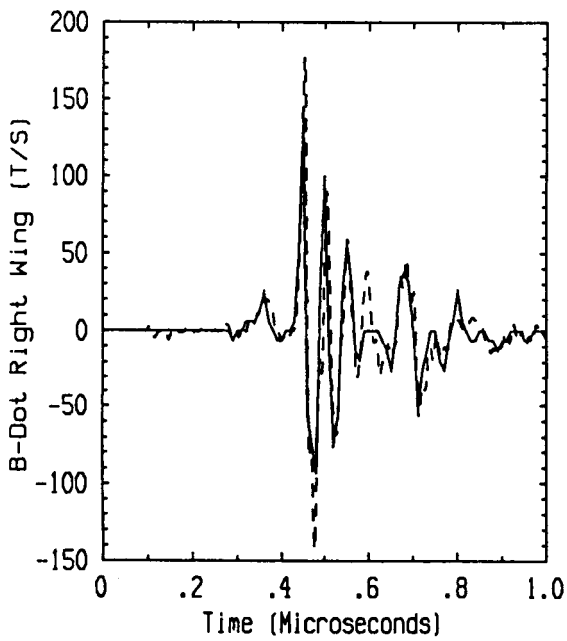
Flight 85.023 Run 005 Strike 002
 - Measured -- Predicted



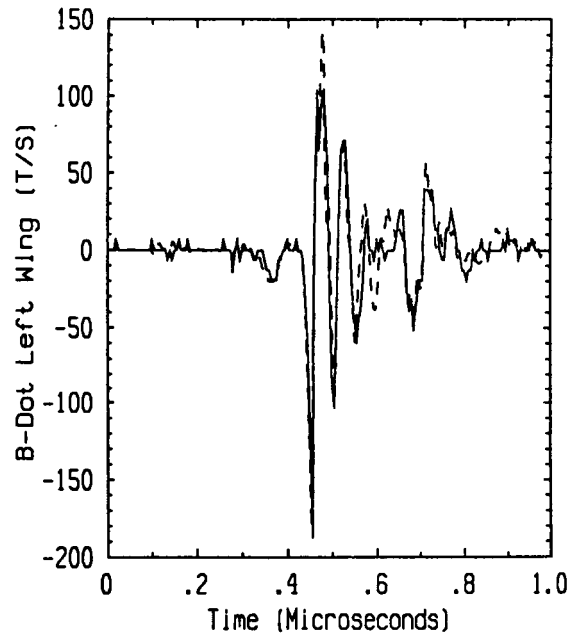
Flight 85.027 Run 001 Strike 001
 - Measured -- Predicted



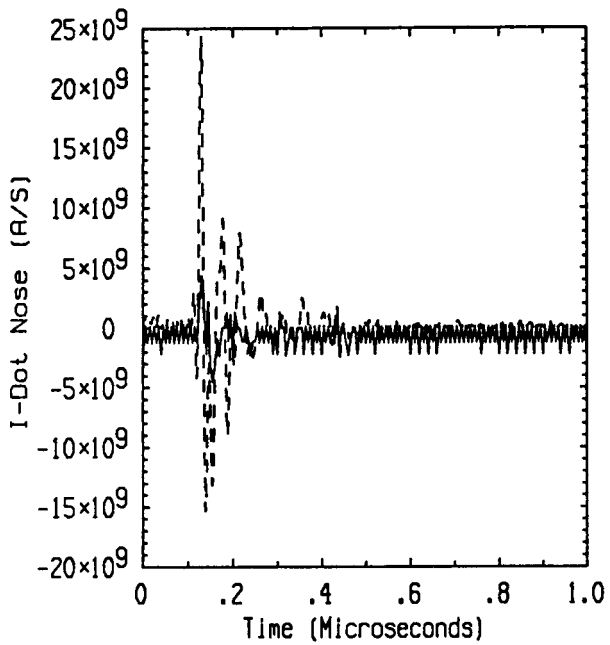
Flight 85.027 Run 001 Strike 001
 - Measured -- Predicted



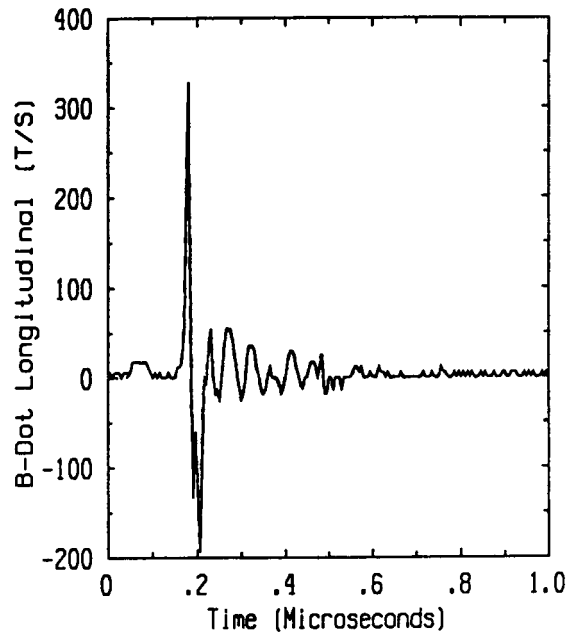
Flight 85.027 Run 001 Strike 001
 - Measured -- Predicted



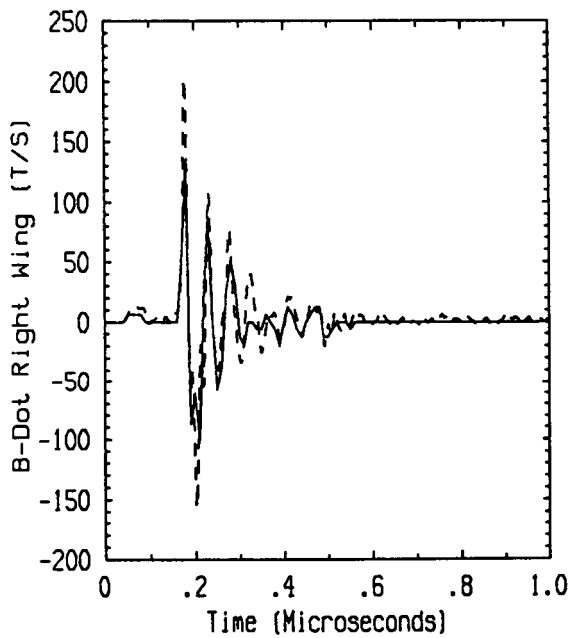
Flight 85.027 Run 001 Strike 001
 - Measured -- Predicted



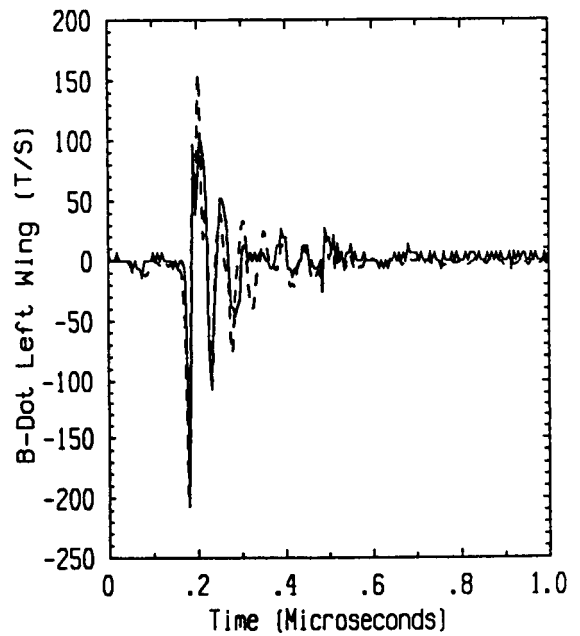
Flight 85.028 Run 001 Strike 001
 - Measured -- Predicted



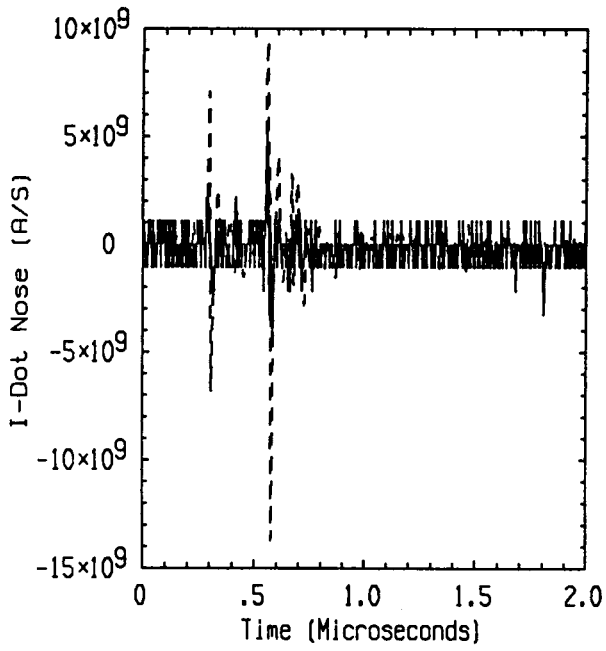
Flight 85.028 Run 001 Strike 001
 - Measured -- Predicted



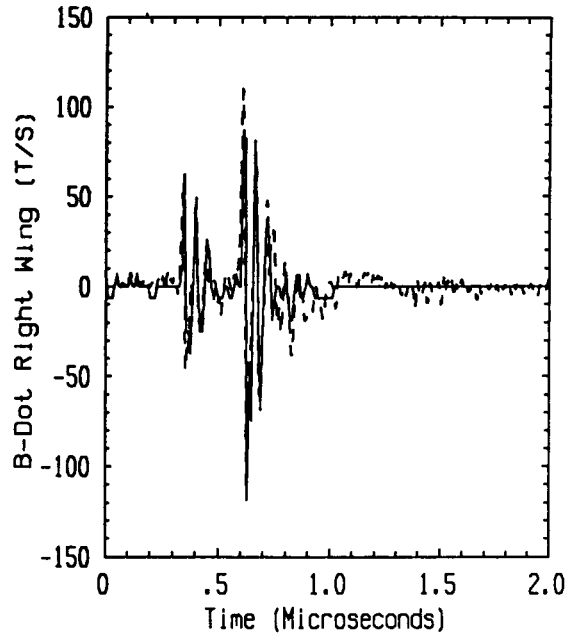
Flight 85.028 Run 001 Strike 001
 - Measured -- Predicted



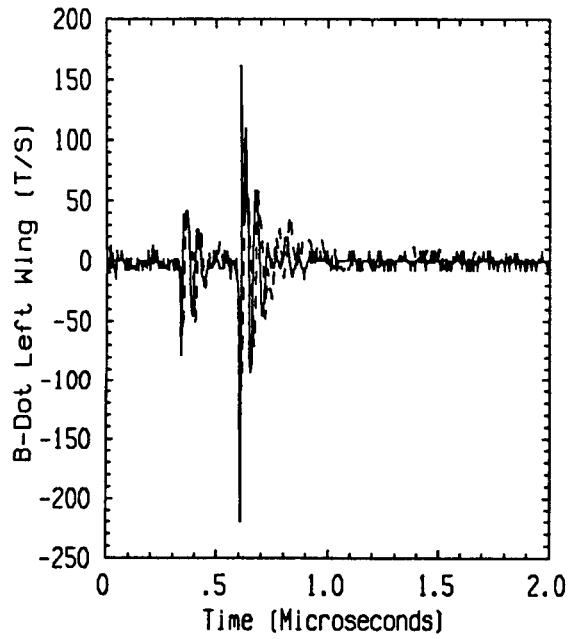
Flight 85.028 Run 001 Strike 001
 - Measured -- Predicted



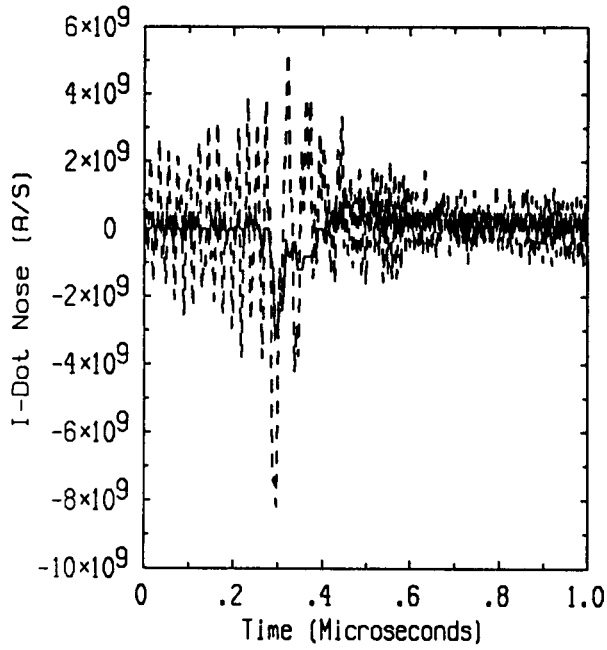
Flight 85.030 Run 001 Strike 001
 - Measured -- Predicted



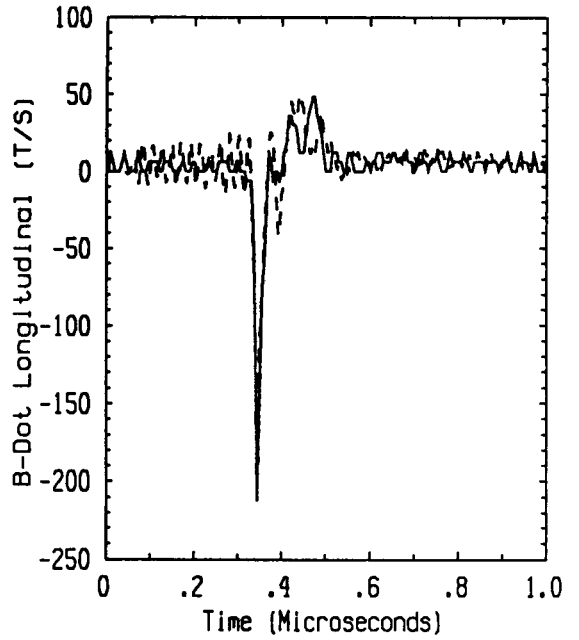
Flight 85.030 Run 001 Strike 001
 - Measured -- Predicted



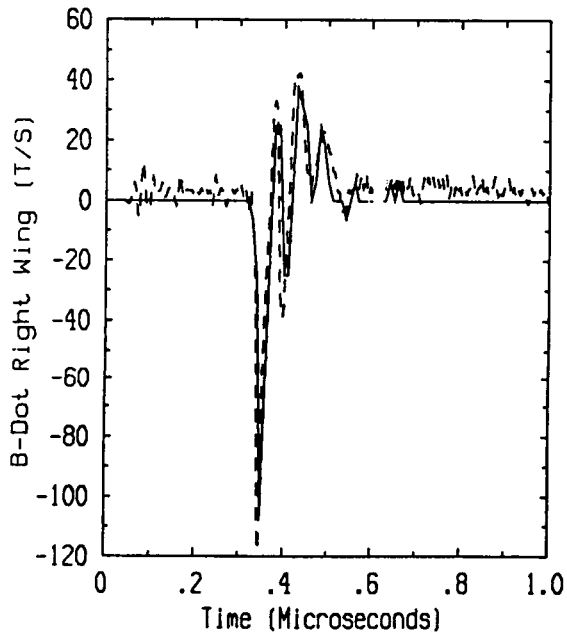
Flight 85.030 Run 001 Strike 001
 - Measured -- Predicted



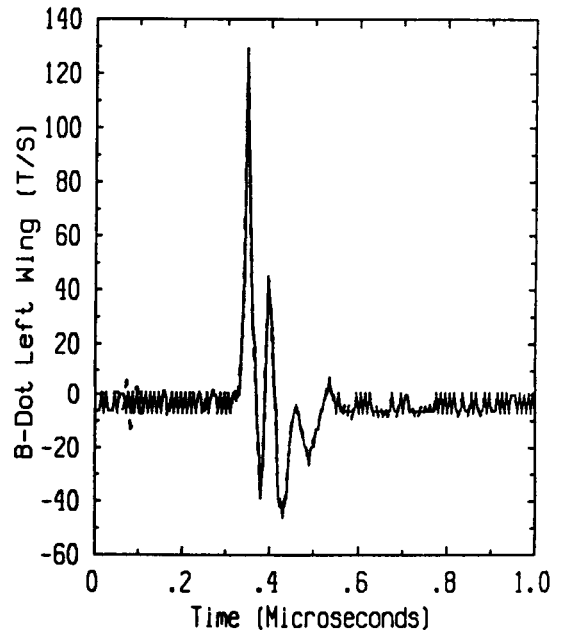
Flight 85.032 Run 001 Strike 001
 - Measured -- Predicted



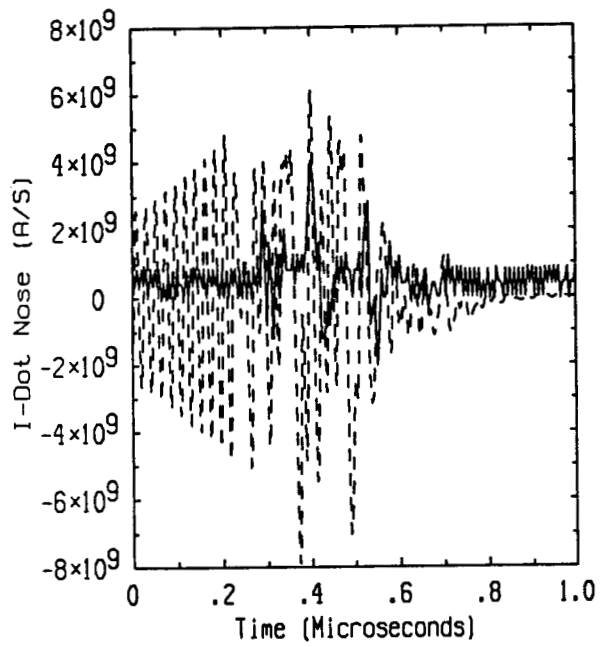
Flight 85.032 Run 001 Strike 001
 - Measured -- Predicted



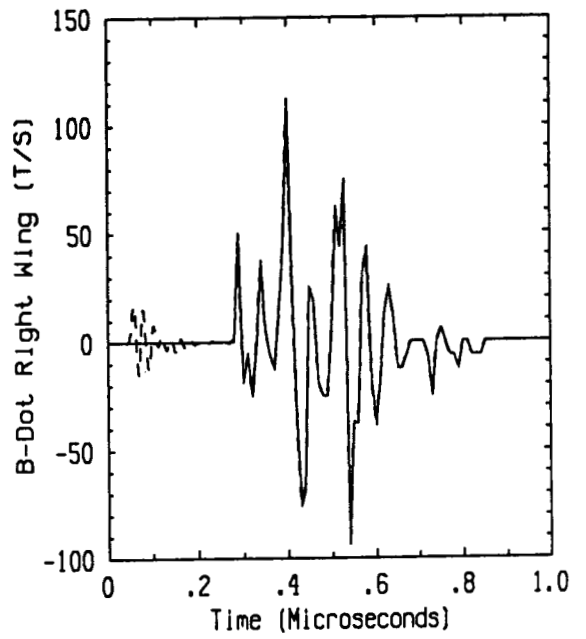
Flight 85.032 Run 001 Strike 001
 - Measured -- Predicted



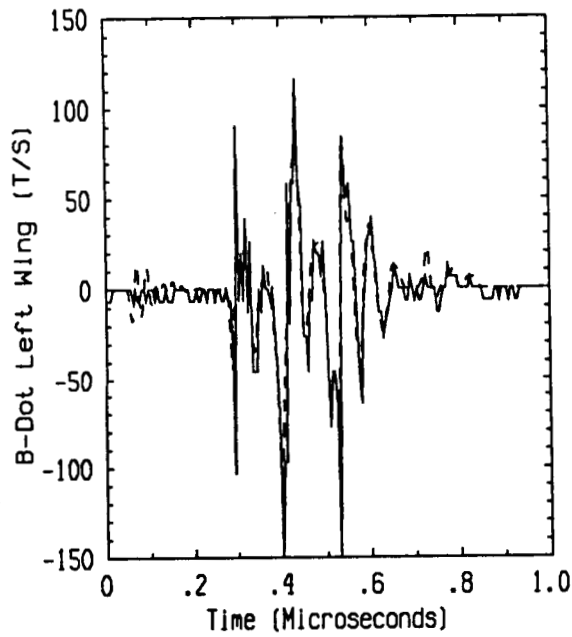
Flight 85.032 Run 001 Strike 001
 - Measured -- Predicted



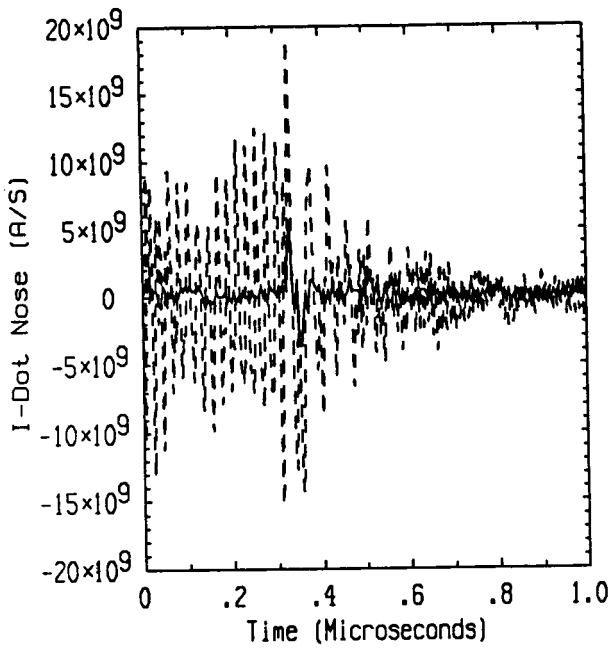
Flight 85.032 Run 002 Strike 002
 - Measured -- Predicted



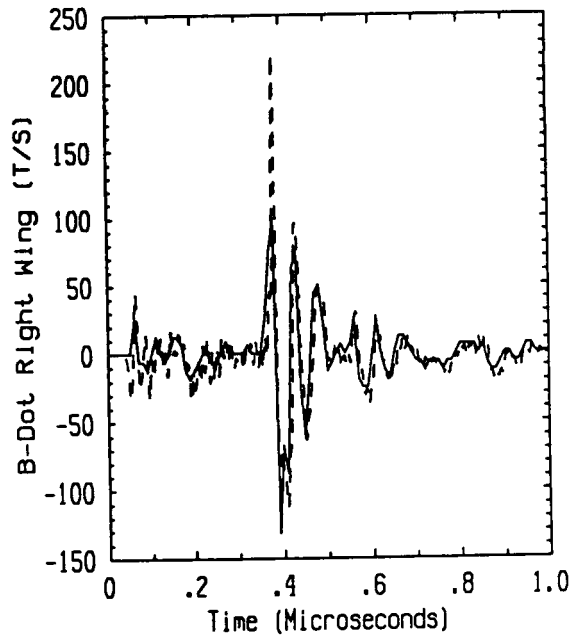
Flight 85.032 Run 002 Strike 002
 - Measured -- Predicted



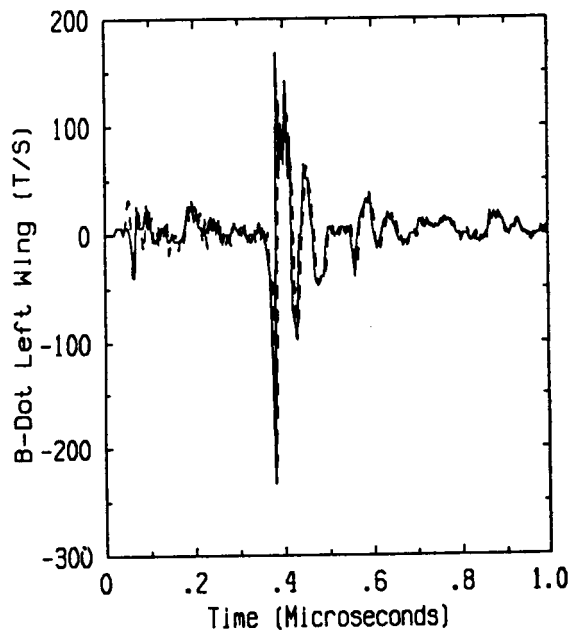
Flight 85.032 Run 002 Strike 002
 - Measured -- Predicted



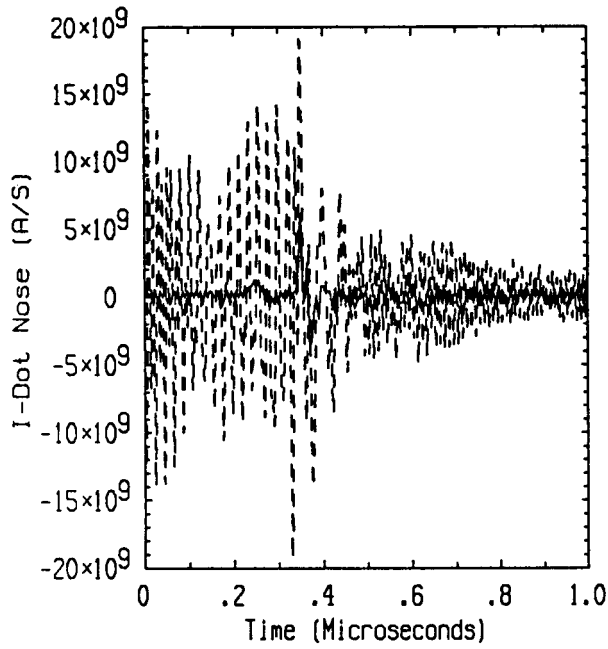
Flight 85.032 Run 003 Strike 003
 - Measured -- Predicted



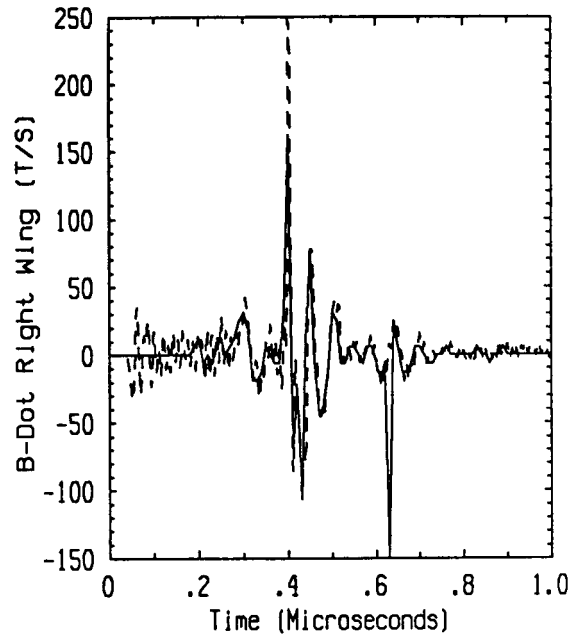
Flight 85.032 Run 003 Strike 003
 - Measured -- Predicted



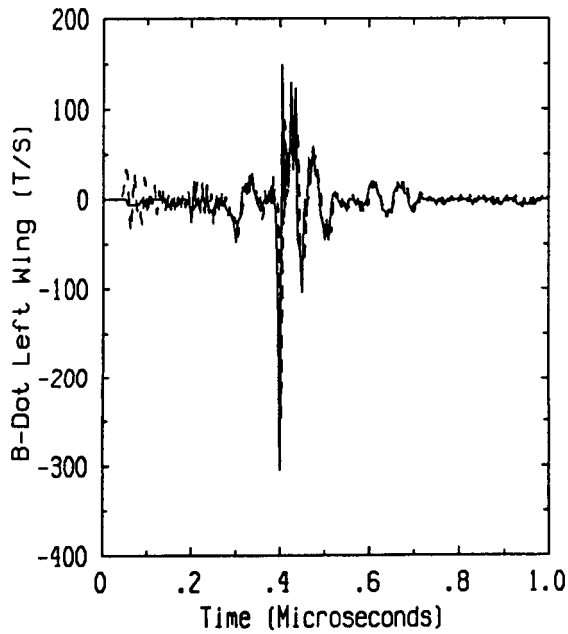
Flight 85.032 Run 003 Strike 003
 - Measured -- Predicted



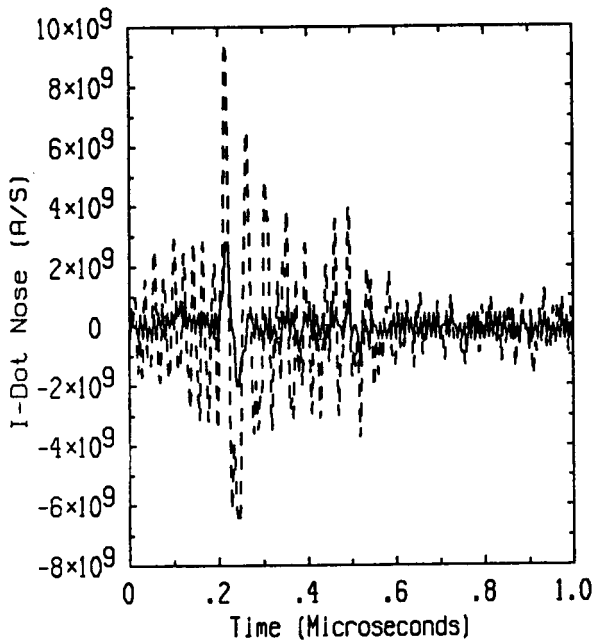
Flight 85.032 Run 004 Strike 004
 - Measured -- Predicted



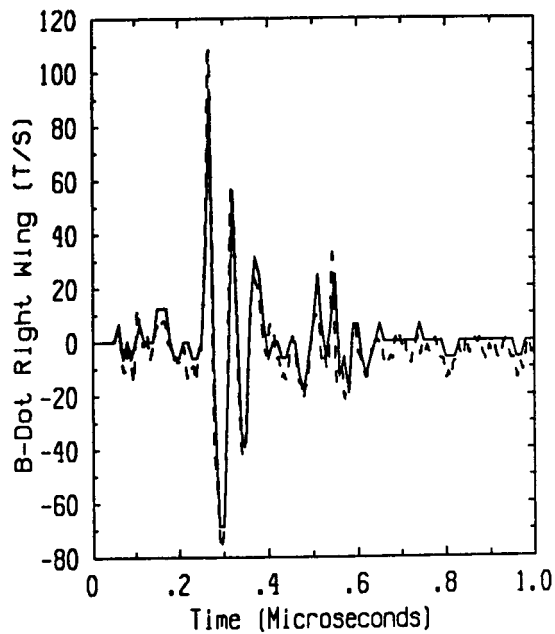
Flight 85.032 Run 004 Strike 004
 - Measured -- Predicted



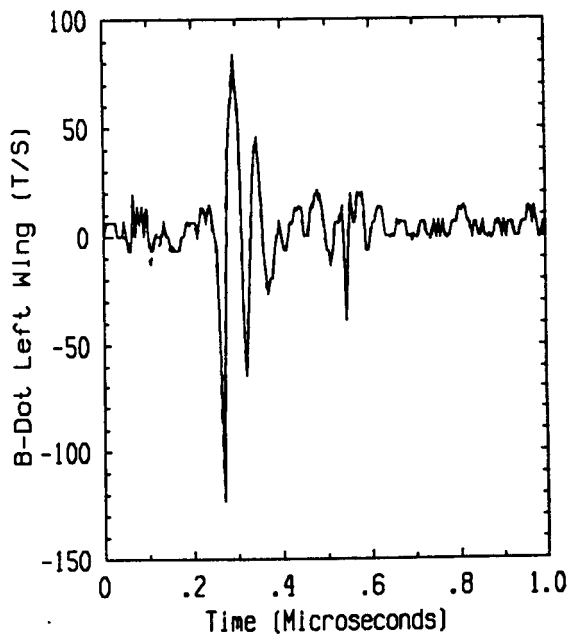
Flight 85.032 Run 004 Strike 004
 - Measured -- Predicted



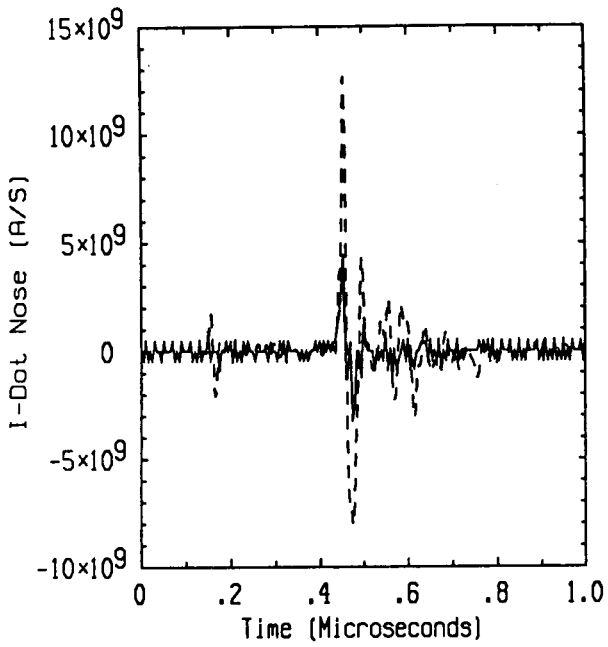
Flight 85.032 Run 005 Strike 005
 - Measured -- Predicted



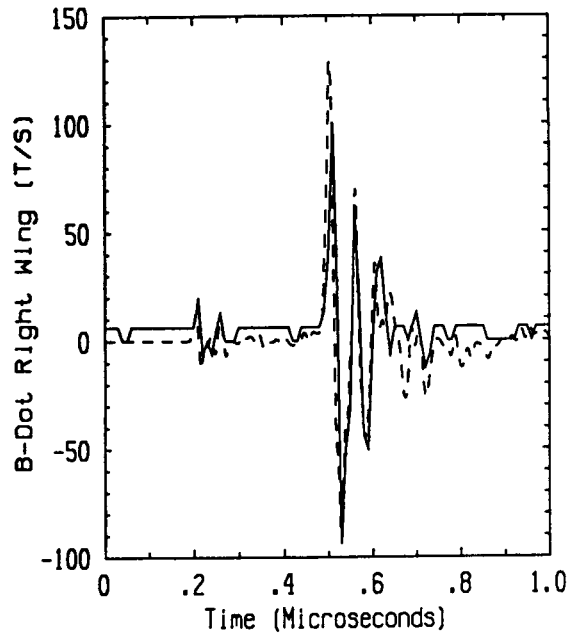
Flight 85.032 Run 005 Strike 005
 - Measured -- Predicted



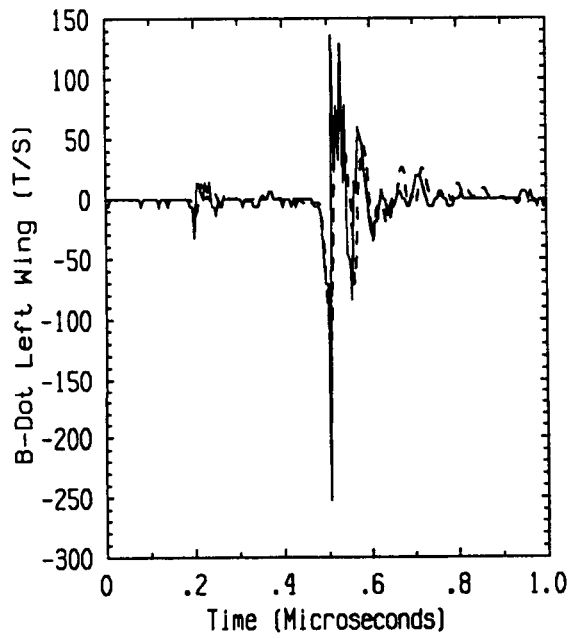
Flight 85.032 Run 005 Strike 005
 - Measured -- Predicted



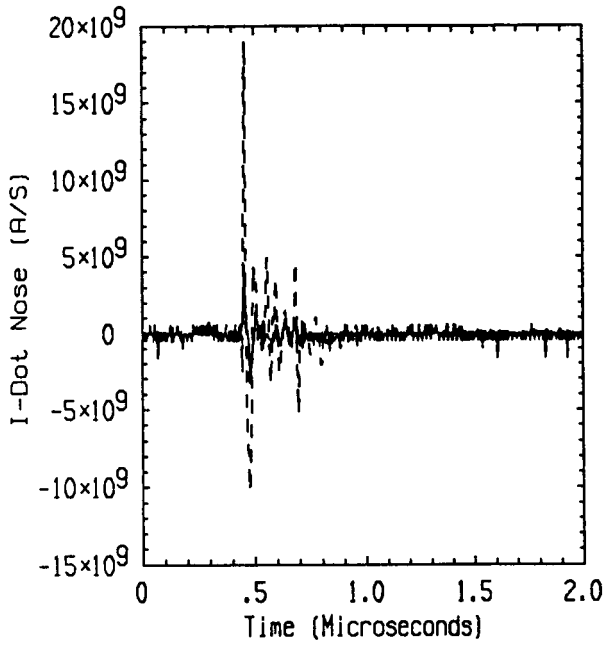
Flight 85.033 Run 001 Strike 001
 - Measured -- Predicted



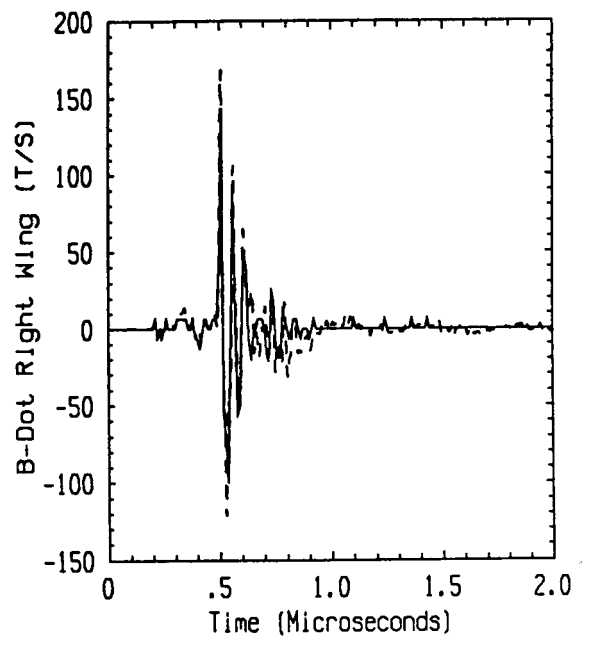
Flight 85.033 Run 001 Strike 001
 - Measured -- Predicted



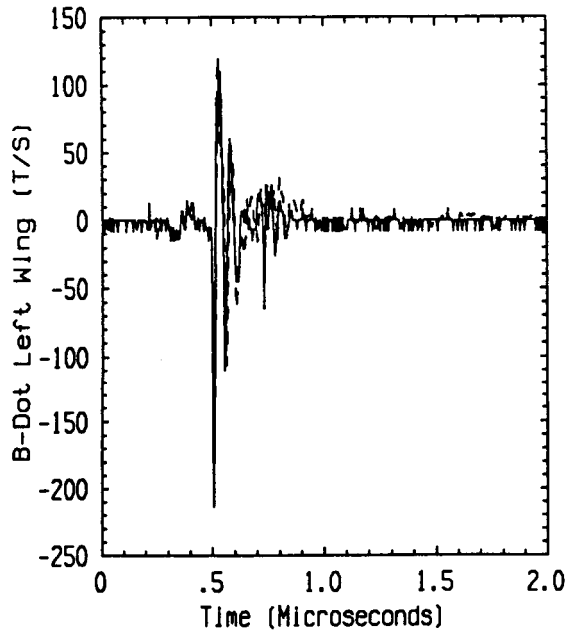
Flight 85.033 Run 001 Strike 001
 - Measured -- Predicted



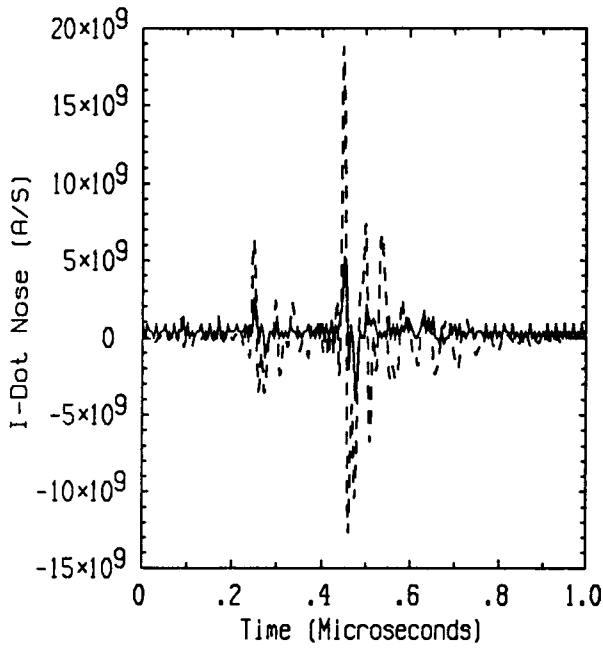
Flight 85.033 Run 003 Strike 003
 - Measured -- Predicted



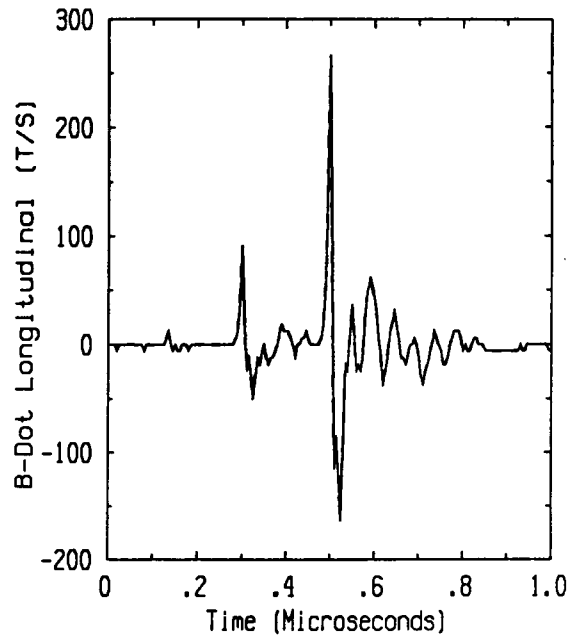
Flight 85.033 Run 003 Strike 003
 - Measured -- Predicted



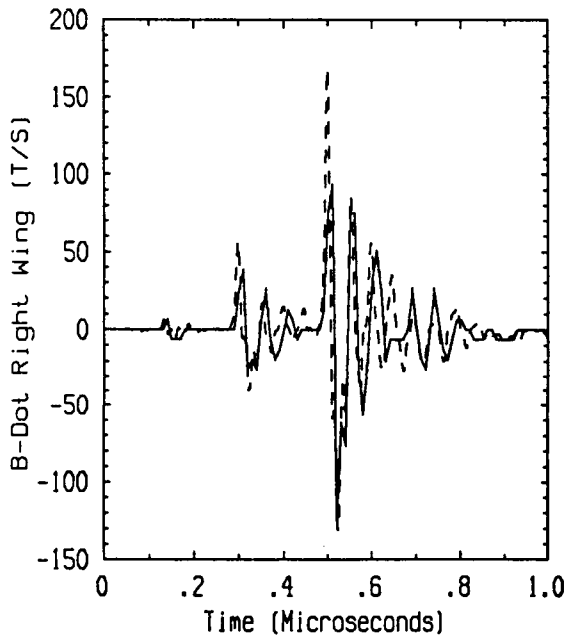
Flight 85.033 Run 003 Strike 003
 - Measured -- Predicted



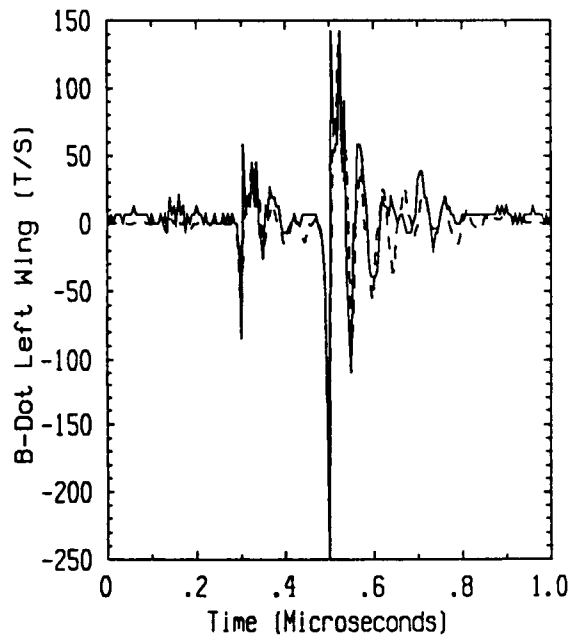
Flight 85.035 Run 001 Strike 001
 - Measured -- Predicted



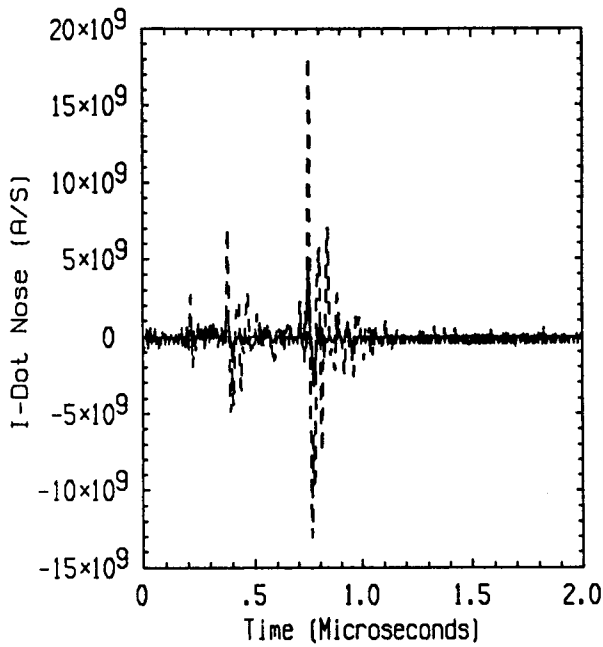
Flight 85.035 Run 001 Strike 001
 - Measured -- Predicted



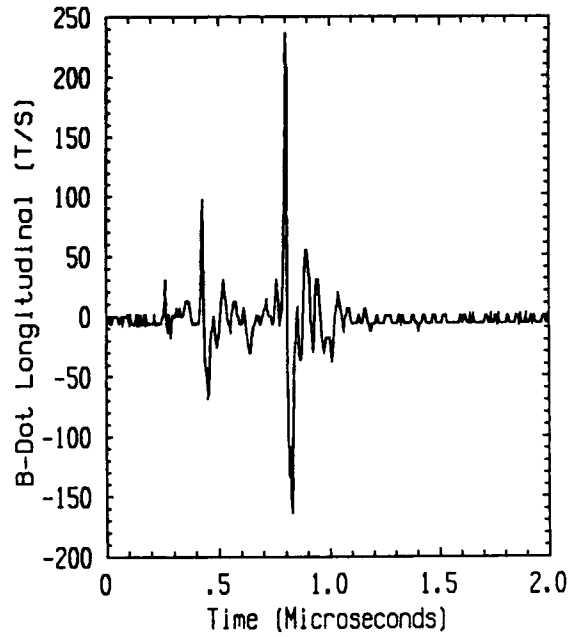
Flight 85.035 Run 001 Strike 001
 - Measured -- Predicted



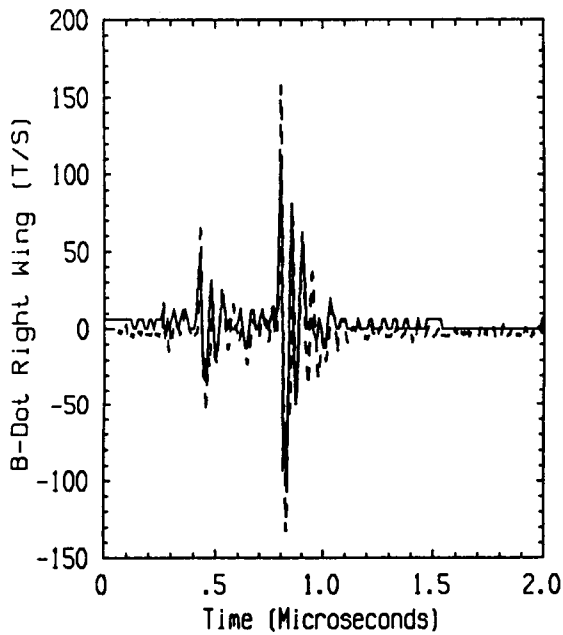
Flight 85.035 Run 001 Strike 001
 - Measured -- Predicted



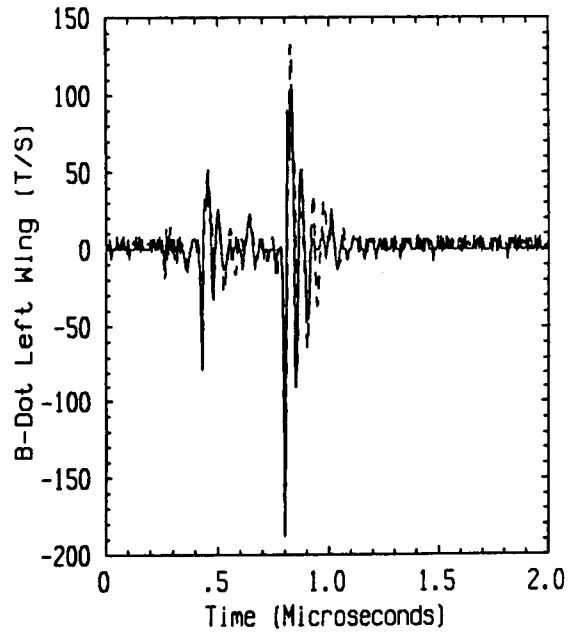
Flight 85.035 Run 002 Strike 002
 - Measured -- Predicted



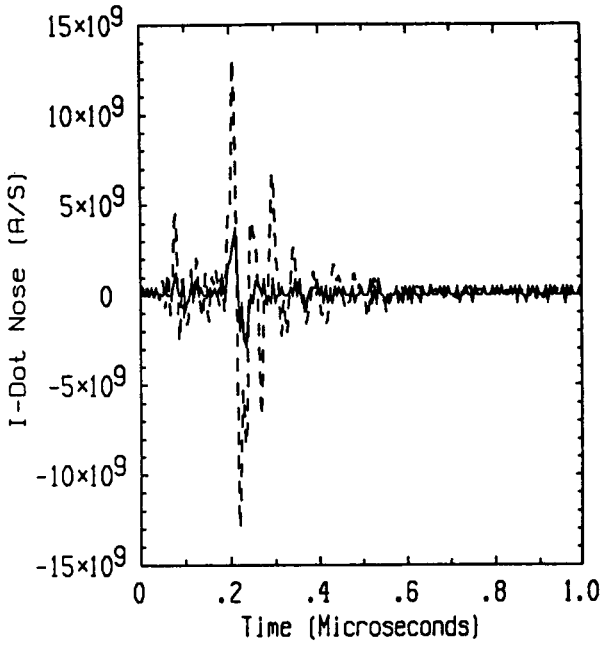
Flight 85.035 Run 002 Strike 002
 - Measured -- Predicted



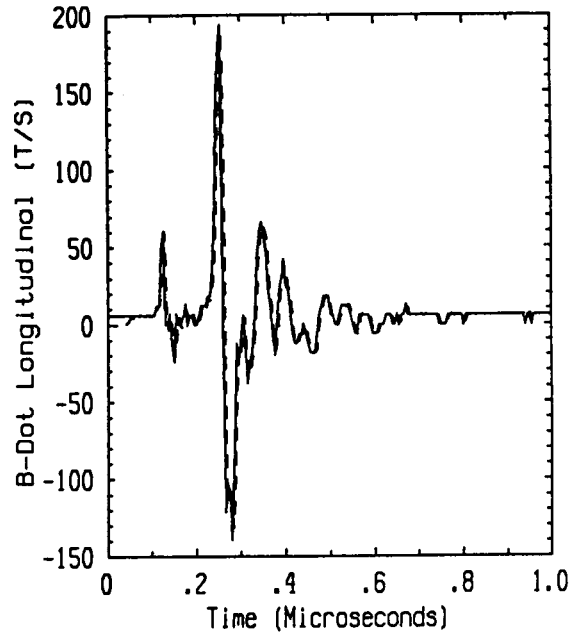
Flight 85.035 Run 002 Strike 002
 - Measured -- Predicted



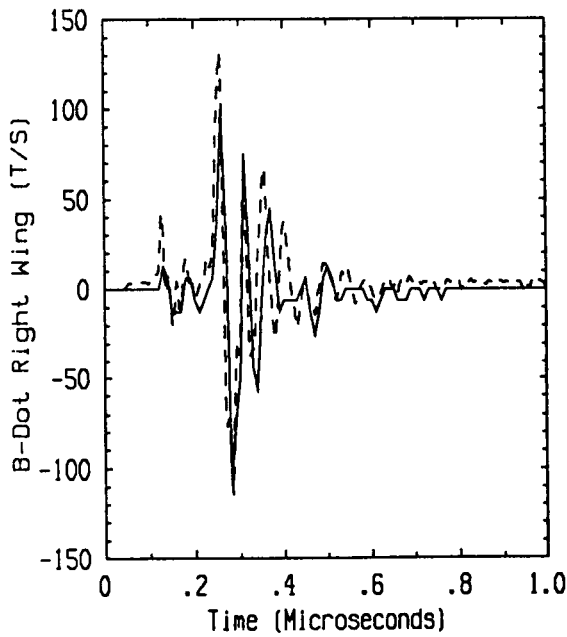
Flight 85.035 Run 002 Strike 002
 - Measured -- Predicted



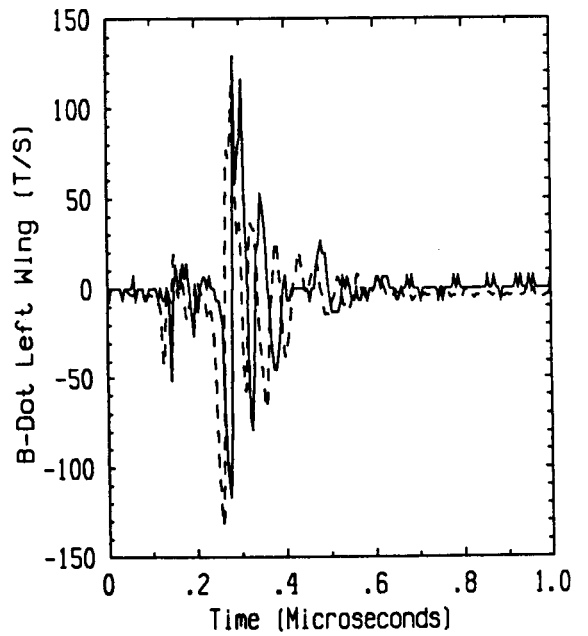
Flight 85.035 Run 003 Strike 003
 - Measured -- Predicted



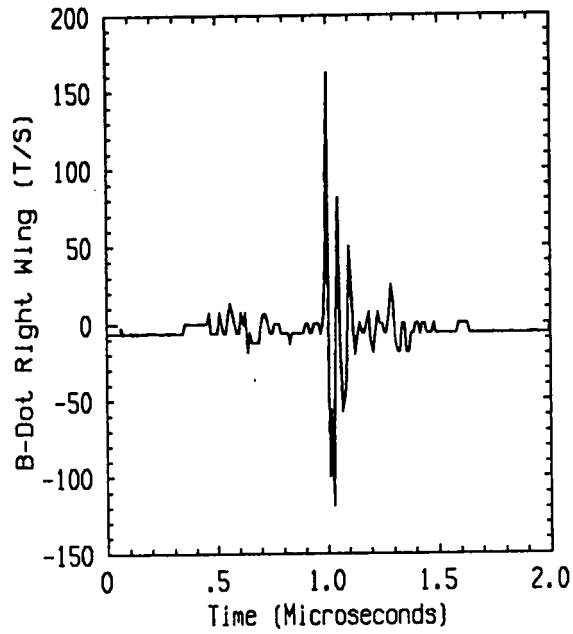
Flight 85.035 Run 003 Strike 003
 - Measured -- Predicted



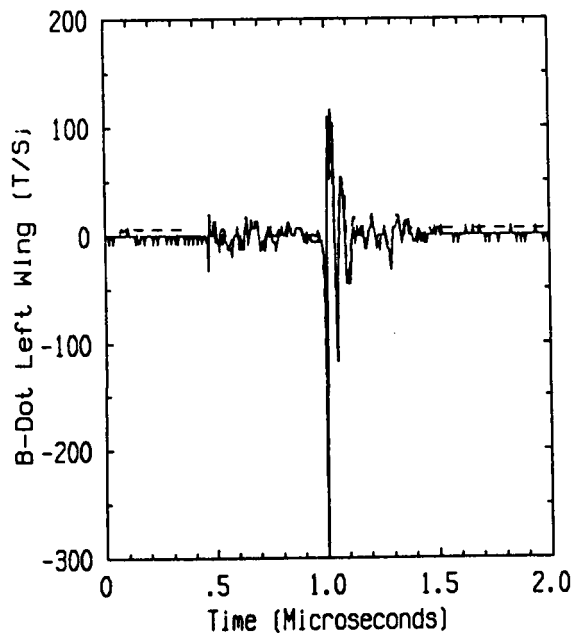
Flight 85.035 Run 003 Strike 003
 - Measured -- Predicted



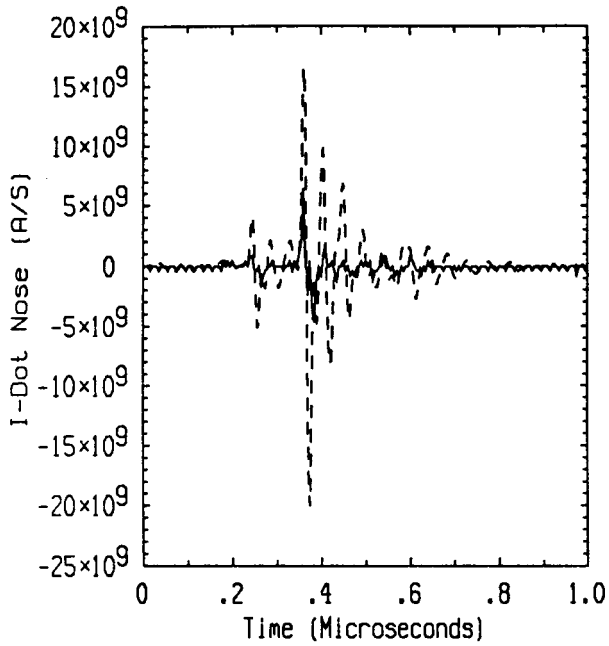
Flight 85.035 Run 003 Strike 003
 - Measured -- Predicted



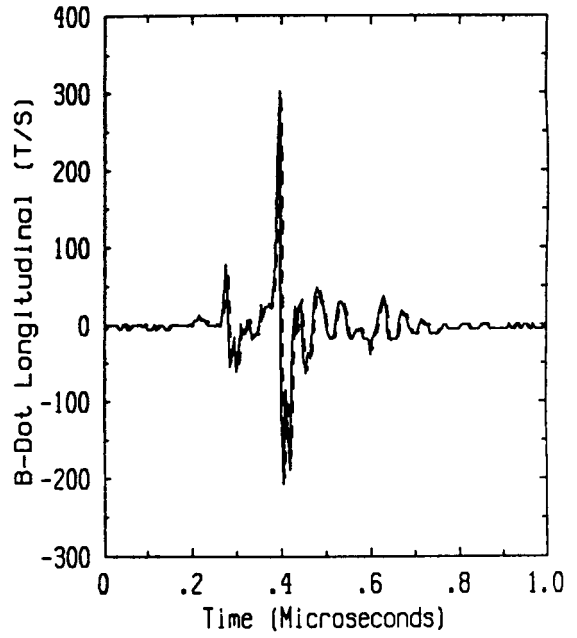
Flight 85.035 Run 006 Strike 006
- Measured -- Predicted



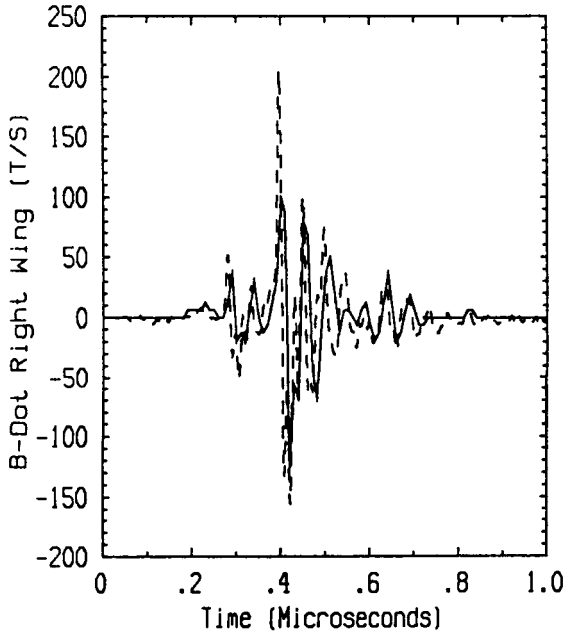
Flight 85.035 Run 006 Strike 006
- Measured -- Predicted



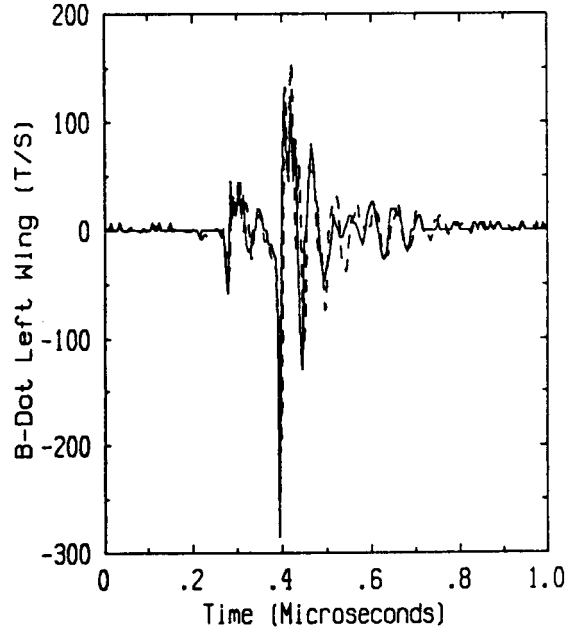
Flight 85.036 Run 001 Strike 001
 - Measured -- Predicted



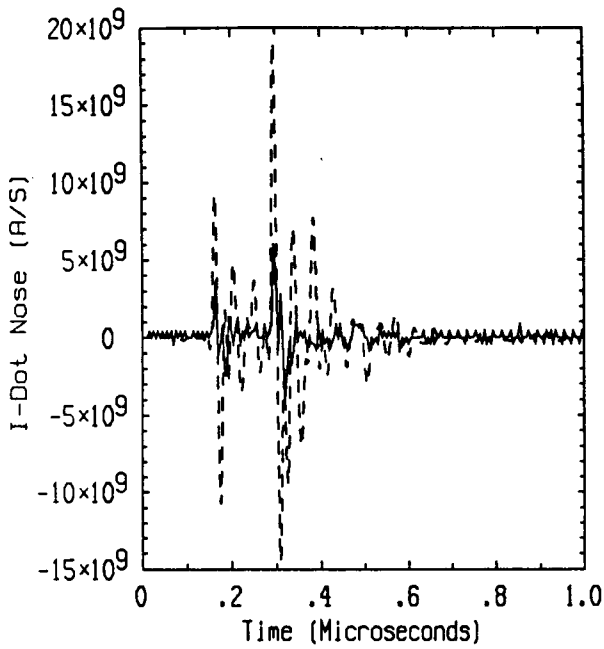
Flight 85.036 Run 001 Strike 001
 - Measured -- Predicted



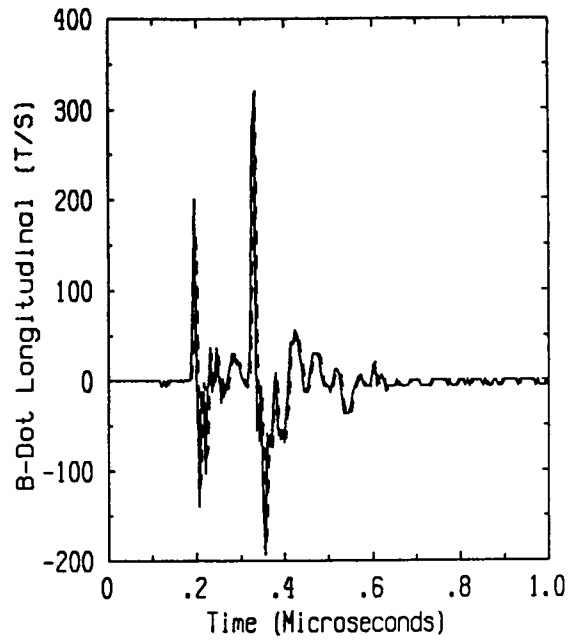
Flight 85.036 Run 001 Strike 001
 - Measured -- Predicted



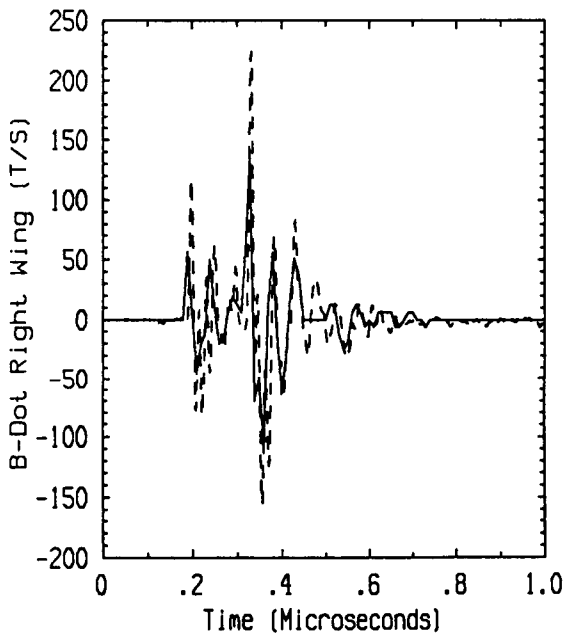
Flight 85.036 Run 001 Strike 001
 - Measured -- Predicted



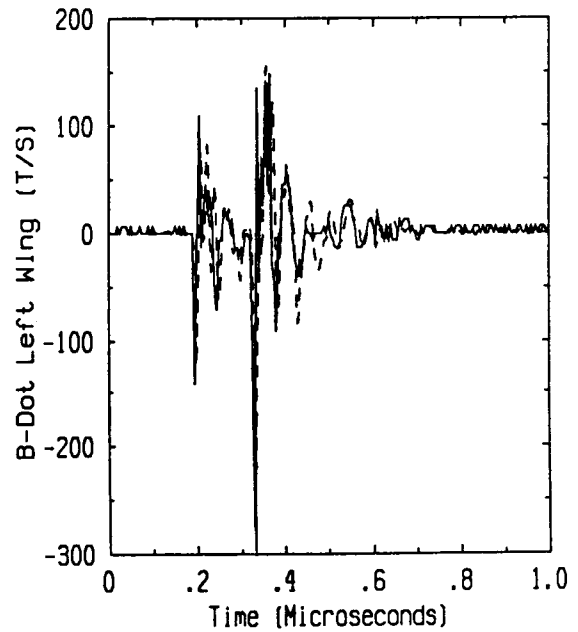
Flight 85.036 Run 003 Strike 003
 - Measured -- Predicted



Flight 85.036 Run 003 Strike 003
 - Measured -- Predicted

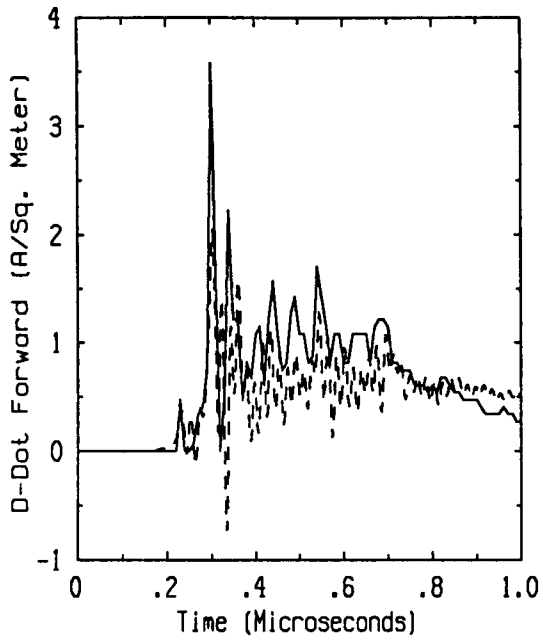


Flight 85.036 Run 003 Strike 003
 - Measured -- Predicted

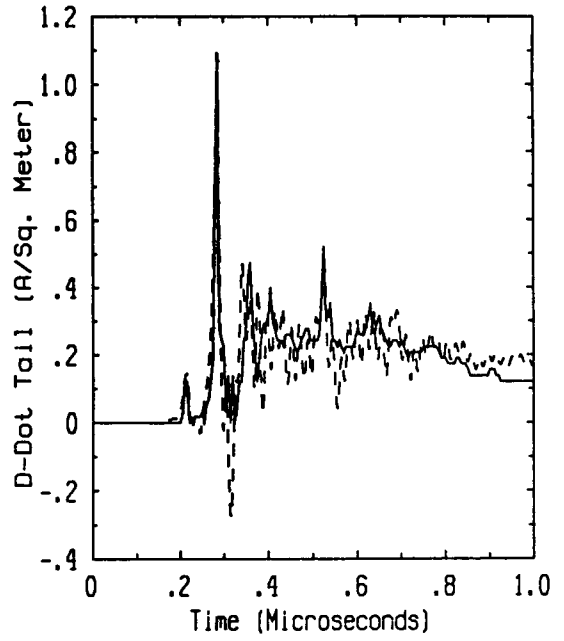


Flight 85.036 Run 003 Strike 003
 - Measured -- Predicted

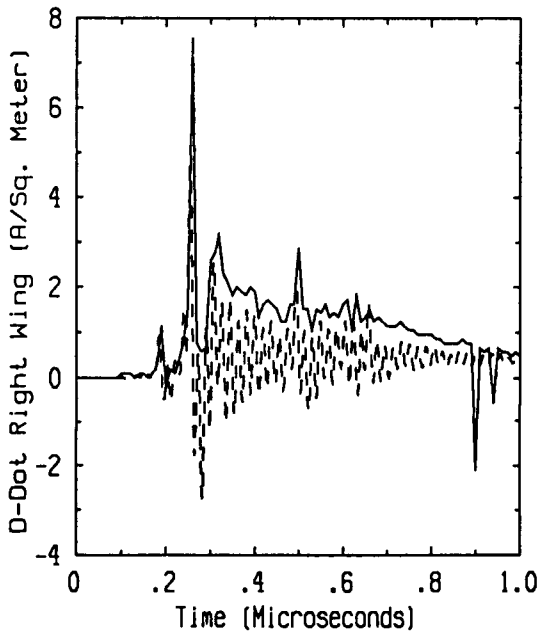
**MEASURED AND CALCULATED SENSOR TRANSIENTS
FOR RIGHT WING ATTACHMENTS**



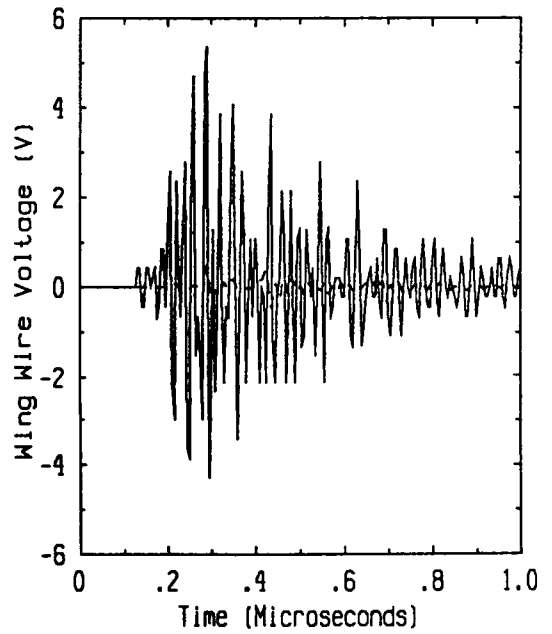
Flight 85.018 Run 002 Strike 001
 - Measured -- Predicted



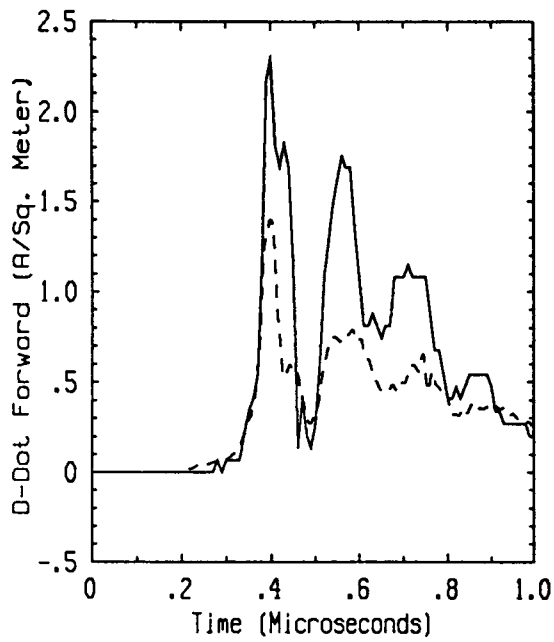
Flight 85.018 Run 002 Strike 001
 - Measured -- Predicted



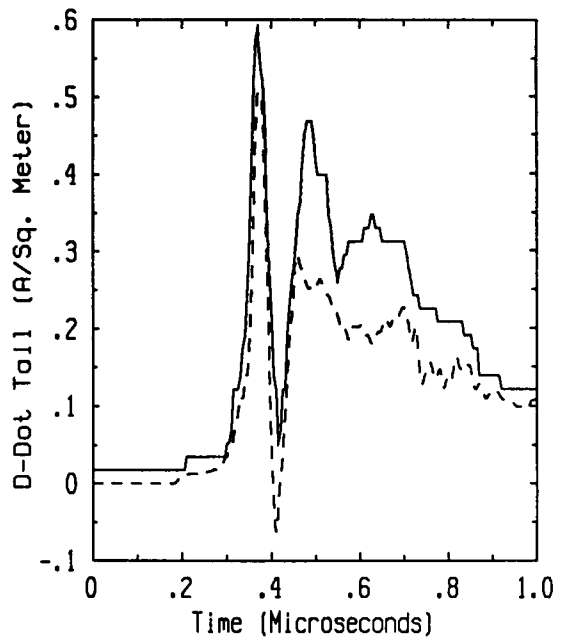
Flight 85.018 Run 002 Strike 001
 - Measured -- Predicted



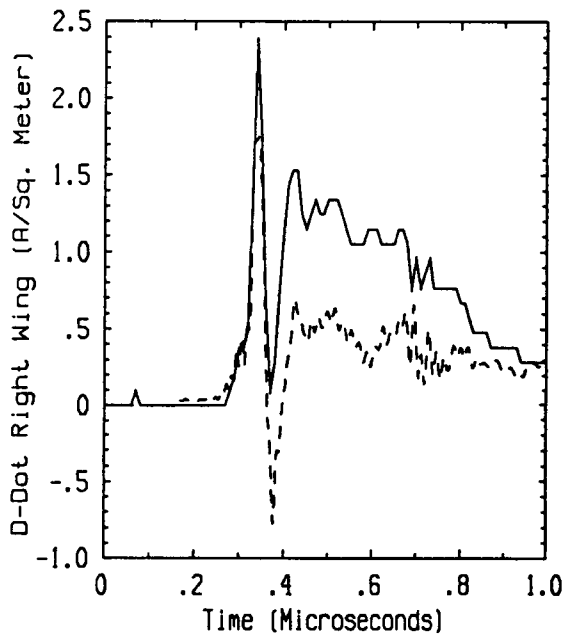
Flight 85.018 Run 002 Strike 001
 - Measured -- Predicted



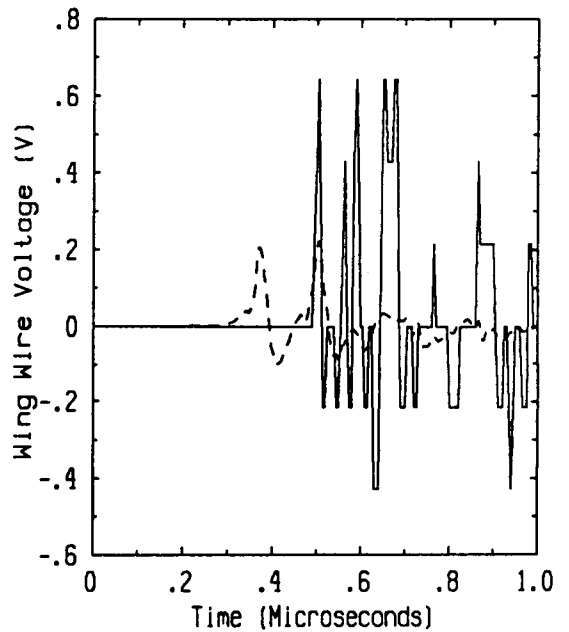
Flight 85.022 Run 003 Strike 003
 - Measured -- Predicted



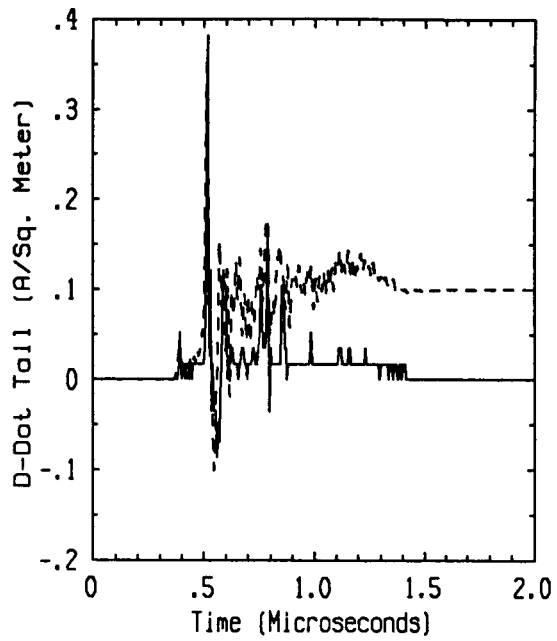
Flight 85.022 Run 003 Strike 003
 - Measured -- Predicted



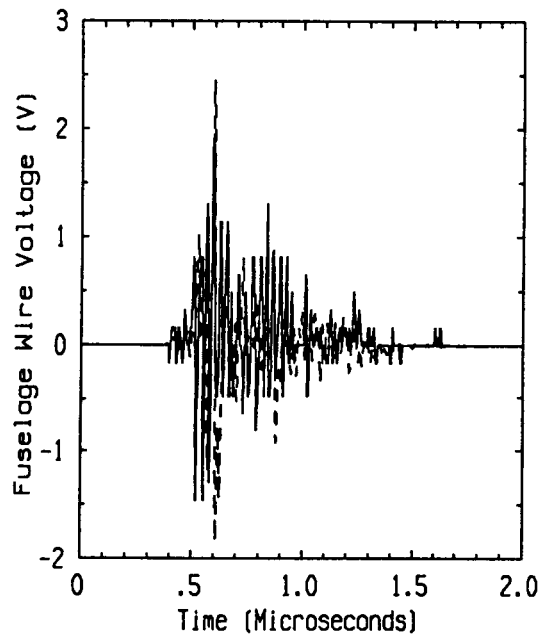
Flight 85.022 Run 003 Strike 003
 - Measured -- Predicted



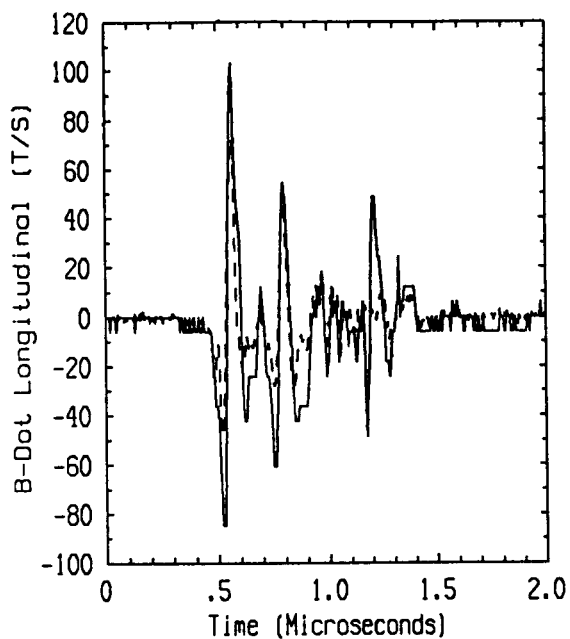
Flight 85.022 Run 003 Strike 003
 - Measured -- Predicted



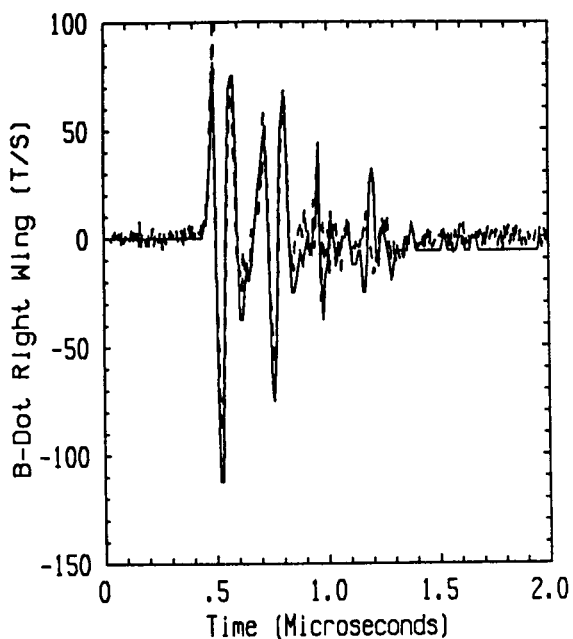
Flight 85.033 Run 002 Strike 002
- Measured -- Predicted



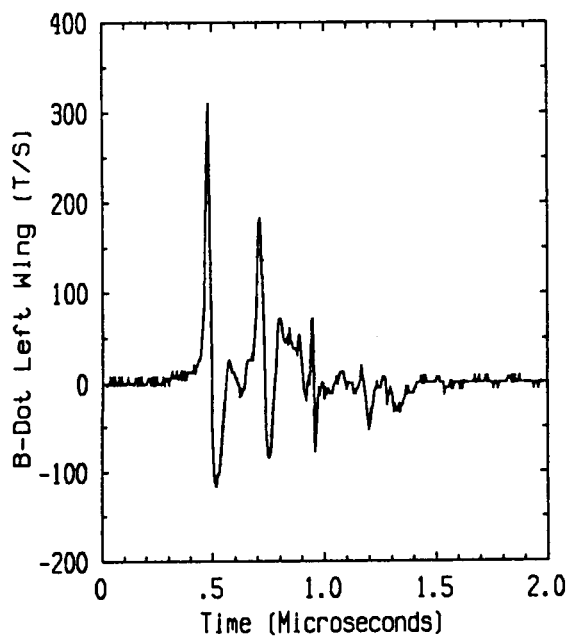
Flight 85.033 Run 002 Strike 002
- Measured -- Predicted



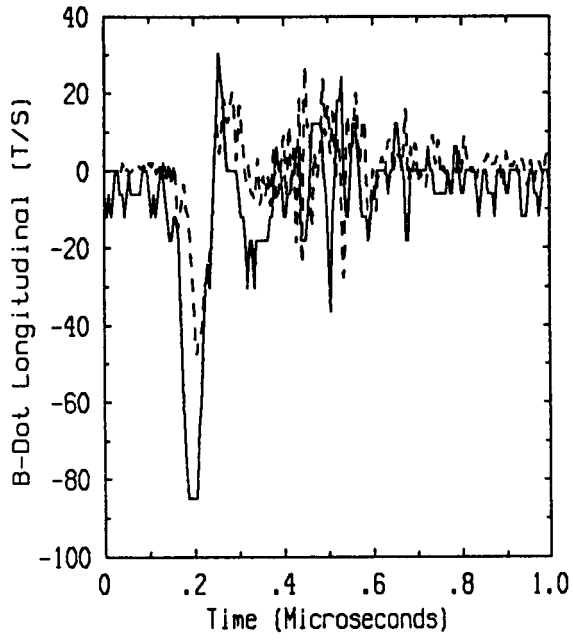
Flight 85.027 Run 002 Strike 002
 - Measured -- Predicted



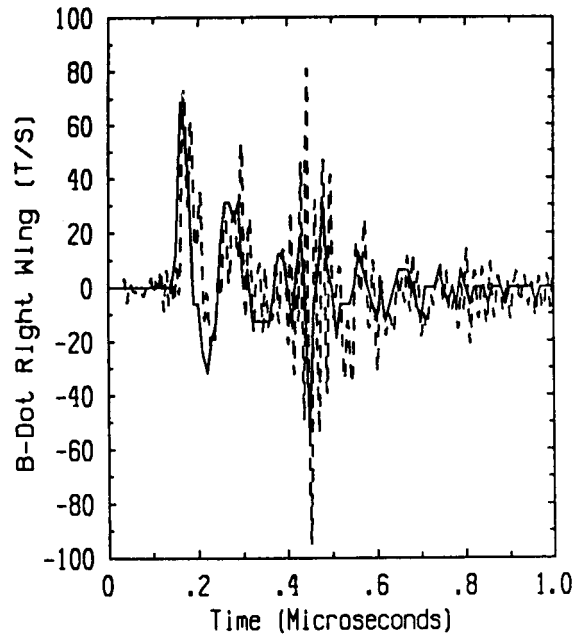
Flight 85.027 Run 002 Strike 002
 - Measured -- Predicted



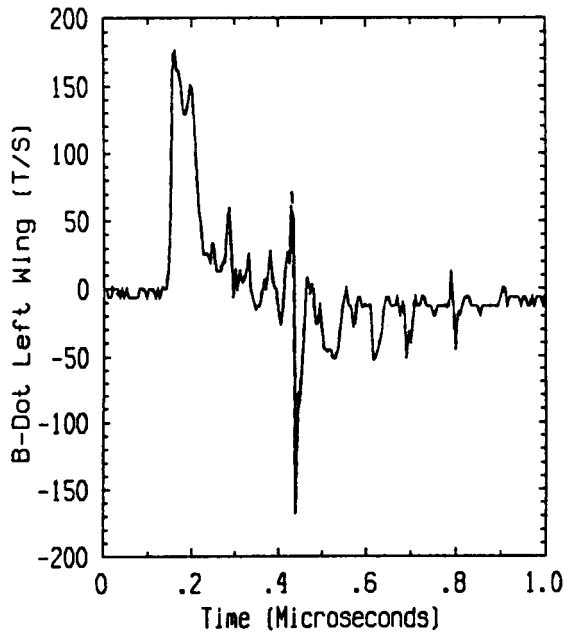
Flight 85.027 Run 002 Strike 002
 - Measured -- Predicted



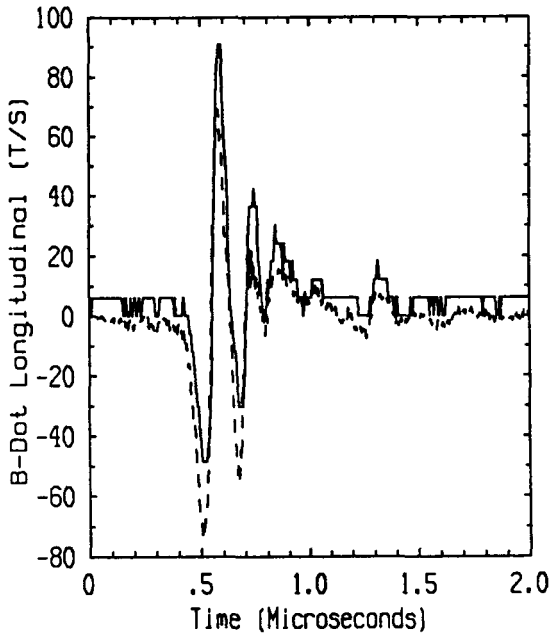
Flight 85.031 Run 001 Strike 001
 - Measured -- Predicted



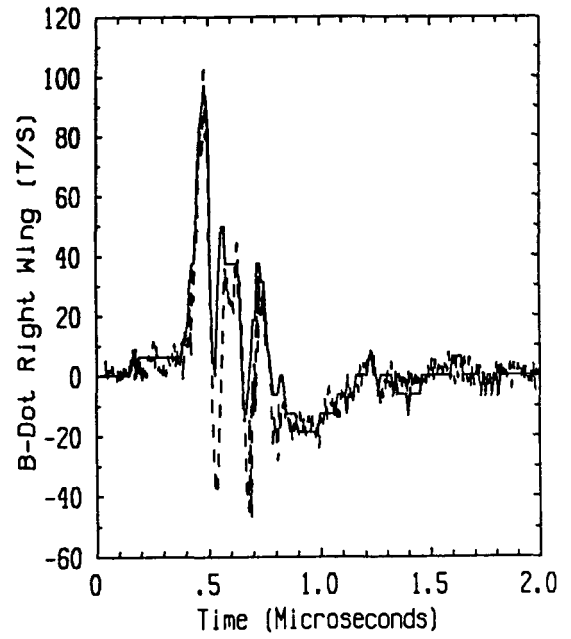
Flight 85.031 Run 001 Strike 001
 - Measured -- Predicted



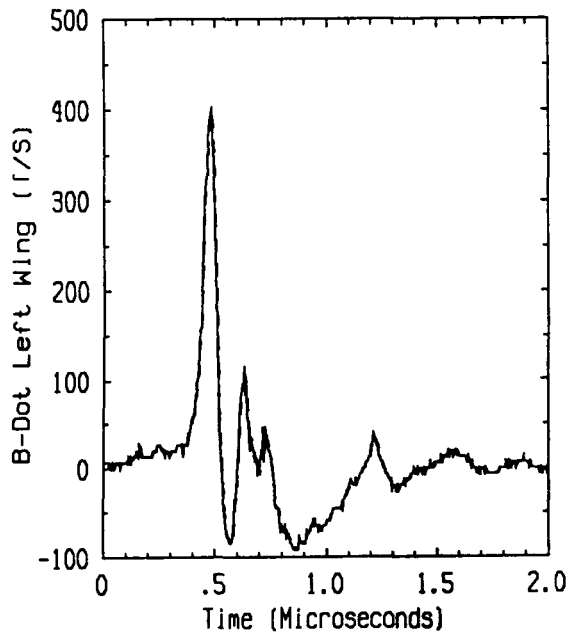
Flight 85.031 Run 001 Strike 001
 - Measured -- Predicted



Flight 85.035 Run 004 Strike 004
 - Measured -- Predicted

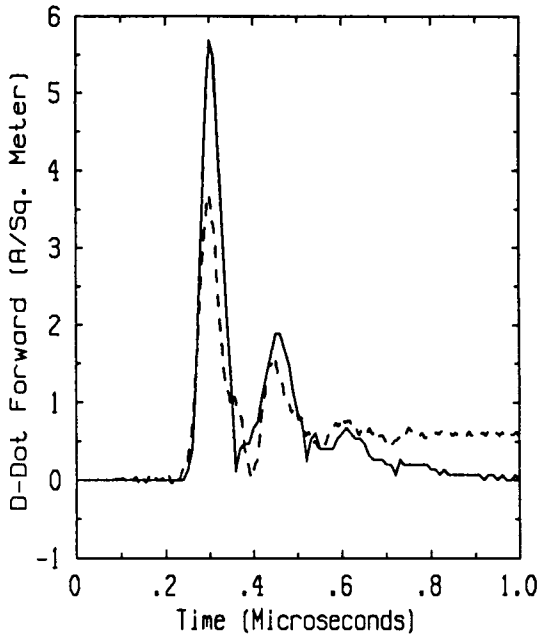


Flight 85.035 Run 004 Strike 004
 - Measured -- Predicted

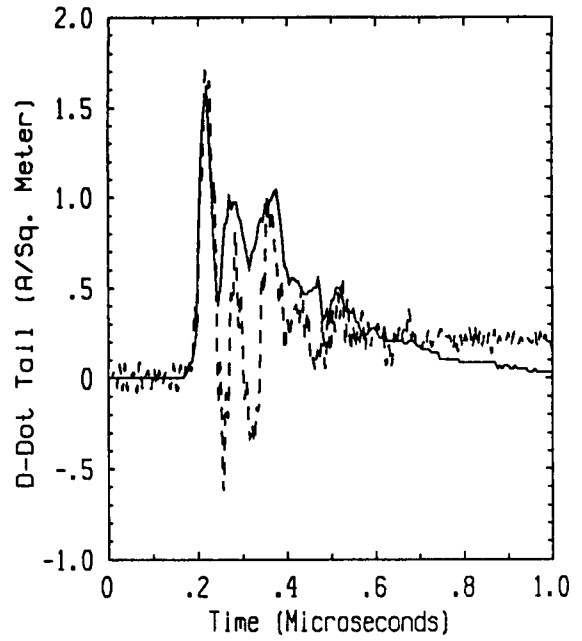


Flight 85.035 Run 004 Strike 004
 - Measured -- Predicted

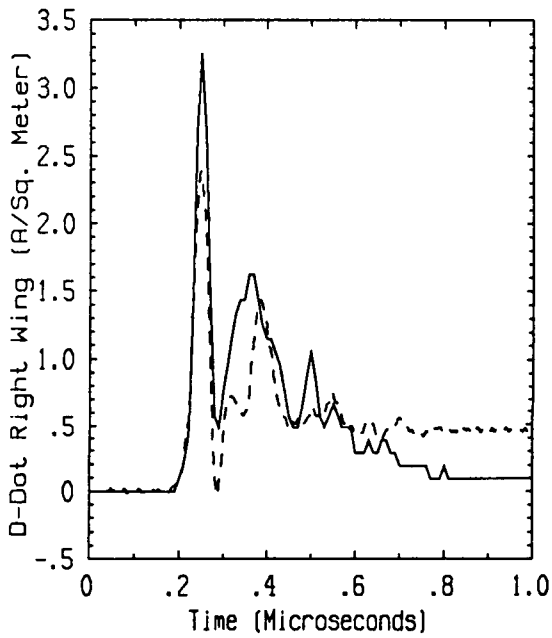
**MEASURED AND CALCULATED SENSOR TRANSIENTS
FOR TAIL ATTACHMENTS**



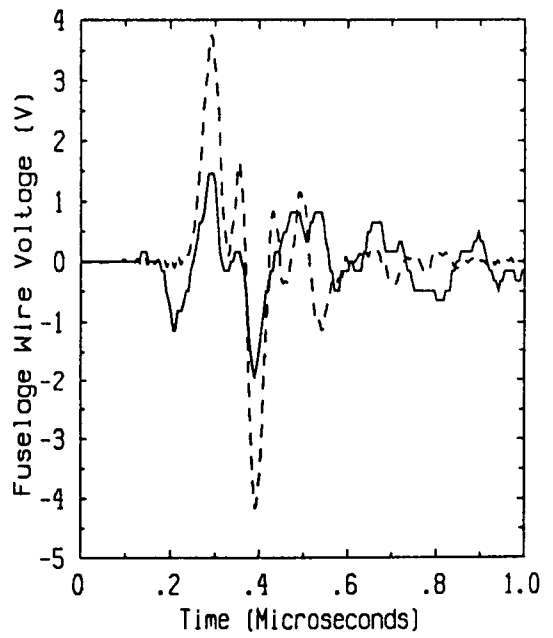
Flight 85.035 Run 005 Strike 005
 - Measured -- Predicted



Flight 85.035 Run 005 Strike 005
 - Measured -- Predicted



Flight 85.035 Run 005 Strike 005
 - Measured -- Predicted



Flight 85.035 Run 005 Strike 005
 - Measured -- Predicted



Report Documentation Page

1. Report No. NASA CR-4250		2. Government Accession No.		3. Recipient's Catalog No.	
4. Title and Subtitle Interpretation of F106B and CV580 In-Flight Lightning Data and Form Factor Determination			5. Report Date September 1989		
			6. Performing Organization Code		
7. Author(s) T. Rudolph, J. Horembala, F. J. Eriksen, H. S. Weigel, J. R. Elliott, S. L. Parker, R. A. Perala			8. Performing Organization Report No. EMA-89-R-33		
			10. Work Unit No. 505-66-21-04		
9. Performing Organization Name and Address Electro Magnetic Applications, Inc. 12567 West Cedar Drive, Suite 250 Lakewood, CO 80228			11. Contract or Grant No. NAS1-17748		
			13. Type of Report and Period Covered Contractor Report		
12. Sponsoring Agency Name and Address National Aeronautics and Space Administration Langley Research Center Hampton, VA 23665-5225			14. Sponsoring Agency Code		
			15. Supplementary Notes Langley Technical Monitor: Felix L. Pitts		
16. Abstract <p>This report deals with two main topics in the area of in-flight aircraft/lightning interaction. The first is the analysis of measured data from the NASA F106B Thunderstorm Research Aircraft and the CV580 research program run by the FAA and Wright-Patterson Air Force Base. The CV580 data was investigated in a mostly qualitative sense, while the F106B data was subjected to both statistical and quantitative analysis using linear triggered lightning finite difference models. The second main topic of the report is the analysis of field mill data and the calibration of the field mill systems. The calibration of the F106B field mill system was investigated using an improved finite difference model of the aircraft having a spatial resolution of one-quarter meter. The calibration was applied to measured field mill data acquired during the 1985 thunderstorm season. The experimental determination of form factors useful for field mill calibration was also investigated both experimentally and analytically. The experimental effort involved the use of conducting scale models and an electrolytic tank. A new analytic technique was developed to aid in the understanding of the experimental results.</p>					
17. Key Words (Suggested by Author(s)) F106B Form Factors Electrolytic Tank Field Mill Calibration CV580 Triggered Lightning			18. Distribution Statement Unclassified-Unlimited Subject Category 47		
19. Security Classif. (of this report) Unclassified		20. Security Classif. (of this page) Unclassified		21. No. of pages 156	22. Price A08